TECHNICAL REPORT H-71-2

THEORETICS IN DESIGN OF THE PROPOSED CRESCENT CITY HARBOR TSUNAMI MODEL

by

San Francisco

U. S. Army Engineer Waterways Experiment Station
CORPS OF ENGINEERS
Vicksburg, Mississippi

TECHNICAL REPORT H-69-9

THEORETICS IN DESIGN OF THE PROPOSED CRESCENT CITY HARBOR TSUNAMI MODEL

by

G. H. Keulegan
J. Harrison
M. J. Mathews

June 1969

Sponsored by

U. S. Army Engineer District
San Francisco

Conducted by

U. S. Army Engineer Waterways Experiment Station
CORPS OF ENGINEERS
Vicksburg, Mississippi

ARMY-MRC VICKSBURG, MISS.

Unclassified

Security Classification

DOCUMENT CONTROL DATA - R & D

(Security classification of title, body of abstract and indexing annotation must be entered when the overall report is classified)

1. ORIGINATING ACTIVITY (Corporate author)
U. S. Army Engineer Waterways Experiment Station
Vicksburg, Mississippi

2a. REPORT SECURITY CLASSIFICATION
Unclassified

2b. GROUP

3. REPORT TITLE
THEORETICS IN DESIGN OF THE PROPOSED CRESCENT CITY HARBOR TSUNAMI MODEL

4. DESCRIPTIVE NOTES (Type of report and inclusive dates)
Final report

5. AUTHOR(S) (First name, middle initial, last name)
Garbis H. Keulegan
John Harrison
Michael J. Mathews

6. REPORT DATE	7a. TOTAL NO. OF PAGES	7b. NO. OF REFS
July 1969	124	27

8a. CONTRACT OR GRANT NO.	9a. ORIGINATOR'S REPORT NUMBER(S)
b. PROJECT NO.	Technical Report H-69-9
c.	9b. OTHER REPORT NO(S) (Any other numbers that may be assigned this report)
d.	

10. DISTRIBUTION STATEMENT
This document has been approved for public release and sale; its distribution is unlimited.

11. SUPPLEMENTARY NOTES	12. SPONSORING MILITARY ACTIVITY
	U. S. Army Engineer District San Francisco, California

13. ABSTRACT

The important wave parameters to be considered for tsunami model studies are wave height and period, and wave-front orientation. The first two of these parameters can be determined by marigraphic measurements or by visual observations; however, wave-front orientation has never been accurately observed at the problem site (Crescent City, Calif.). A digital computer program was written to plot wave rays from three recent epicentral locations to Crescent City to obtain approximate tsunami-front orientations. The refraction diagrams were checked by comparing the computed and actual arrival times of the wave fronts. The actual arrival times were obtained from recording tide stations at Crescent City and Hilo, Hawaii. Initial wave-front orientations near the earthquake epicenter were either assumed or taken from the literature. The frequency distribution of wave heights at Crescent City is a necessary consideration in the overall study. The period of record for tsunamis at Crescent City is too short to determine the frequency distribution of the wave heights; thus, an attempt was made to correlate the tsunami records from particular stations in the San Francisco and Hilo Harbor areas so that the Crescent City record could be artificially lengthened. Correlation between the Hilo Harbor and Crescent City data indicates that the 1964 tsunami at Crescent City was abnormally severe. Effects of distance on wave-height attenuation were investigated and compared with theoretical predictions. On the basis of these considerations, a tentative frequency relation was derived and a risk-duration relation was prepared from the frequency relation. The selected values of the test-wave dimensions (height and period) and orientation determine, to a considerable extent, the model configuration necessary to ensure results sufficiently accurate for purposes of the model study. Since experience in the design and operation of long-period wave

DD FORM 1 NOV 65 1473 REPLACES DD FORM 1473, 1 JAN 64, WHICH IS OBSOLETE FOR ARMY USE.

Unclassified

Security Classification

THE CONTENTS OF THIS REPORT ARE NOT TO BE USED FOR ADVERTISING, PUBLICATION, OR PROMOTIONAL PURPOSES. CITATION OF TRADE NAMES DOES NOT CONSTITUTE AN OFFICIAL ENDORSEMENT OR APPROVAL OF THE USE OF SUCH COMMERCIAL PRODUCTS.

Unclassified
Security Classification

14. KEY WORDS	LINK A		LINK B		LINK C	
	ROLE	WT	ROLE	WT	ROLE	WT
Crescent City Harbor						
Hydraulic models						
Tsunamis						
Water waves						

13. ABSTRACT (Continued)
models is scant, it was deemed necessary to conduct preliminary tests utilizing a pneumatic wave generator in a two-dimensional flume. The results of these tests were compared with theoretical predictions from an idealized mathematical model and on the basis of these tests, a preliminary model design was proposed. Further two-dimensional testing is deemed necessary before a satisfactory design of the three-dimensional model can be accomplished.

Unclassified
Security Classification

FOREWORD

The theoretical study described herein was requested by the District Engineer, U. S. Army Engineer District, San Francisco, in a letter to the Office, Chief of Engineers, dated 15 September 1967; authority to perform the investigation was granted by the Office, Chief of Engineers, in an indorsement dated 7 November 1967. The investigation was conducted during the period December 1967 to August 1968.

The study was conducted in the Hydraulics Division of the U. S. Army Engineer Waterways Experiment Station under the direction of Mr. E. P. Fortson, Jr., Chief of the Hydraulics Division, and Mr. R. Y. Hudson, Chief of the Wave Dynamics Branch. The investigation was conducted by Dr. G. H. Keulegan, Resident Consultant, CPT J. Harrison, Military Assistant, and Mr. M. J. Mathews, Research Hydraulic Engineer.

Directors of the Waterways Experiment Station during the conduct of this investigation and preparation and publication of this report were COL John R. Oswalt, Jr., CE, and COL Levi A. Brown, CE. Technical Directors were Messrs. J. B. Tiffany and F. R. Brown.

CONTENTS

NOTATION

a	Radius of zero contour of the theoretical island in fig. C1; constant used in an integration formula
A	Constant used in equation D17
A, A_1, A_2 B, B_1, B_2 C, C_1, C_2 D, D_1, D_2 E, E_1, E_2	Coefficients used in the surface fitting procedure of the computer program
b	Radius of the largest contour of the theoretical island in fig. C1; constant used in an integration formula
b_b	Physical distance between wave rays at a point of unknown wave height, h_b
b_o	Physical distance between wave rays at a point of known wave height, h_o
B	Constant used in equation D14
BW	Effective bandwidth of band-pass filter
C	Tsunami celerity in the open ocean; $C = \sqrt{gH}$
C_1	Constant found in equation B9; $C_1 = \left(\frac{\eta_o}{1 + \eta_o}\right)^{1/2}$
C_2	Constant found in equation C15
D	Time in years in equation 26
e_s	Probable error inherent in the estimate
f_1	Fundamental frequency of a resonating body; equation 1
h	height of initial wave from generator; elevation above mean water level
h_b	Unknown wave height
h_c	Open-ocean wave height near Crescent City shelf
h_h	Open-ocean wave height near Hilo shelf
h_o	Known wave height
h_t	Wave height after t hours of travel

h_1 Wave height after one hour of travel

H Depth of water through which wave ray is passing; assumed water depth on a Mercator map; mean water depth at any location in a channel

$H_{(i,j)}$ Depth value assigned to an intersection within a grid of depth values

H_o Initial water level in flume before release; water depth at wave generator; water depth; water depth over a shelf at a distance L from the shore (equation D1)

H_{P_1} Water depth at a random point P_1 within a grid of depth values

H_1 Appointed depth defined in fig. D1; maximum depth of ocean surrounding theoretical island

J_o Bessel function of order zero of the first kind

J_1 Bessel function of order one of the first kind

k_1 Constant between 0.06 and 0.10 depending on the air space and the aperture openings of the pneumatic wave generator

K Constant; $K = \frac{C}{H^{1/2}}$; $K^2 = C_1^{-2} - 1$; radius of curvature of a curve in rectangular coordinates; constant; $K = \frac{\sigma^2 L^2}{gH_o}$

K_o Bessel function of order zero of the second kind

K_1 Bessel function of order one of the second kind

ℓ Length of sloping channel

L Water-surface length; length of submerged shelf off Crescent City

m Curve fitting coefficient

n Curve fitting coefficient; ratio of $\frac{\Delta x}{\Delta x_o}$ and $\frac{\Delta y}{\Delta y_o}$; degree of freedom

N Average frequency of occurrence of tsunamis of equal or greater height h ; factor used in the solution of equation D30

$$N = \frac{T\sqrt{gH_o}}{L} = \frac{4\pi}{2K^{1/2}}$$

$P(x,y)$ Arbitrary point on a curve in x , y coordinate system

P_o, P_1, P_2 Successive computation points along a wave ray

q	Risk associated with an equal or greater event occurring during a given time period D years
r	Polar coordinate measure of distance $r = \frac{x}{\cos \theta}$; radius of hypothetical island between zero and maximum contour
r'	$r' = \frac{\partial r}{\partial \theta}$
r''	$r'' = \frac{\partial^2 r}{\partial \theta^2}$
R	Radius of the earth, assuming spherical shape
s	Distance along a wave ray
S	Vertical model scale
SL	Sample length
S_1	Ray path over a given Mercator map
t	Time; tsunami travel time $t = \int_{s_1} \frac{ds}{V}$
T	Period of forcing function; wave period
T_c	Fundamental period of bay oscillation; tsunami travel time from source to the Crescent City area
T_{cr}	Critical resonant period for a given body of water
T_h	Tsunami travel time from source to Hilo area
T_p	Assumed period of the 1964 tsunami $T_p = 28$ min
u	Dimensionless horizontal velocity component
U	Wave velocity
V	Wave celerity on a Mercator map; wave celerity
V_o	Tsunami celerity, $V_o = \sqrt{gH_o}$
x	Measurement of length; part of total length of water surface L
x,y	Length of grid square edge in x and y direction, respectively (Note: $x = y$); lengths measured on a Mercator map corresponding to x_o and y_o ; coordinate locations in Cartesian coordinate system
x_o,y_o	Lengths measured on a sphere of radius R
x_1	Distance from shore to beginning of shelf
$y(t)$	Periodic signal
Y_n	Amplitude of nth component of a Fourier series
Y_o,Y_1,Y_2,Y_3	Amplitudes of respective components in a Fourier series

z $z = \sinh y$

α Slope of a given basin

δ Dimensionless depth parameter

$\left.\begin{matrix}\delta x \\ \delta y\end{matrix}\right\}$ Coordinates of the random point P_1 measured from $H_{(i,j)}$

Δp_i Amount that suction pressure in pneumatic generator is decreased upon opening air valves

Δp_o Pneumatic generator suction pressure prior to opening air valves

Δx_o Elementary length on a parallel of latitude ψ

Δy_o Elementary length on a meridian of longitude ϕ

ζ Dimensionless length parameter

η Dimensionless depth parameter; maximum elevation above mean, equation E7; $\left(\frac{dx}{dy}\right)^2$ on a Mercator map

θ Wave ray angle measured positive counterclockwise from the positive x-axis; angle in polar coordinates; variable in equation D12

θ_a Angle shown in fig. C2 which is the angle between the positive x-axis and the intersection of a wave ray with the island's zero contour

θ_b Angle shown in fig. C2 which is the angle between the x-axis and the intersection of a wave ray with the island's maximum contour

θ_o Wave ray angle measured positive counterclockwise from the positive x-axis

θ_L $\theta_L = 2K^{1/2}$

λ Constant (taken equal to 0.4) related to nozzle energy loss in the pneumatic wave generator

ξ Dimensionless length or depth parameter

ρ Water density

σ $\sigma = 2\pi/T$

τ Dimensionless time parameter

ϕ Degrees of longitude

ϕ_n Phase angle of nth component of a Fourier series

ψ Degrees of latitude

CONVERSION FACTORS, BRITISH TO METRIC UNITS OF MEASUREMENT

British units of measurement used in this report can be converted to metric units as follows:

Multiply	By	To Obtain
inches	2.54	centimeters
feet	0.3048	meters
miles	1.609344	kilometers
square feet	0.092903	square meters
feet per second per second	0.3048	meters per second per second

SUMMARY

The important wave parameters to be considered for tsunami model studies are wave height and period, wave-front orientation, and the frequency of occurrence of waves of different heights. The first two of these parameters can be determined by marigraphic measurements or by visual observations; however, wave-front orientation, which is an important variable in the construction and operation of a model, has never been accurately observed at the problem site (Crescent City, Calif.). A digital computer program was written to plot wave rays from three recent epicentral locations to Crescent City to obtain approximate tsunami-front orientations and to compute refraction coefficients in the Crescent City area. The refraction diagrams were checked by comparing the computed and actual arrival times of the wave fronts. The actual arrival times were obtained from recording tide stations at Crescent City and Hilo, Hawaii. Initial wave-front orientations near the earthquake epicenter were either assumed or taken from the literature.

The frequency distribution of wave heights at Crescent City is a necessary consideration in the overall study. The period of record for tsunamis at Crescent City is too short to determine the frequency distribution of the wave heights; thus, an attempt was made to correlate the tsunami records from particular stations in the San Francisco and Hilo Harbor areas so that the Crescent City record could be artificially lengthened. Correlation between the Hilo Harbor and Crescent City data indicates that the 1964 tsunami at Crescent City was abnormally severe. Effects of distance on wave-height attenuation were investigated and compared with theoretical predictions. On the basis of these considerations, a tentative frequency relation was derived and a risk-duration relation was prepared from the frequency relation.

The selected values of the test-wave dimensions (height and period) and orientation determine, to a considerable extent, the model configuration necessary to ensure results sufficiently accurate for purposes of the model study. Since experience in the design and operation of long-period wave models is scant, it was deemed necessary to conduct preliminary tests utilizing a pneumatic wave generator in a two-dimensional flume. The results of these tests were compared with theoretical predictions from an idealized mathematical model, and on the basis of these tests, a preliminary model design was proposed. Further two-dimensional testing is deemed necessary before a satisfactory design of the three-dimensional model can be accomplished.

THEORETICS IN DESIGN OF THE PROPOSED CRESCENT CITY HARBOR TSUNAMI MODEL

PART I: INTRODUCTION

1. Crescent City, Calif., with a resident population of approximately 3200, is located on the northern California coast approximately 20 miles* from the California-Oregon border. The combination of nearshore undersea topography, resonant characteristics of the surrounding nearshore area, and exposed position on the coast makes Crescent City particularly susceptible to tsunamis originating anywhere in the Pacific seismic belt.

2. The primary purposes of this investigation were to conduct a theoretical study of tsunamis with particular emphasis on their occurrence at Crescent City, and to provide input data for a hydraulic model which is to be used to determine the characteristics of proposed barrier plans to protect the city and harbor of Crescent City from future tsunamis. Because of the magnitude of this many-faceted problem, it was decided to divide the study into four major sections, namely, the wave input for the proposed model, the tsunami refraction problem, the frequency of occurrence of tsunamis of various heights at Crescent City, and the flume tests conducted to determine details of the proposed model.

3. In the Crescent City Harbor tsunami model, as in any model of the same scope and nature, one of the primary elements to consider is that of wave input. In a general sense this involves decisions as to the magnitude, form, and period of the critical waves in a specific tsunami wave train. Equally important is the orientation of the wave fronts approaching the harbor area, which determines the alignment of the wave generator during model testing. Unfortunately, owing to the early destruction of the harbor tide gages during the 1964 tsunami, the magnitude and form of the waves for this occurrence could not be accurately determined. The disastrous effects of this particular tsunami appear to have been associated

---

* A table of factors for converting British units of measurement to metric units is given on page xiii.

with extensive inundation by a rising horizontal water surface instead of a borelike configuration sometimes associated with tsunamis.[1] The limit of the inundation is well defined, and accordingly, verification of the model processes will rely solely on the limits of this inundation.

4. To determine the wave directions at the positions of the model wave generator, a new tsunami refraction diagram technique was developed by the authors. Refraction diagrams were prepared for three recent tsunamis (Alaska, 1964; Chile, 1960; and Kamchatka, 1952), and wave-front patterns charted from each of the sources were determined for the nearshore areas at Crescent City and Hilo, Hawaii. Van Dorn's 10-min wave-front configuration[2] was used as the starting position for ray trajectories for the Alaskan tsunami. Starting lines for the other two tsunamis were assumed by the investigators.

5. In the selection of test waves for the Crescent City Harbor tsunami model, the question arises as to whether the effectiveness of protective structures should be determined for tsunami intensities greater than the one that occurred in 1964. In this connection, a study was made to ascertain the probability of the occurrence of tsunamis at Crescent City with more critical dimensions than those of the 1964 tsunami. The frequency distribution of tsunamis at Hilo Harbor was determined from a considerable number of occurrences, and it was assumed that the Hilo frequency distribution is similar to that for Crescent City. The correlation of the observed tsunami heights for these two localities was examined in light of the tsunami sources.

6. After the orientation, height, and period of the test waves have been selected, the linear scales of the model and the extent of the sea area lying between the wave generator and the harbor, which must be included within the model limits, can be determined. The extent of the required sea area is related to the number of wave cycles to be simulated in the operation of the model. The greater the sea area, the larger the number of cycles that can be reproduced in the model, and the more accurate will be the observable wave phenomena. Cost considerations, however, impose restrictions on the allowable space; yet it is essential that the model sea area be of such size that a minimum of one initial wave cycle

is completed. Therefore, the necessary condition is that the fundamental period of the resonant oscillation of the model sea, between the coast and the generator, correspond to the largest period of the prototype waves selected for testing. Tests in a two-dimensional wave flume became necessary to develop the basic ideas concerning this aspect in the design of the proposed three-dimensional model. The results of these tests are presented herein.

PART II: TSUNAMI CHARACTERISTICS AT CRESCENT CITY, CALIF.

Maximum Observed Height of the 1964 Tsunami

7. Crescent City is located at a point on the California coast that is particularly susceptible to the damaging effects of tsunamis. The largest tsunami recorded at Crescent City was the one generated by the 1964 Alaskan earthquake. Fig. 1 is a reproduction of the marigram of the 1964 tsunami taken from the wave gage at Citizen's Dock in Crescent City Harbor.

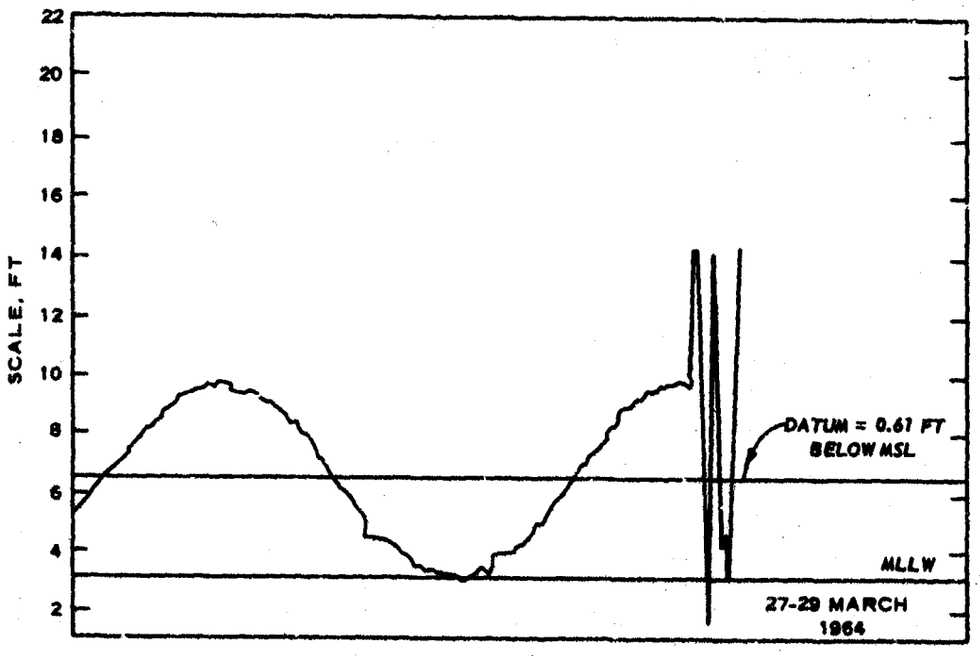

Fig. 1. Gage record of 1964 tsunami at Crescent City

8. The first problem was that of organizing the information contained in the various reports concerning the observed heights of the 1964 tsunami at Crescent City. After reviewing the available data, it is believed that the tide gage at Citizen's Dock was rendered inoperable by the wave crest preceding the largest wave. Therefore, in order to assimilate the tsunami observations, the sequence of wave crests has been designated

as shown in fig. 2.* Accordingly, the wave crest that destroyed the tide gage was the fourth crest, while the largest wave was the fifth crest. The dashed lines in fig. 2 indicate Wilson's extrapolations of the wave record.

9. Since it was considered undesirable to rely on an extrapolation of the crest height for the fifth crest from the existing record, observations of eyewitnesses were the only available means of estimating the rise and fall characteristics of the fifth and largest crest. The observations from four sources are tabulated in fig. 3. It is interesting to note that there is a large degree of disagreement as to the magnitudes of the crest heights, even for crests that were recorded by the tide gage. This may be due in part to the disagreement as to what constituted

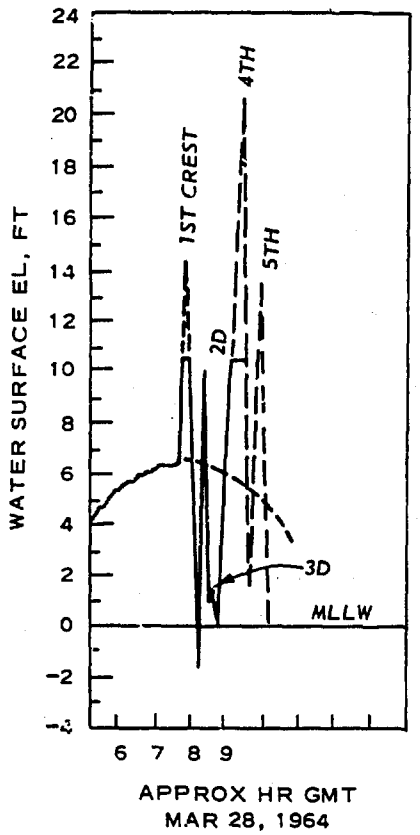

Fig. 2. Wave configuration of 1964 tsunami (from Wilson)

	TUDOR[5]	WILSON[1]	WIEGEL[3]	MAGOON[4] USAED, SF
1ST CREST	14.5	14.5	16.1	
1ST TROUGH	0.2	-2.0	-2.0	
2D CREST	12.0	10.0	11.0	
2D TROUGH	2.2	0.8	0.8	
3D CREST	2.6	1.0	1.5	
3D TROUGH	2.2	0.0	0.0	
4TH CREST	20.5	20.8	17.2	
4TH TROUGH		1.0	-5.5 (-4 TO -7)	-5.5 (-4 TO -7)
5TH CREST		13.5	18.5 (18 TO 19)	18.5 (18 TO 21)
5TH TROUGH				-2.0 (0 TO -4)

HEIGHT VALUES FOR 1964 TSUNAMI (IN FT REFERRED TO MLLW)

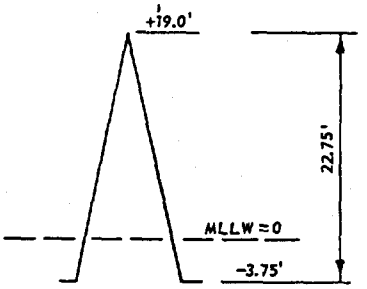

Fig. 3. The selected design wave

* Fig. 2 is from reference 1; crest notations have been added.

distinct troughs and crests. The fifth crest and preceding trough heights were reported by Wiegel[3] and Magoon[4] after extensive interviews with reliable observers who were on or near Citizen's Dock during the tsunami. As a result, the reported heights should be within a tolerable range of accuracy. For this report, and for any subsequent model testing, an assumed maximum wave with the height characteristics shown at the bottom of fig. 3 was selected.

Period of the 1964 Tsunami

10. Tudor,[5] in reconstructing the Crescent City marigram for the 1964 Alaskan tsunami, gives the following times (PST) for the occurrences of the crests: first crest 2352, 27 March; second crest 0020 and fourth crest 0115, 28 March. What Tudor calls the fourth crest has been indicated in this report as the fifth crest. Accordingly, the period of the first wave is 28 min and the mean period of the sequence of the first four waves is 27.6 min. This value can be compared with the periods of the corresponding tsunami observations on the northwestern coast of the United States. These periods are approximately as follows:

Location	Period, min	Location	Period, min
Neah Bay, Wash.	31	Rincon Island, Calif.	30
Friday Harbor, Wash.	31	Santa Monica, Calif.	26
Astoria, Oreg.	30	Los Angeles, Calif.	30
San Francisco, Calif.	30	Newport Bay, Calif.	31
Alameda, Calif.	30	La Jolla, Calif.	31
Avila Beach, Calif.	30	San Diego, Calif.	31

The above values, which were obtained by scanning the tsunami tide gage records shown by Spaeth and Berkman,[6] are close enough to the periods of waves assigned to Crescent City so that the value of T_p = 28 min can be selected as the characteristic period of 1964 Alaskan tsunami. Tide gage records of the 1964 tsunami at other localities show the presence of waves of other periods that are missing in the corresponding record for

Crescent City owing to the early destruction of the gage. These may be inferred from the very complete gage records taken at Crescent City during the 1960 tsunami from Chile.

Spectral Analysis of a Portion of the 1960 Tsunami Records

11. A useful method for describing a vibrating environment, whether it be random, periodic, or a mixture of both, is to determine the spectral composition of the response data representing the environment. Several different spectral density functions might be conceived and employed to describe the frequency composition of random or periodic vibration responses of which two are amplitude spectra and power spectra. Each of the periodic spectra consists of discrete components at specific frequencies and harmonics of these frequencies; for random vibration data, each of the spectra is continuous with responses possible at any or all frequencies in the spectrum.

12. Because of the relatively small number of visually obvious discrete frequencies, the wave records of the May 1960 tsunami at Crescent City were treated as periodic vibration data. Any periodic signal $y(t)$ can be expressed by a Fourier series as follows:[7]

$$y(t) = Y_0 + Y_1 \sin (2\pi f_1 t + \phi_1) + Y_2 \sin (4\pi f_1 t + \phi_2) + Y_3 \sin (6\pi f_1 t + \phi_3) + \ldots$$

$$= Y_0 + \sum_1^\infty Y_n \sin (2\pi n f_1 t + \phi_n) \qquad (1)$$

where f_1 is the fundamental frequency in cps, Y_n is the amplitude of the nth component, and ϕ_n is the phase angle of the nth component. A description in terms of the harmonic amplitudes and frequencies is possible by frequency spectrum analysis and is presented as the remainder of this section.

13. Mr. J. L. Ferguson of the WES Electronic Data Reduction Lab undertook the task of producing the amplitude spectra (frequency versus

wave-height plots) for a portion of the Crescent City tsunami height record of May 1960. The record submitted for analysis was an average of the readings taken at Citizen's Dock and Dutton's Dock in Crescent City Harbor. The average record was done by hand by personnel of the Hilo Model Branch, U. S. Army Engineer District, Honolulu, in 1965. Because of the 2-min phase lag between the response at the two locations, each of the records was offset 1 min before the average heights were computed. The results of this effort are presented as figs. 5-8.

14. The steps taken in processing the pictorial wave record prior to reduction by the analog wave analyzer are outlined below:

a. The pictorial record of the tsunami was transferred to a digital magnetic tape (in a compatible BCD format) by a pencil-line follower (Edwin Industries model PF10A). The follower digitized and recorded the y-coordinates (from a prescribed base line) at 1-mm horizontal increments along the entire 18.5-hr pictorial record.

b. A digital to analog conversion was then effected by a small digital computer (Scientific Controls Corporation model 650-2), and the resulting analog signal was processed by the wave analyzer (Gulton Ortholog model OR-WA/1) diagrammed in fig. 4.

15. Each of the frequency spectra (figs. 5-8) was generated by a slow-moving filter or "window" of the indicated bandwidth. The entire

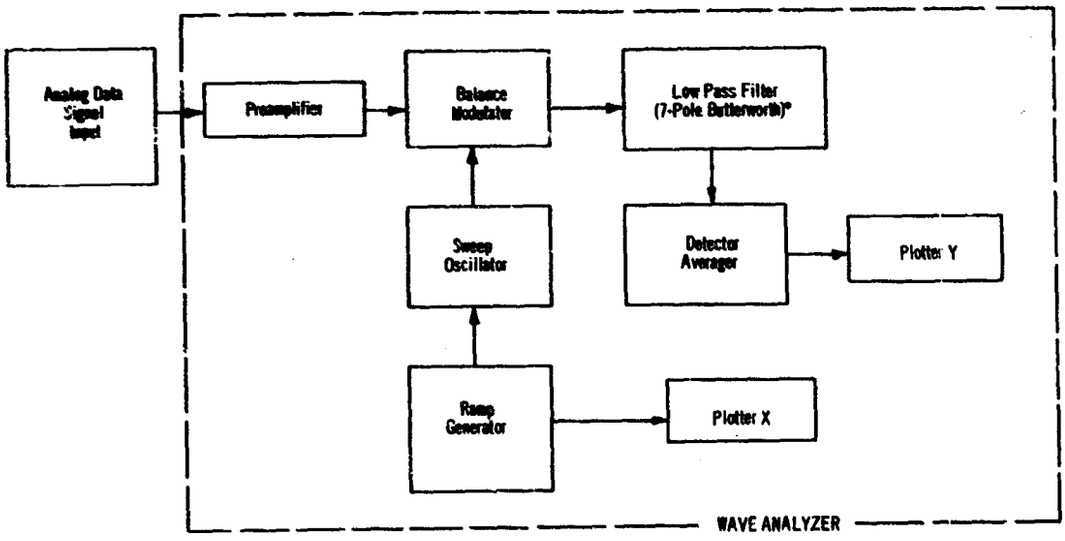

* Butterworth filters are discussed in most comprehensive texts dealing with the theory of electrical filters.

Fig. 4. Analog wave analyzer

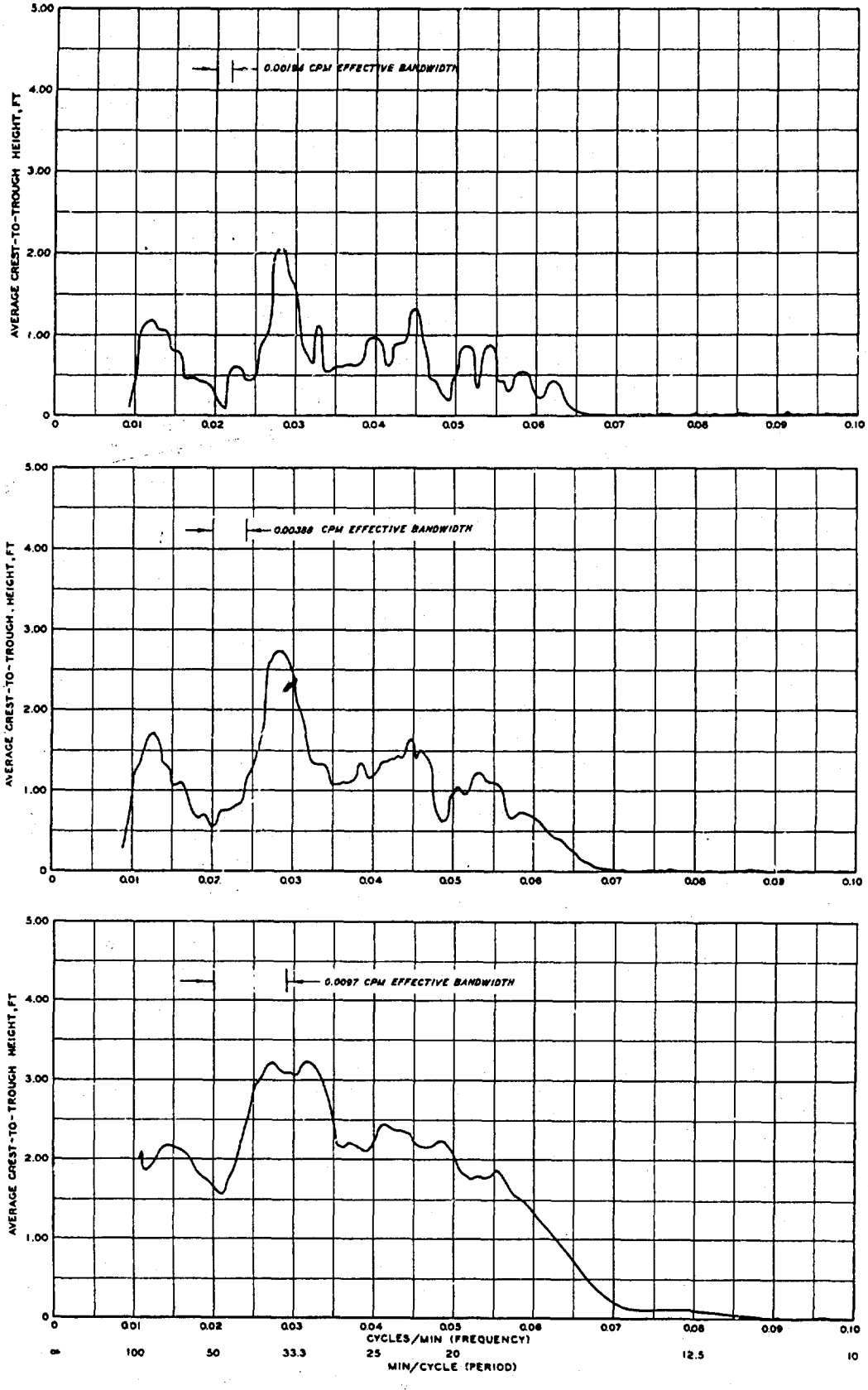

Fig. 5. Frequency spectra for entire tsunami record, 0530 to 2400 hr, 23 May 1960, at Crescent City with 0.00194-, 0.00388-, and 0.0097-cpm filters

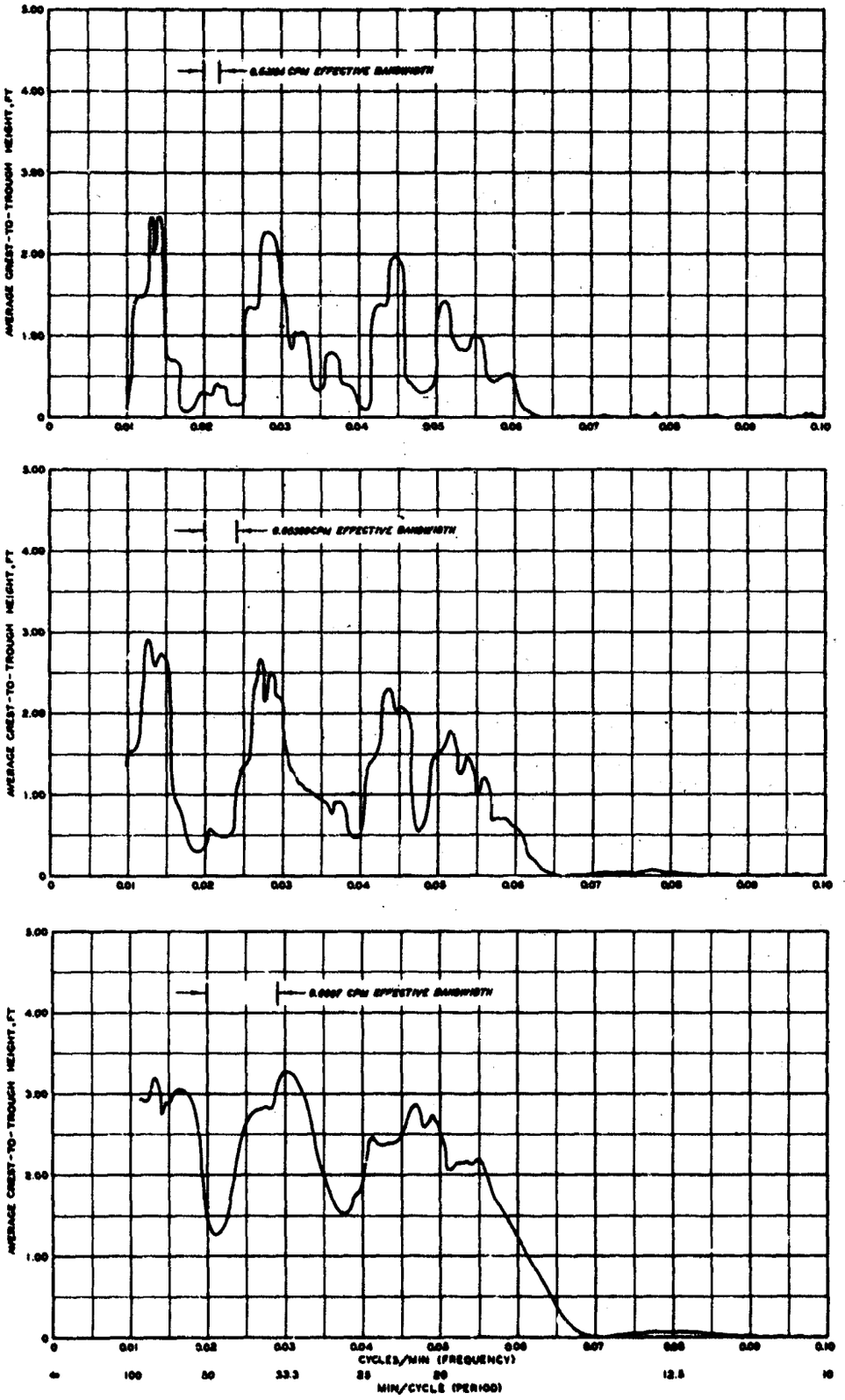

Fig. 6. Frequency spectra for the period 0530 to 1300 hr, 23 May 1960, at Crescent City with 0.00194-, 0.00388-, and 0.0097-cpm filters

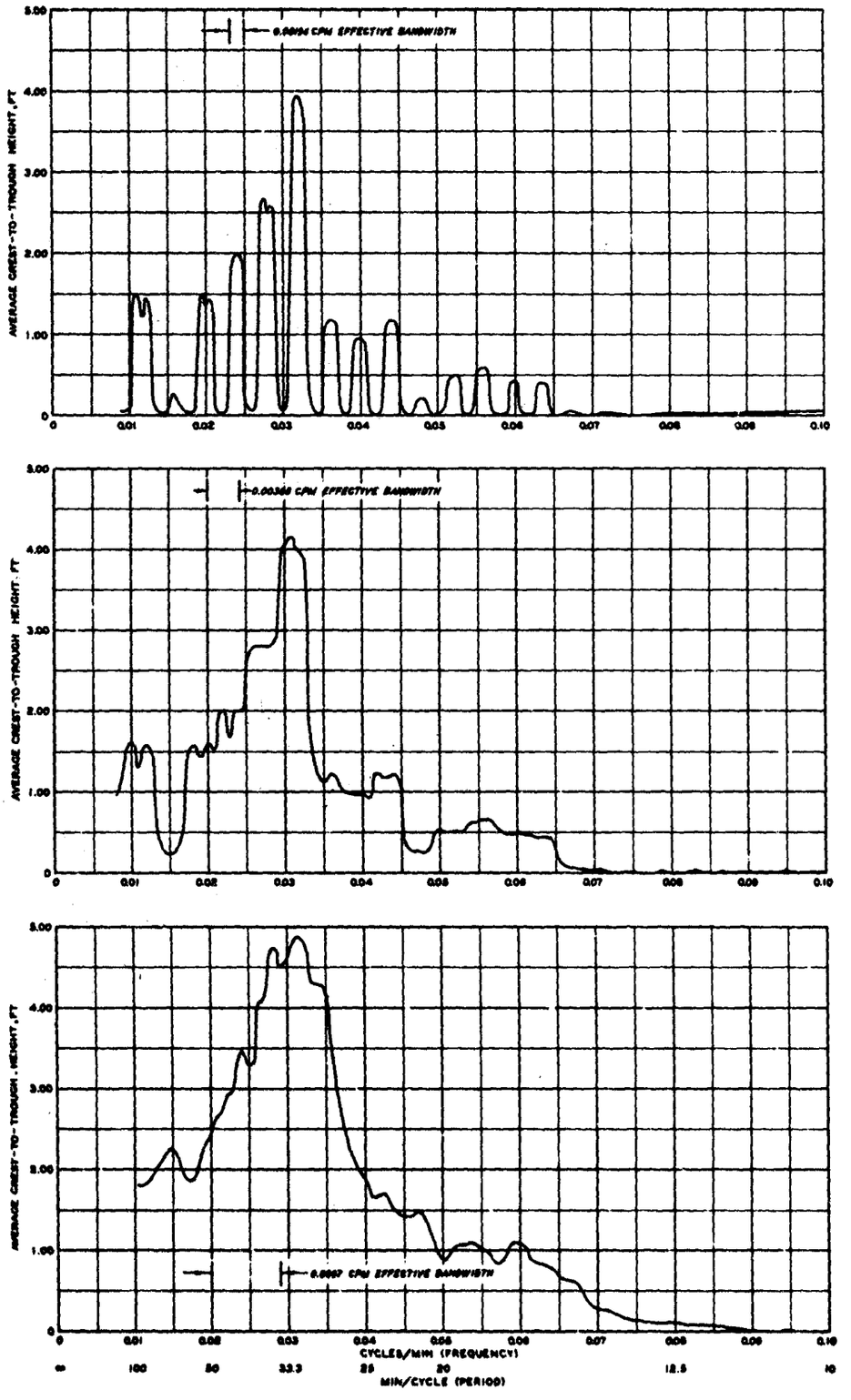

Fig. 7. Frequency spectra for the period 1300 to 1700 hr, 23 May 1960, at Crescent City with 0.00194-, 0.00388-, and 0.0097-cpm filters

//

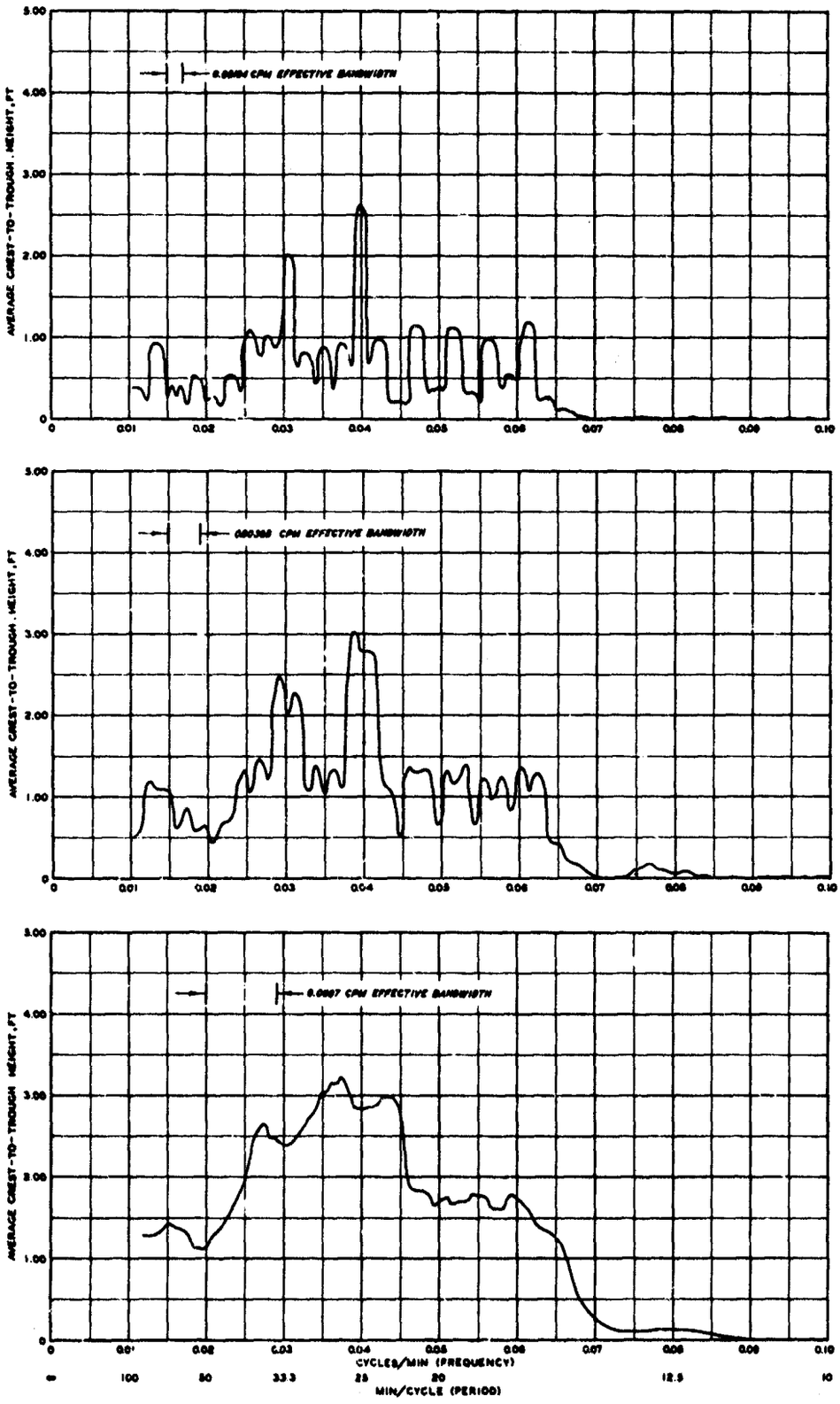

Fig. 8. Frequency spectra for the period 1700 to 2400 hr, 23 May 1960, at Crescent City with 0.00194-, 0.00388-, and 0.0097-cpm filters

analog wave record signal was continuously cycled through the analyzer and the window position moved so slowly across the spectrum that any wave height may be considered as being associated with its discrete frequency. All signal amplitudes of a particular frequency were averaged (by means of an RC averaging network within the wave analyzer) over the entire time period to obtain the average wave height. This height, as shown in the plots, would not be comparable to a maximum height as measured from the wave record. Since none of the frequencies appeared at all times on the wave record, the heights shown on the spectrum plots are lower than the maximum heights measured on the pictorial record with the heights for the least occurring frequencies being the most out of proportion.

16. Each of the four separate record lengths of the 1960 tsunami at Crescent City was subjected to analysis using three separate window widths. The entire record (from 0530 to 2400 hr, 23 May 1960) was analyzed first. The record was then divided into three parts, 0530 to 1300 hr, 1300 to 1700 hr, and 1700 to 2400 hr; and separate analyses were performed on each of these parts. Because of the amplitude averaging technique and the distribution of the wave record spectral frequencies, the plotted height increased as the window width increased for the three separate analyses of the four series of runs.

17. The statistical methods commonly used to establish confidence limits with respect to the accuracy of the wave-height measurements, shown in figs. 5-8, are the statistical coefficient of variation and the chi-square distribution.[8]

18. The statistical coefficient of variation expresses the probable error, e_s, as

$$e_s = \frac{1}{\sqrt{BW \times SL}} \qquad (2)$$

where

e_s = probable error inherent in the estimate

BW = effective bandwidth of band-pass filter

SL = sample length (in units corresponding to the bandwidth)

Moody[8] states that this method should not be used when the numerical value

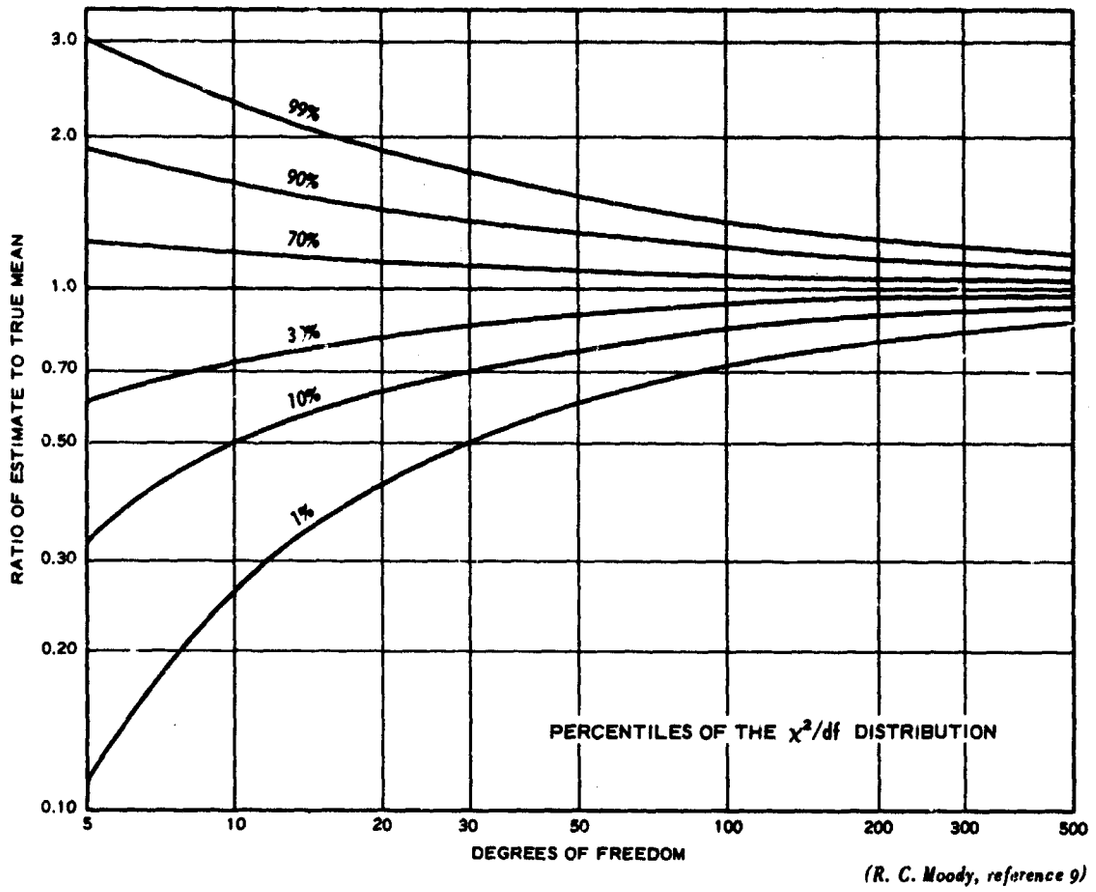

Fig. 9. Chi-square distribution chart for establishing confidence levels of amplitude spectra

of e_s exceeds 0.20 (20 percent). Table 1 shows that all values of e_s exceed 20 percent; therefore, the chi-square distribution method (fig. 9) must be used. The abscissa of fig. 9 is in units of degrees of freedom, the ordinate is in units of the ratio of the estimated to the true value, and the parameter is the confidence band.

19. Degrees of freedom are given by

$$n = 2 \times BW \times SL \tag{3}$$

where

n = degree of freedom

20. Confidence levels for each of the time intervals studied, with their corresponding bandwidths, are shown in fig. 9. A large number of degrees of freedom are required to obtain a high confidence in an estimate. Equation 3 shows that this can be accomplished by using either wider filter bandwidths or longer sample lengths. For reasonable sample lengths the problem is most acute at the low-frequency end of the spectrum because of the narrowness of the filter required to resolve the resonances.

21. It should be noted from fig. 9 that, while degrees of freedom in excess of 100 do not produce proportionately more confidence, those observations with less than 20 degrees of freedom produce such wide confidence intervals that they are of questionable value.

22. While one cannot place any confidence in the fact that the plotted heights are peak values, the predominant periods of 80.0, 33.0, 22.0, and 18.0 min are clearly defined in all cases and can be accepted with confidence. These predominant periods are in good agreement with those mentioned in the following discussion of resonance, which were computed by considering the oscillations of the Crescent City area from the offshore shelf to the beach.

Resonance

23. The Omori principle that the tsunami periods observed in a bay are nearly the same as those of the usual secondary oscillations of that bay has been confirmed by Honda, Terada, and Isitani.[10] The principle is shown to be valid in the undulations of numerous bays along the coasts of the Pacific Ocean and the Sea of Japan. Suda and Seki in their study of the Atacam tsunami of 1922 and of the Aleutian tsunami of 1923 found that the second and third harmonics of the fundamental periods are highly predominant in bay areas.[11] The latter finding appears to apply also to the undulations of the 1960 tsunami at Crescent City.

24. The Omori principle suggests that the greater tsunami heights observed in some bays should also be examined on the basis of resonance. Wilson[1] observes that the excessive heights noted at Port Alberni, Canada, during the 1964 Alaskan tsunami were brought about because of the parabolic

variation of channel depths, with the width being nearly constant. Likewise, the greater heights observed at Port Littleton, New Zealand, were due to the uniformly sloping floor of the channel. For the analyses of these two cases, Wilson makes a judicial application of Lamb's treatment of the oscillation of bays of such configurations, imposing the condition that the mouths of the bays are nodal lines.[1]

25. Similarly, the periods of oscillations of the offshore shelf in the proximity of Crescent City, as shown in fig. 10, have been considered. The shelf is regarded as sloping uniformly with the depth of the shelf H_c = 350 ft, and the length of the shelf L = 16 nautical miles. Assuming that the depth at the coast is nil, computations for the periods of the various harmonics give values of 89, 35, 18, 15, and 13 min, which curiously enough are in approximate agreement with the periods found in the spectral analysis of the 1960 tsunami. Other computations were also made, assuming that the shelf at the coast has a finite depth. However, the effect of this assumption is to increase the value of the fundamental periods. A more thorough treatment of shelf oscillations is presented in Appendix D. Noting that the shelf environment enclosing Crescent City may be regarded as approximating a semielliptic basin, Wilson makes use of an analysis by Goldsborough[12] and finds a satisfactory agreement between the observed and computed periods of the 1960 tsunami.

26. Hilo Bay and the sea vicinity of Crescent City are both susceptible to resonance. Since the periods of the fundamental oscillations of these two localities are different, the magnification of heights in each will be different for a given tsunami of a definite period. Another consideration which may be significant is the following. The phenomenon of resonance is most conveniently observed with standing waves in rectangular basins. Experience shows that as the periods of the forcing oscillations are decreased from an initially large value and are made to approach the period of the greatest fundamental oscillation of the basin, the wave magnification in the basin increases steadily to a limiting value. Then, when the period of the forcing oscillation is further decreased even by a small value, the wave magnification decreases markedly. There was an evidence of this in the Hilo Bay model study. As the main object of that

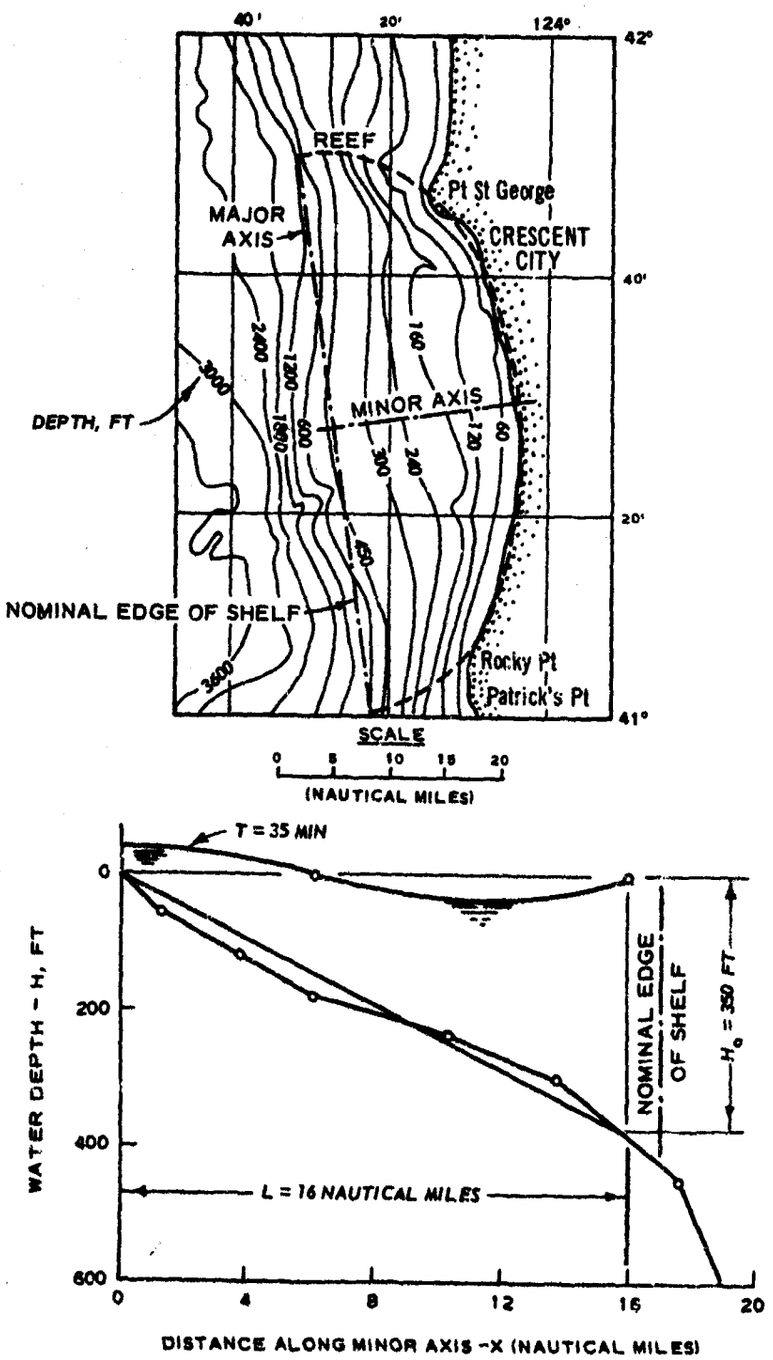

Fig. 10. Crescent City shelf location and dimensions

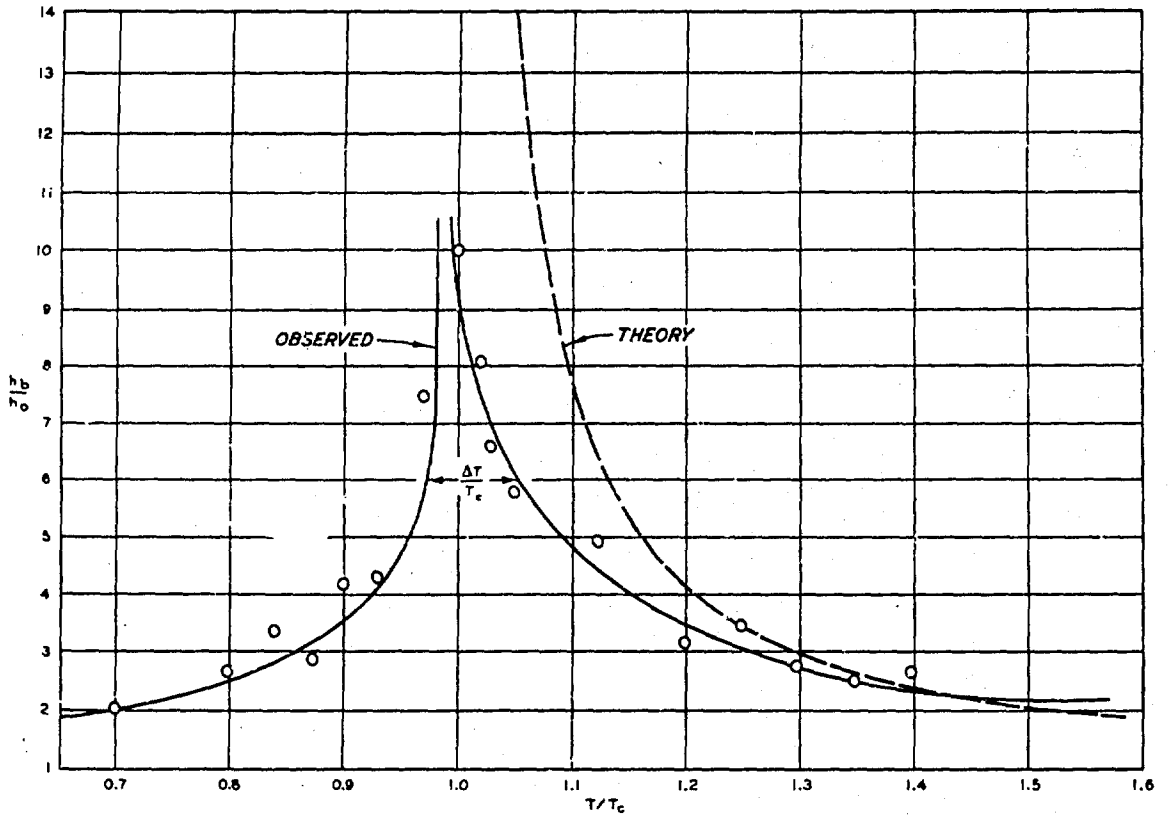

Fig. 11. Wave amplification in Hilo Bay; pilot model study

study was to examine the effect of model distortion, for the simplicity and the purity of observed results, the bay barrier was completed forming a truncated bay. The average results of the magnification ratio $\frac{h_b}{h_o}$, h_b being the wave height at the barrier and h_o the wave height at the bay mouth, from all the tests are shown in fig. 11 as a function of $\frac{T}{T_c}$ (T being the period of the forcing waves and T_c the fundamental period of oscillation).[13] There is a marked peak in the magnification values at $\frac{T}{T_c} = 0.99$. Accordingly, the interval $\frac{\Delta T}{T_c}$ for which the waves are appreciably magnified is about $\frac{\Delta T}{T_c} = 0.075$. In the same figure the theoretical magnification curve is also given.[14]

27. Eventually the question will be asked whether there is a discernible and consistent correlation between the tsunami heights observed

at Hilo Bay and those in the sea approaches of Crescent City. The above discussions suggest that correlation may be noted for the situations where the tsunami waves have periods which are removed from the periods of the fundamentals of the localities by an amount of about $\Delta T = 0.075T_c$ or greater.

PART III: PREPARATION OF TSUNAMI REFRACTION DIAGRAMS

Theoretical Development

28. After a considerable literature search it was deemed desirable to use the digital computer facilities at the U. S. Army Engineer Waterways Experiment Station (WES) to prepare the refraction diagrams. In January 1968, the main computer center utilized an 8000-space main memory GE-225 computer and an off-line Calcomp 750 incremental plotter. Attempts were first made to modify existing computer programs for use on the GE-225; however, the existing programs not only proved difficult to modify but did not incorporate all the features considered necessary for this particular problem. Therefore, a computer program was written specifically for tsunami refraction.

29. Ippen[15] presents the basic equation for wave ray refraction as:

$$\frac{d\theta}{ds} = \frac{1}{C}\left(\sin\theta\,\frac{\partial C}{\partial x} - \cos\theta\,\frac{\partial C}{\partial y}\right) \tag{4}$$

where, considering an x, y rectangular coordinate system, $\frac{d\theta}{ds}$ represents the change in the angle θ with respect to the distance moved along the ray (ds) and $\frac{\partial C}{\partial x}$ and $\frac{\partial C}{\partial y}$ represent the partial derivatives of the velocity in the x- and y-directions, respectively. C is the wave celerity and θ the instantaneous angular orientation of the ray.

30. Consider two positions, P_o and P_1, on a ray moving in the x-, y-plane as shown in fig. 12; P_o and P_1 represent two successive points on the ray with a velocity of travel at each point of $C = \sqrt{gH}$. Considering H as the depth of water through which this ray travels,

$$\frac{\partial C}{\partial x} = \frac{1}{2}\,g^{1/2}\,H^{-1/2}\,\frac{\partial H}{\partial x}$$

and

$$\frac{1}{C}\,\frac{\partial C}{\partial x} = \frac{1}{2H}\,\frac{\partial H}{\partial x} \tag{5}$$

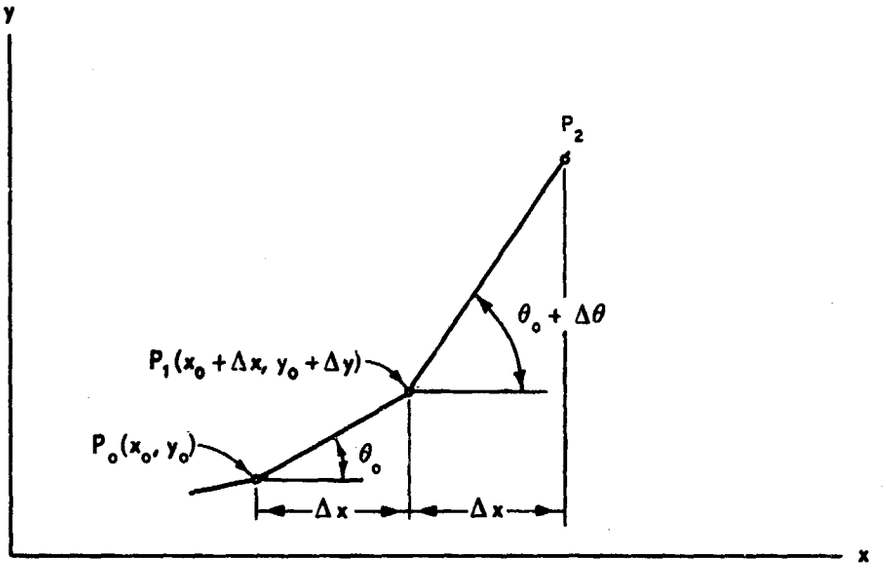

Fig. 12. Wave ray notation

In a like manner,

$$\frac{1}{C}\frac{\partial C}{\partial y} = \frac{1}{2H}\frac{\partial H}{\partial y} \tag{6}$$

Substitution of equations 5 and 6 into equation 4 yields

$$\frac{d\theta}{ds} = \frac{1}{2H}\left(\sin\theta\,\frac{\partial H}{\partial x} - \cos\theta\,\frac{\partial H}{\partial y}\right) \tag{7}$$

Noting that $\sin\theta = \frac{dy}{ds}$ and $\cos\theta = \frac{dx}{ds}$, equation 7 becomes

$$\frac{d\theta}{ds} = \frac{1}{2H}\left(\frac{dy}{ds}\frac{\partial H}{\partial x} - \frac{dx}{ds}\frac{\partial H}{\partial y}\right) \tag{8}$$

Using a small increment for ds allows

$$ds = \sqrt{dx^2 + dy^2}$$

or

$$ds = dx\sqrt{1 + \left(\frac{dy}{dx}\right)^2} \tag{9}$$

Substitution of equation 9 into equation 8 yields

$$\frac{d\theta}{ds} = \frac{1}{2H}\left(\frac{dy}{dx}\frac{\partial H}{\partial x} - \frac{\partial H}{\partial y}\right)\left[\frac{1}{\sqrt{1+\left(\frac{dy}{dx}\right)^2}}\right] \tag{10}$$

Smail[16] shows that the curvature $\frac{d\theta}{ds}$ of a curve $y = f(x)$ at a point $P(x,y)$ in rectangular coordinates is given by:

$$\frac{d\theta}{ds} = \frac{\frac{d^2y}{dx^2}}{\left[1+\left(\frac{dy}{dx}\right)^2\right]^{3/2}} \tag{11}$$

where $\frac{d^2y}{dx^2}$ and $\left(\frac{dy}{dx}\right)^2$ are to be evaluated at $P(x,y)$. Therefore, equating equation 10 to equation 11 yields

$$\frac{\frac{d^2y}{dx^2}}{\left[1+\left(\frac{dy}{dx}\right)^2\right]^{3/2}} = \frac{1}{2H}\left(\frac{dy}{dx}\frac{\partial H}{\partial x} - \frac{\partial H}{\partial y}\right)\frac{1}{\sqrt{1+\left(\frac{dy}{dx}\right)^2}}$$

or

$$\frac{d^2y}{dx^2} = \left(\frac{dy}{dx}\frac{\partial H}{\partial x} - \frac{\partial H}{\partial y}\right)\left[1+\left(\frac{dy}{dx}\right)^2\right]\frac{1}{2H} \tag{12}$$

A Taylor's expansion of the function of $(y_o + \Delta y)$ yields

$$y_o + \Delta y = y_o + \frac{dy}{dx}\Delta x + \frac{1}{2}\frac{d^2y}{dx^2}\Delta x^2 + \ldots$$

or, considering only the first three terms,

$$\Delta y = \frac{dy}{dx}\Delta x + \frac{1}{2}\frac{d^2y}{dx^2}\Delta x^2 \tag{13}$$

Substitution of equation 12 into equation 13 yields

$$\Delta y = \frac{dy}{dx}\Delta x + \frac{1}{4H}\left(\frac{dy}{dx}\frac{\partial H}{\partial x} - \frac{\partial H}{\partial y}\right)\left[1+\left(\frac{dy}{dx}\right)^2\right]\Delta x^2 \tag{14}$$

Equation 14 shows that by starting with known values of H, $\frac{dy}{dx}$, $\frac{\partial H}{\partial x}$, $\frac{\partial H}{\partial y}$ at P_o, and for an assigned value of Δx, one can compute the Δy of point P_1. The location of P_1 is then simply $x_o + \Delta x$, $y_o + \Delta y$.

31. To move from P_1 to point P_2, it is necessary to know $\frac{dy}{dx}$ at P_1. So, $\frac{dy}{dx}$ at P_1 is $\tan(\theta_o + \Delta\theta)$ and it can be shown that

$$\tan(\theta_o + \Delta\theta) = \tan\theta_o + (1 + \tan^2\theta_o)\,\Delta\theta \tag{15}$$

Equation 10 can be written as

$$\frac{\Delta\theta}{\Delta s} = \frac{1}{2H}\left(\frac{dy}{dx}\frac{\partial H}{\partial x} - \frac{\partial H}{\partial y}\right)\frac{1}{\sqrt{1 + \left(\frac{dy}{dx}\right)^2}}$$

or

$$\Delta\theta = \frac{1}{2H}\left(\frac{dy}{dx}\frac{\partial H}{\partial x} - \frac{\partial H}{\partial y}\right)\Delta x \tag{16}$$

Therefore, $\left(\frac{dy}{dx}\right)_{P_1} = \left(\frac{dy}{dx}\right)_{P_o} + \frac{1}{2H}\left[1 + \left(\frac{dy}{dx}\right)^2\right]\left(\frac{dy}{dx}\frac{\partial H}{\partial x} - \frac{\partial H}{\partial y}\right)\Delta x$

or from equation 12

$$\left(\frac{dy}{dx}\right)_{P_1} = \left(\frac{dy}{dx}\right)_{P_o} + \left(\frac{d^2y}{dx^2}\right)_{P_o}\Delta x \tag{17}$$

32. The time of travel along an increment Δs is given by

$$\Delta t = \frac{(\Delta x^2 + \Delta y^2)^{1/2}}{\sqrt{gH}} \tag{18}$$

Thus, for a given starting position (x,y), initial angle $\frac{dy}{dx}$, and computational increment Δx, the corresponding Δy increment can be calculated. This next point's (P_1 in fig. 12) coordinates ($x_o + \Delta x$, $y_o + \Delta y$) and the computed $\left(\frac{dy}{dx}\right)_{P_1}$ then become the basis for computation to P_2.

This process is continued throughout the length of the ray.

33. It is apparent from equation 14 that it is necessary to determine the depth at a given point (such as P_o) in order to progress to the next point (P_1). Equation 14 shows that the incremental computation of the orthogonal path is expressed as a function of $H(x,y)$, so the path of the ray can be constructed across a grid of water depths, each having an x- and y-dimension in the grid area.

34. A regular, square grid of finite boundaries was overlaid on a map showing the area through which the waves were to travel, and depth values were assigned to each of the grid intersections. In general, however, the points for which a depth value is required (beginning points of each incremental segment) will not fall on the regular grid points, so it is necessary to interpolate for the required values of the depth.

35. Dobson[17] utilized a least squares method to fit a surface of 12 grid points in the immediate vicinity of the area of interest and Wilson[18] used a least squares fit to the four closest depth values to calculate the depth at an arbitrary point within a grid square. It is apparent that very few surfaces can be accurately described by a second degree equation when applied to the entire grid; but when it is fitted locally, in a mosaic manner, it is a relatively accurate method for interpolating the depth at intermediate points. Of course, the method would yield best results if the ocean bottom was a second order surface, but should yield satisfactory results if a small enough grid is used. The method used to find the interpolated depth as well as $\frac{\partial H}{\partial x}$ and $\frac{\partial H}{\partial y}$ is outlined in the following paragraphs.

36. Fig. 13 shows the grid points surrounding the area of interest in which it is desired to find the depth at a randomly placed point P_1. This can be done if the depths at each grid intersection are known. It was decided that best results could be obtained if two surfaces were fit through the area of interest and if the depth were computed for the random point P_1 which is the average of these two surface fits; likewise, it was considered best to utilize the average values of $\frac{\partial H}{\partial x}$ and $\frac{\partial H}{\partial y}$ computed from each of these two surfaces.

37. One may solve for the depth at point P_1, H_{P_1}, using

equation 19 where the coefficients A , B , C , D , and E are computed by taking the average values of two sets of coefficients obtained from two different surface fits through the same area.

$$H_{P_1} = H_{(i,j)} + A\,\delta x + B\,\delta y + C\,\delta x\,\delta y + D\,\delta x^2 + E\,\delta y^2 \qquad (19)$$

38. If one considers the depth values $H_{(i,j)}$, $H_{(i+2,j)}$, $H_{(i,j-1)}$, $H_{(i+1,j+1)}$, $H_{(i+1,j-1)}$, and $H_{(i,j+1)}$ as shown in fig. 14, the set of simultaneous equations 20 may be used to solve for the first set of coefficients.

39. Another surface fit through the area of interest considering the depths shown in fig. 15 will yield another set of coefficients describing a second order surface passing through the same area of interest. The set of simultaneous equations used to solve for a second set of coefficients is shown as equation 21.

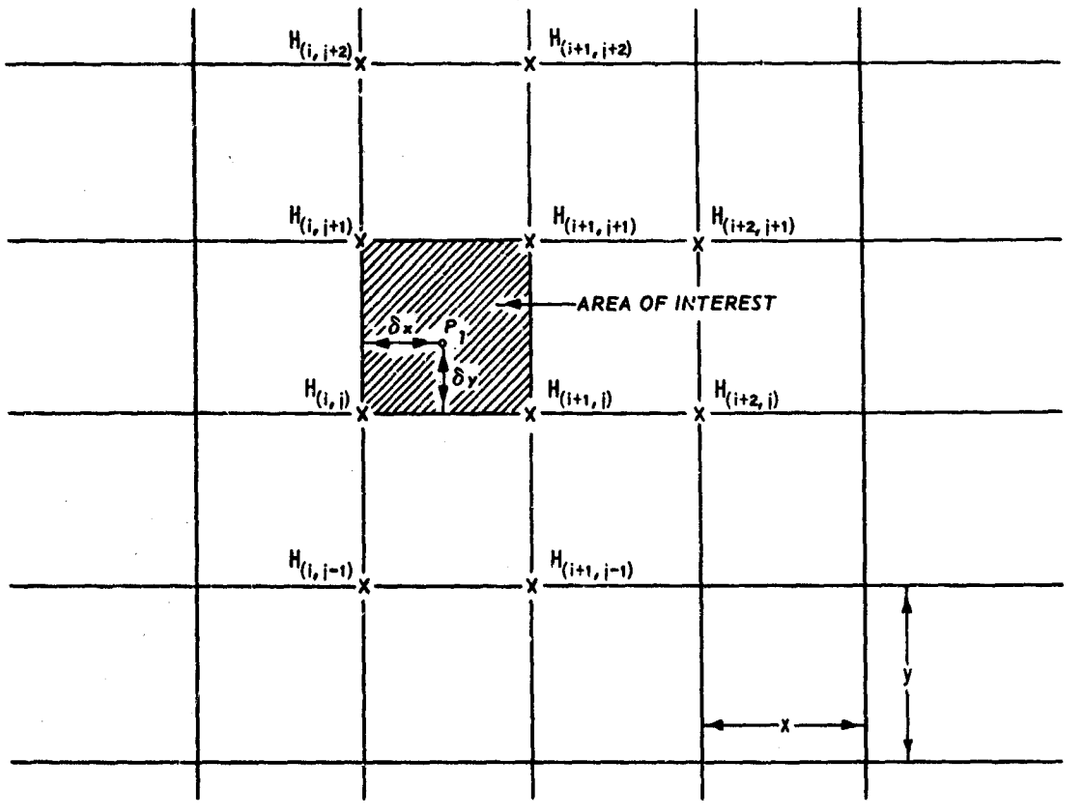

Fig. 13. Arrangement of grid points for surface fitting procedure

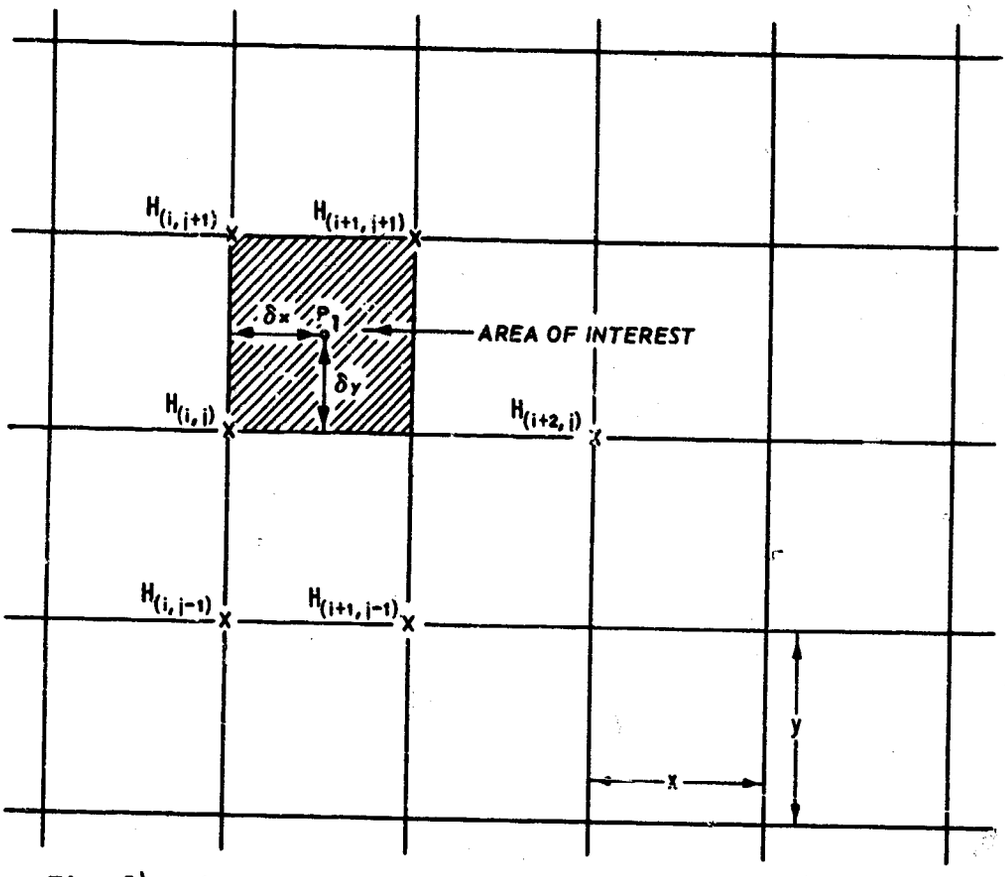

Fig. 14. Arrangement of grid points for fitting the first surface through the area of interest

$$
\left.
\begin{aligned}
H_{(i+2,j)} &= H_{(i,j)} + 2A_1x + 4D_1x^2 \\
H_{(i,j+1)} &= H_{(i,j)} + B_1y + E_1y^2 \\
H_{(i,j-1)} &= H_{(i,j)} - B_1y + E_1y^2 \\
H_{(i+1,j+1)} &= H_{(i,j)} + A_1x + B_1y + C_1xy + D_1x^2 + E_1y^2 \\
H_{(i+1,j-1)} &= H_{(i,j)} + A_1x - B_1y - C_1xy + D_1x^2 + E_1y^2
\end{aligned}
\right\} \qquad (20)
$$

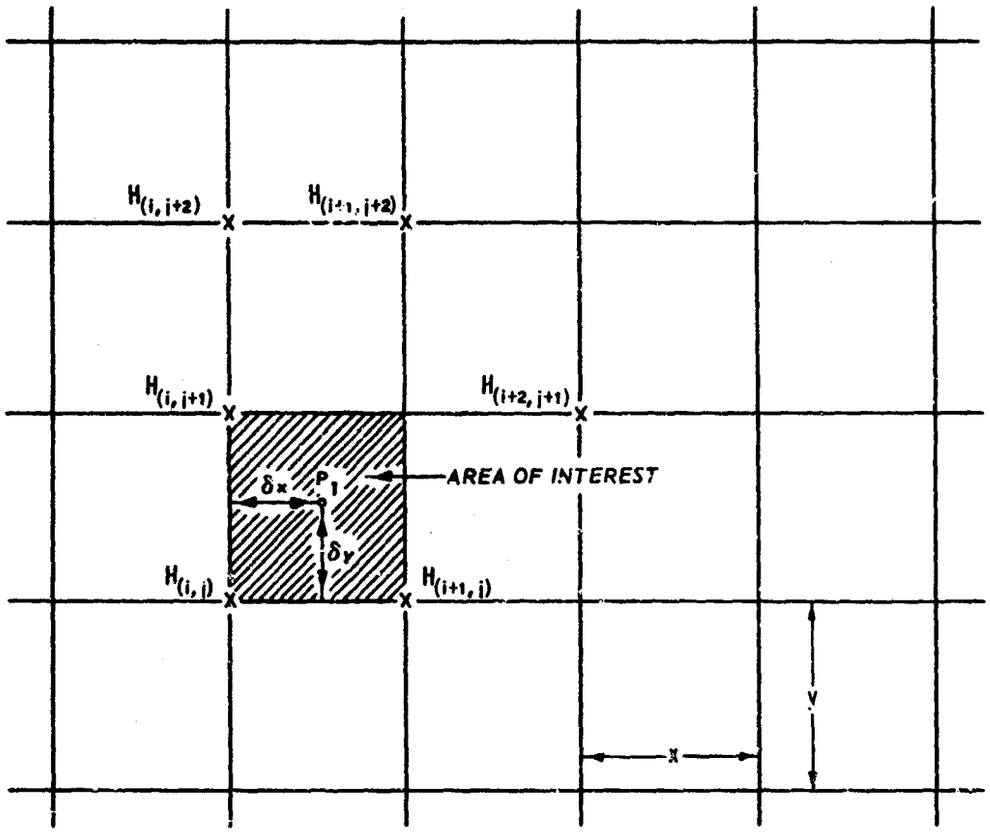

Fig. 15. Arrangement of grid points for fitting the second surface through the area of interest

$$\left.\begin{aligned}
H_{(i+1,j)} &= H_{(i,j)} + A_2x + D_2x^2 \\
H_{(i,j+1)} &= H_{(i,j)} + B_2y + E_2y^2 \\
H_{(i,j+2)} &= H_{(i,j)} + 2B_2y + 4E_2y^2 \\
H_{(i+2,j+1)} &= H_{(i,j)} + 2A_2x + B_2y + 2C_2xy + 4D_2x^2 + E_2y^2 \\
H_{(i+1,j+2)} &= H_{(i,j)} + A_2x + 2B_2y + 2C_2x^2 + 4E_2y^2
\end{aligned}\right\} \quad (21)$$

40. The average value for each of these two sets of coefficients is given by

$$\left.\begin{aligned} A &= \frac{A_1 + A_2}{2} \\ B &= \frac{B_1 + B_2}{2} \\ C &= \frac{C_1 + C_2}{2} \\ D &= \frac{D_1 + D_2}{2} \\ E &= \frac{E_1 + E_2}{2} \end{aligned}\right\} \qquad (22)$$

Substitution of these coefficient values and the correct values for the locations $(\delta x, \delta y)$ of the randomly spaced point in the grid square into equation 19 will yield the depth (Hp_1) at the random point. Partial differentiation of equation 19 with respect to x and y, respectively, will yield

$$\frac{\partial H}{\partial x} = A + C\delta y + 2D\delta x \qquad (23)$$

and

$$\frac{\partial H}{\partial y} = B + C\delta x + 2E\delta y$$

Computer Program

41. A listing of the program with an explanation of the program variables and an example of input data are presented in Appendix A. The depth values used as input data for the program were a weighted average of three independently obtained depths. One of the sources used was the ocean depths averaged over areas of one-degree squares of latitude and longitude[19] and compiled as computer printout available from the National Oceanographic Data Center. The second and third sources of depth data (both

from the U. S. Naval Oceanographic Office) were an unpublished collection of ocean sounding sheets at an approximate scale of 1:800,000, and the H.O. series of charts at an approximate scale of 1:5,990,000. The plots that were obtained from the computer were referenced to the 1:5,990,000 series charts.

42. The presentation of a geoidal surface (the earth) on a map requires that the representation be distorted in some way. Most Mercator projections (the most common charting method for maps used for navigation and ocean studies) are projected in true scale at 0° latitude (the equator) with the distortion becoming greater the farther one moves from the equator as shown in fig. 16. At a given point on a Mercator map the distortion is the same in all directions and is equal to the secant of the latitude at which one is located (i.e., at 60° north or south latitude a Mercator map is distorted by a factor of 2.0).

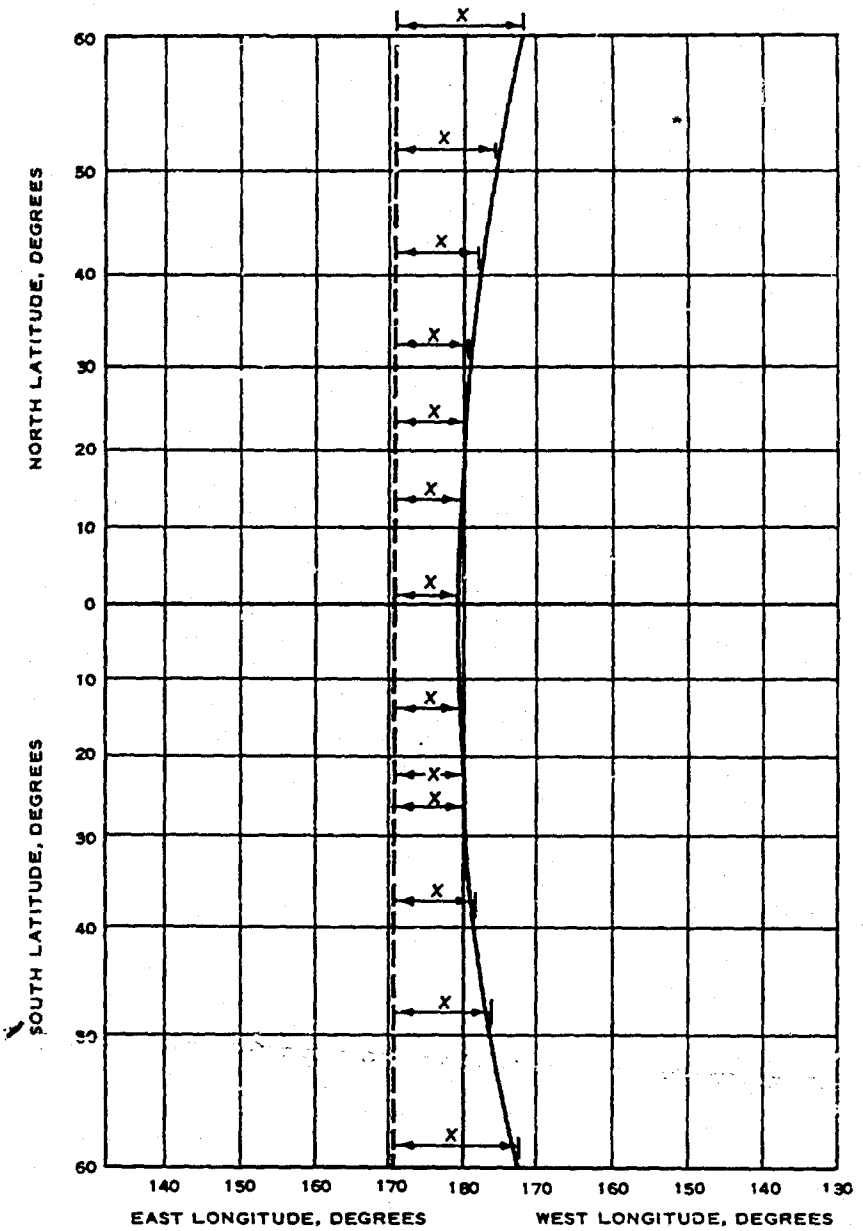

Fig. 16. Equal distances represented at different latitudes on a Mercator projection

To get a true picture of wave travel over large distances and particularly through many degrees of latitude, one must compensate for this distortion.

43. Two methods of compensation were considered for this study. Dr. Ledolph Baer of the Lockheed-California Company has devised an essentially undistorted flat representation of the earth's surface by drawing a map on an icosahedral-gnomonic projection.[20] The earth's surface was divided into 20 sections and each of these sections was individually projected (using a gnomonic projection) onto a flat surface with the center point of each section being the tangent point between the earth and the map. Each of the sections is therefore undistorted at its center, but becomes increasingly distorted toward the edges of that individual section.

44. The second method studied, and the one adopted for application to this problem, was to distort each computed or assigned Δ distance by the secant of the latitude of its location. Careful examination of the theoretical treatment of the problem revealed that this could be easily accomplished by multiplying each of the depth values which were to be input to the program by the square of the secant of the latitude at which these depth values were located. A rigorous treatment of this is presented in Appendix B. This multiplication was performed before inputting the depth data; therefore, all the depth values of the input data grid shown in Appendix A have already been multiplied by the secant squared of the latitude of their respective location. This has the effect of showing the wave path on the map as if it had taken place on the earth's surface and had then been transferred point by point to the map.

45. To test the foregoing numerical techniques, it was deemed necessary to compare the computer-drawn refraction diagrams with those obtained by a closed solution of wave refraction around a given island shape. Such an example is described in Appendix C.

Refraction Diagrams

46. The refraction diagrams computed and drawn by the previously described technique are shown in figs. 17-25. The figures show three recent tsunami-front patterns (Alaska, 1964; Chile, 1960; and Kamchatka, 1952) from each of the given sources to Crescent City and Hilo, Hawaii. The

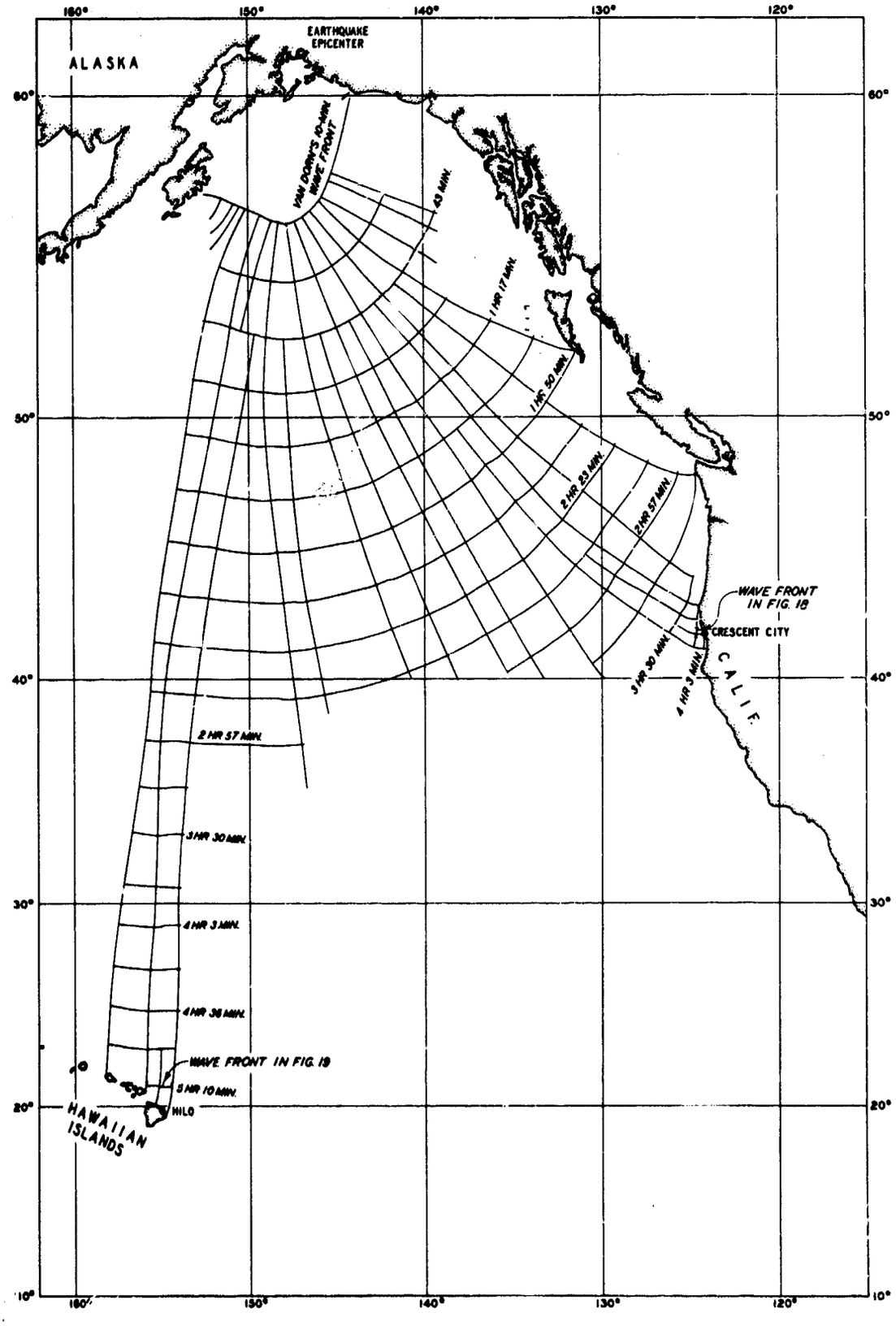

Fig. 17. Refraction diagram for Alaskan tsunami of March 28, 1964

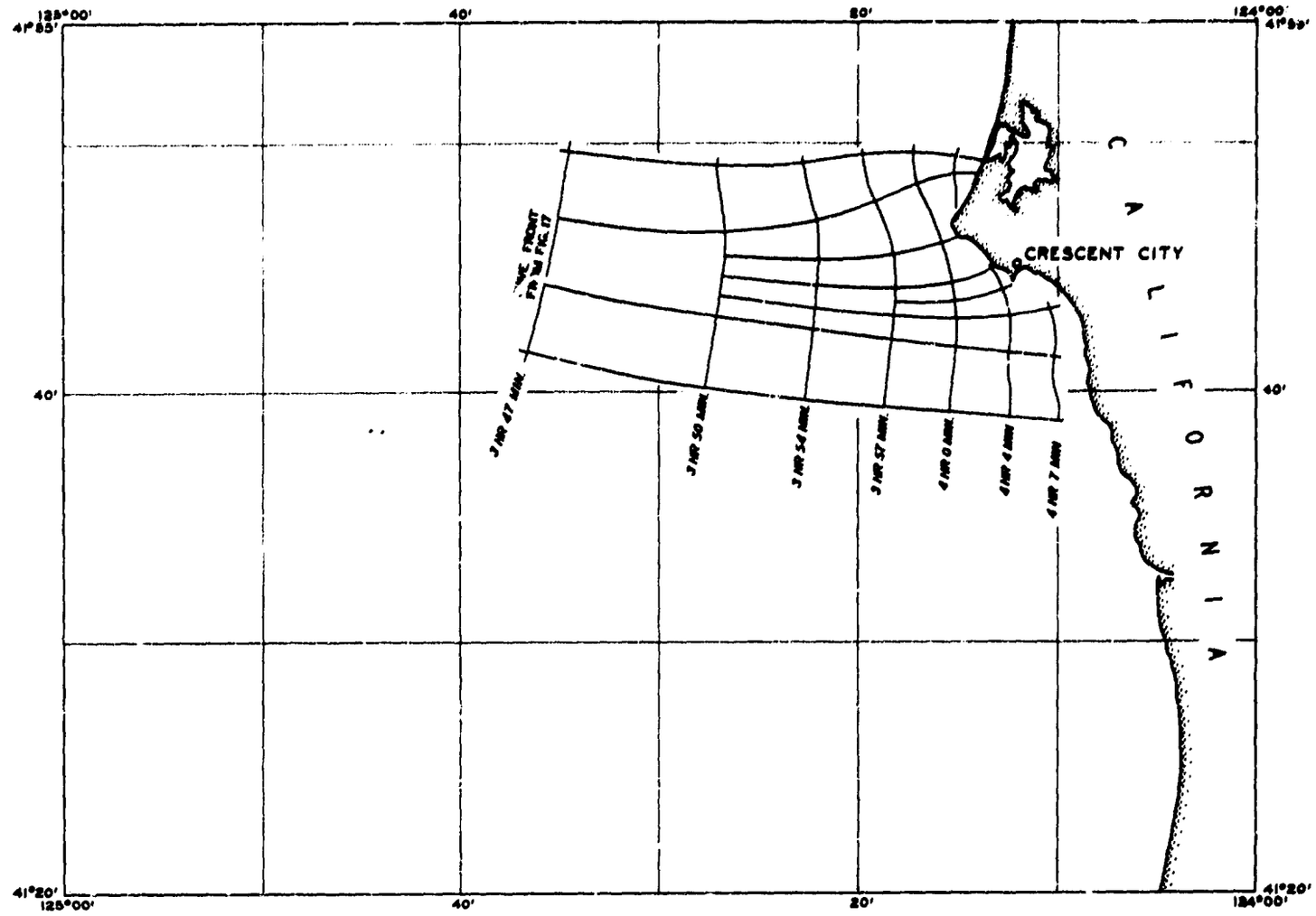

Fig. 18. Refraction diagram in the Crescent City area from the Alaskan tsunami of March 28, 1964

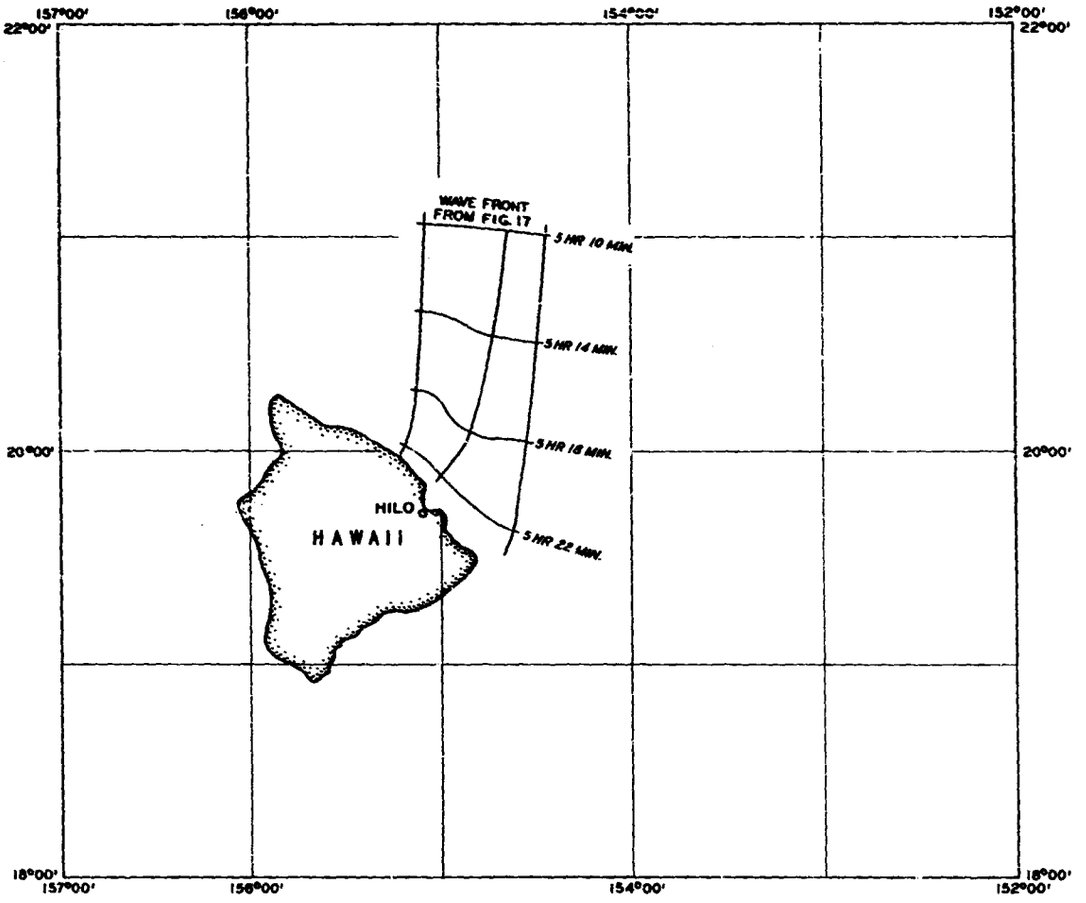

Fig. 19. Refraction diagram in the Hilo area from the Alaskan tsunami of March 28, 1964

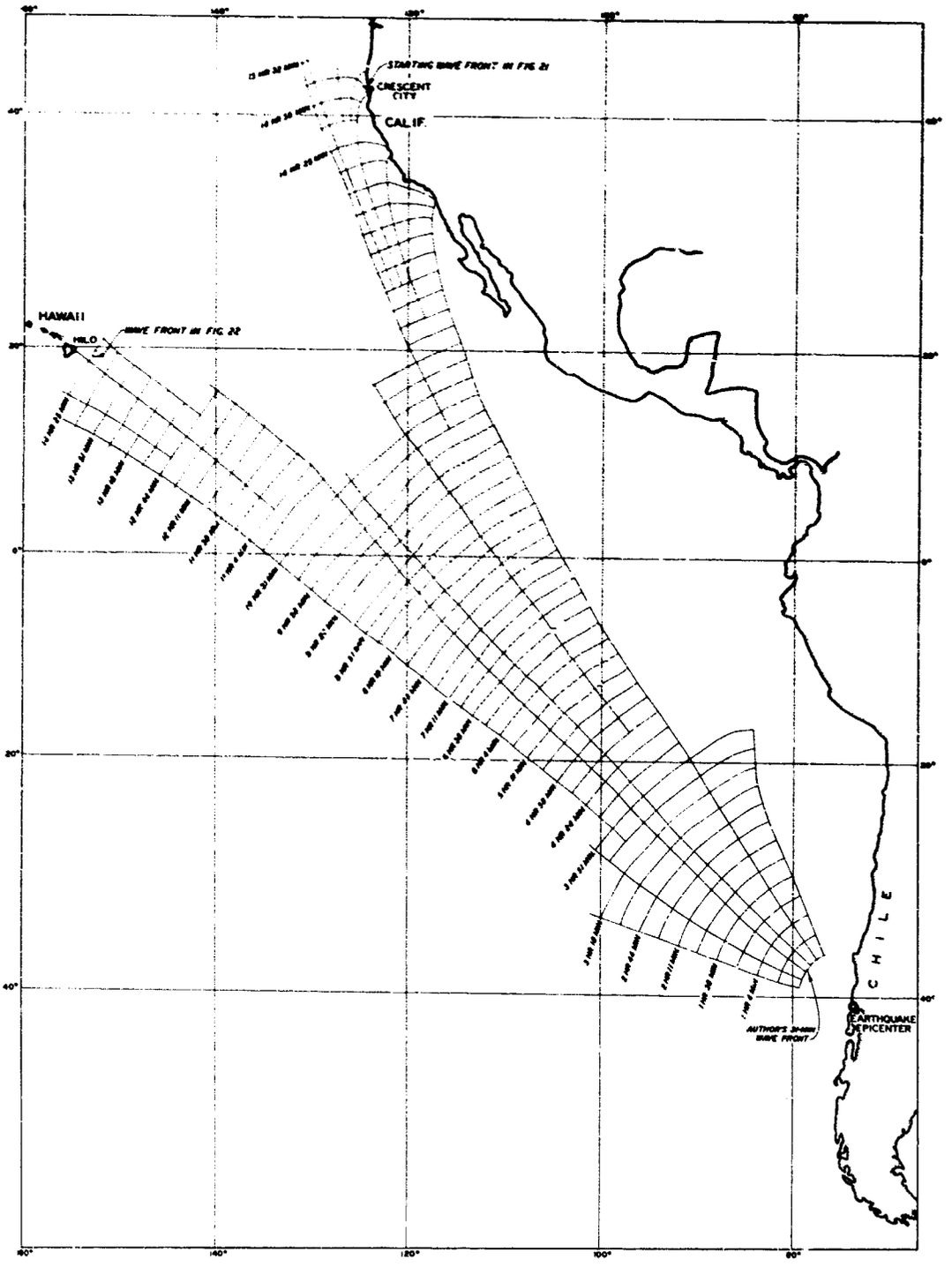

Fig. 20. Refraction diagram for Chilean tsunami of May 22, 1960

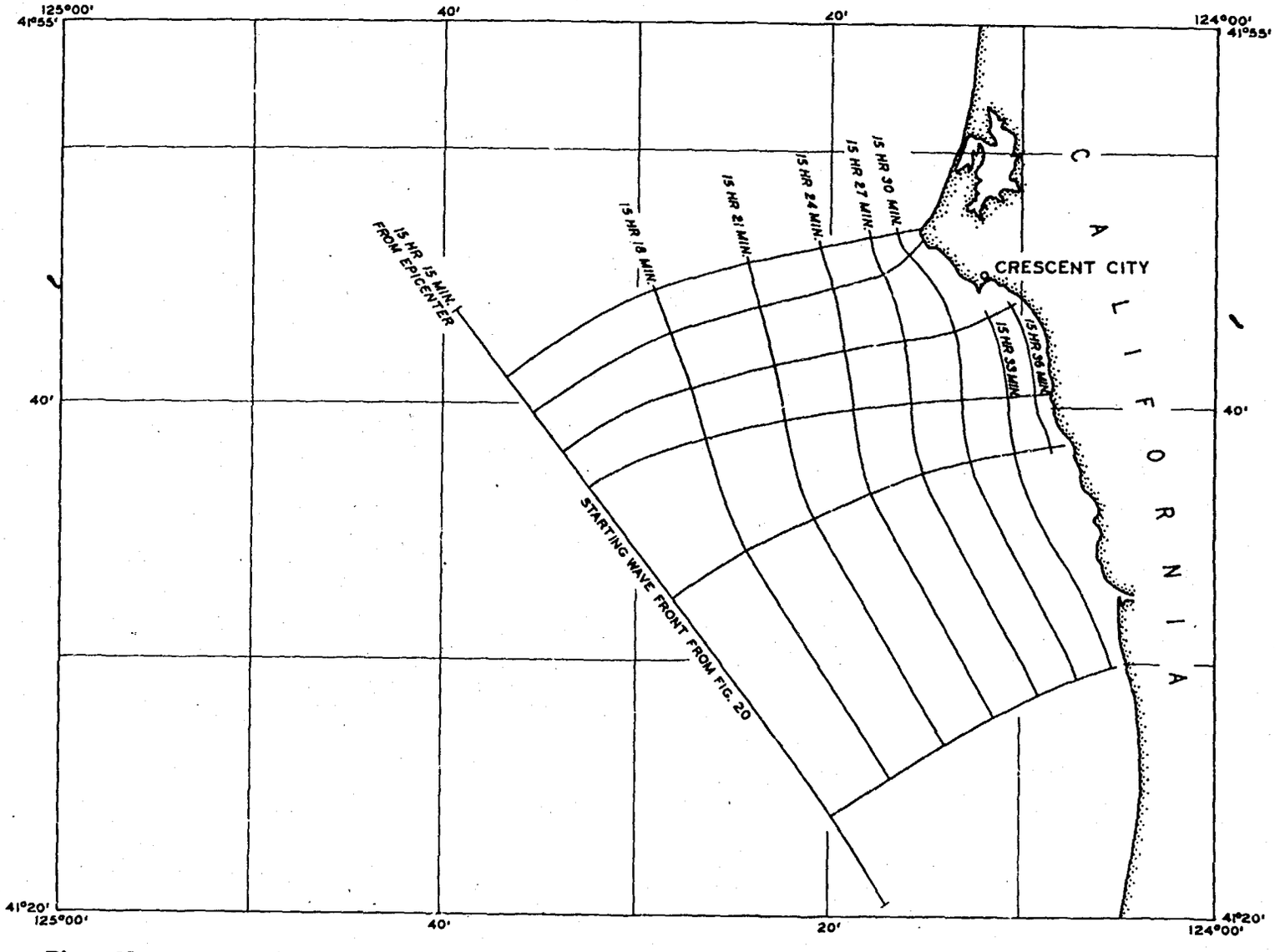

Fig. 21. Refraction diagram in Crescent City area from Chilean tsunami of May 22, 1960

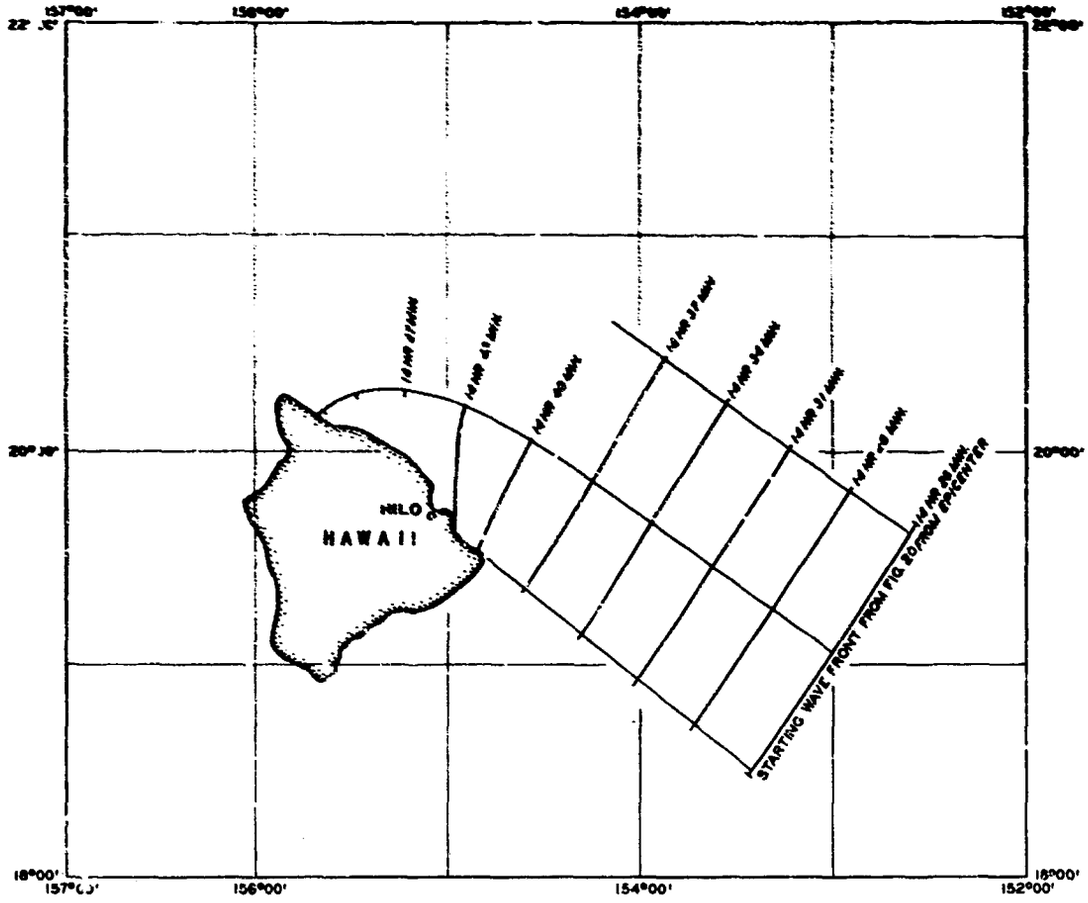

Fig. 22. Refraction diagram in Hilo area
from Chilean tsunami of May 22, 1960

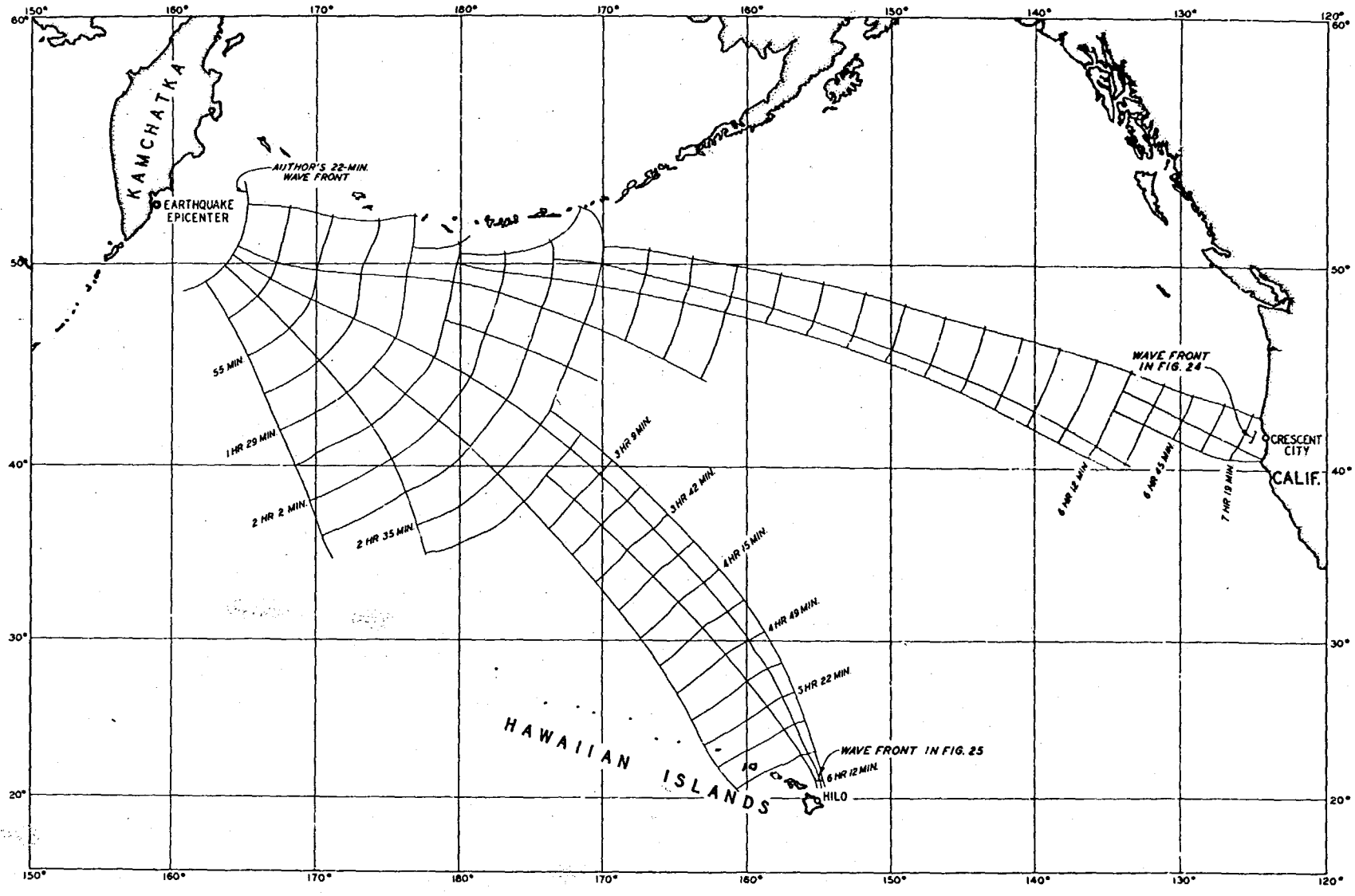

Fig. 23. Refraction diagram for Kamchatka tsunami of November 4, 1952

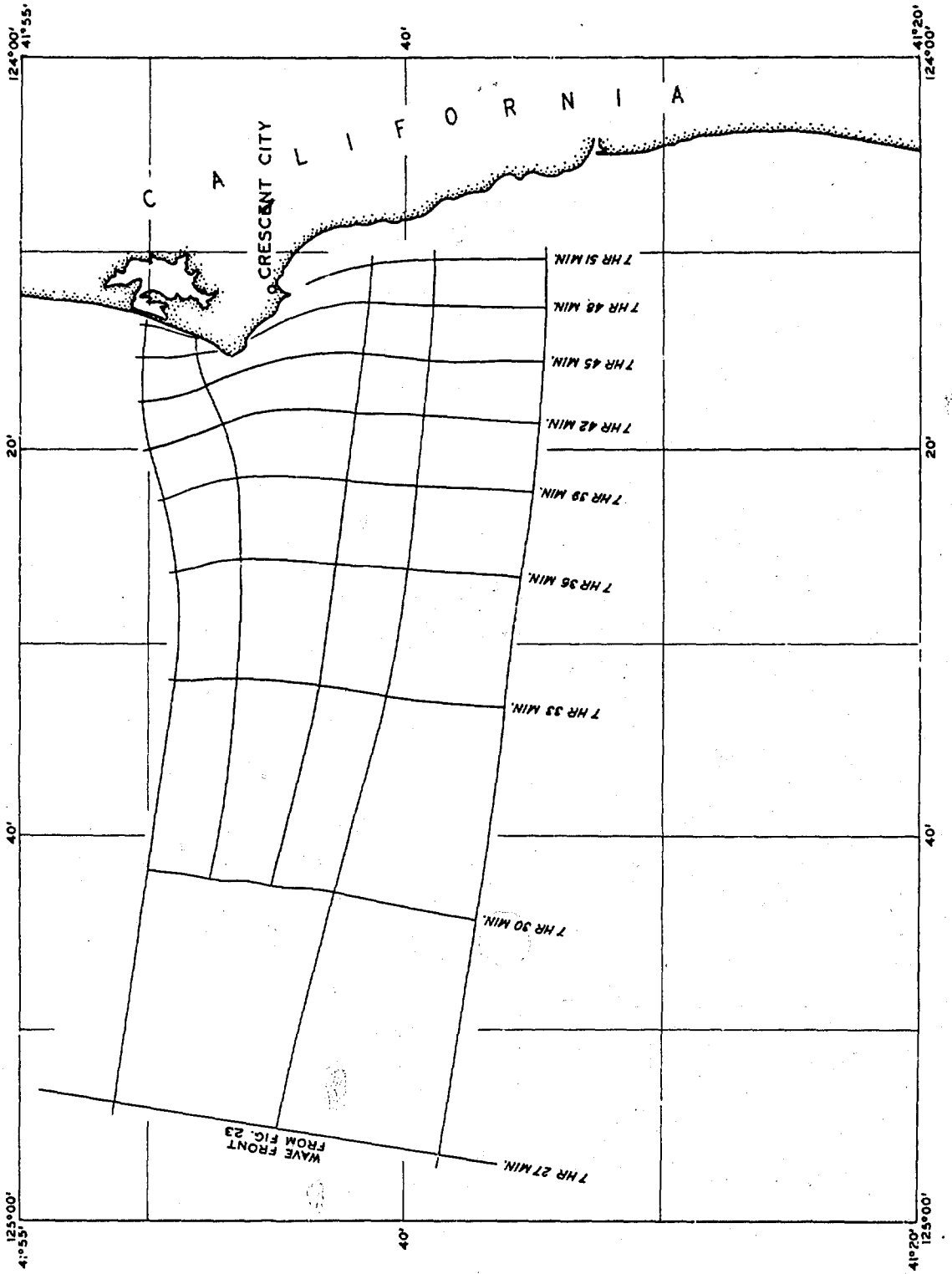

Fig. 24. Refraction diagram in Crescent City area from Kamchatka tsunami of November 4, 1952

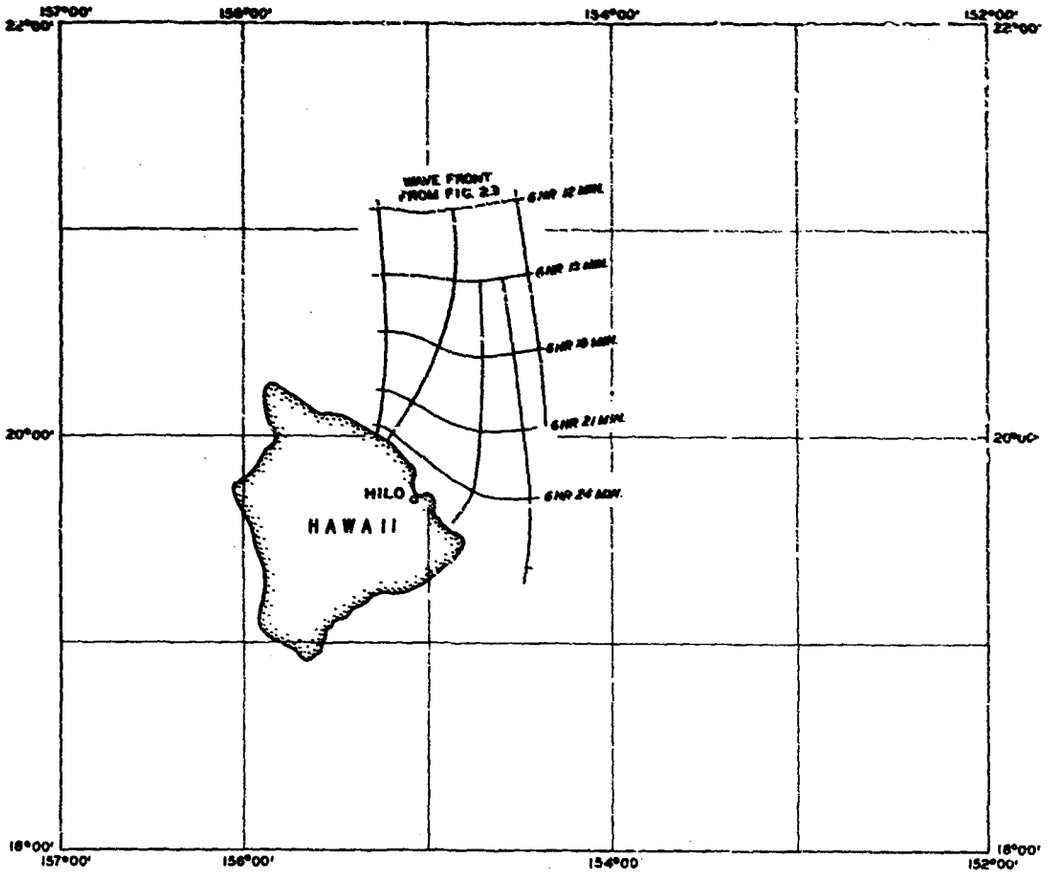

Fig. 25. Refraction diagram in Hilo area from Kamchatka tsunami of November 4, 1952

waves were drawn through the open ocean areas on 1:6,000,000-scale maps and upon arrival in the nearshore areas of Crescent City and Hilo, the tsunami fronts were transferred to a larger scale map (1:196,948 in the case of Crescent City and 1:1,650,000 in the case of Hilo) and continued to very near the two respective points of interest.

47. The tsunami fronts from each of the three locations are clearly defined in the Crescent City area, thus describing definite wave fronts for model wave generator placement. The tsunami-front patterns approach coincidence from the three sources as they approach Crescent City.

48. Refraction theory dictates that the wave height h_b (shown in fig. 26) will be

$$h_b = h_o \left(\frac{b_o}{b_b} \right)^{1/2} \tag{24}$$

where

h_o = known wave height at any distance x from the epicenter

b_o = physical distance between rays at some known wave height (h_o)

b_b = physical distance between rays at a point at which one is seeking a wave height h_b

Assuming that h_o is a constant known quantity for each of the beginning tsunamis at a given location, the quantity $(b_o/b_b)^{1/2}$ should give the relative wave heights at any other desired location for the same tsunami. The distances b_o and b_b were scaled from the small-scale sheets, and the quantity $(b_o/b_b)^{1/2}$ for the nearshore areas at Hilo and Crescent City is shown in the following tabulation:

Tsunami	Hilo, Hawaii	Crescent City, Calif.
Alaska 1964	$\left(\frac{b_o}{b_b} \right)^{1/2} = 0.6$	$\left(\frac{b_o}{b_b} \right)^{1/2} = 0.3$
Chile 1960	0.2	0.09
Kamchatka 1952	0.6	0.08

It must be noted that one could obtain different values for the ratio

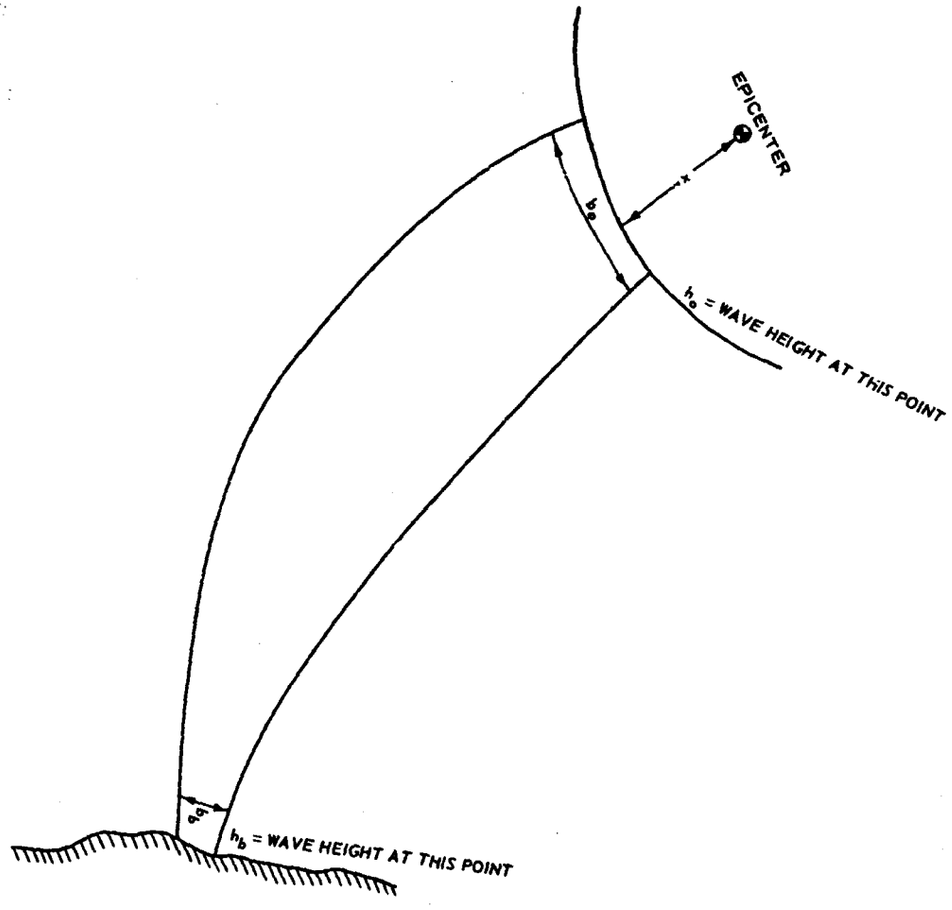

Fig. 26. Refraction notation

$(b_o/b_b)^{1/2}$ by choosing another point such as halfway between the tsunami source and the point of interest for the measurement of h_o and b_o. Since the tsunami height h_o probably does not vary much in the open ocean, the selection of any other point will undoubtedly change the final nearshore wave height h_b by changing the $(b_o/b_b)^{1/2}$ ratio.

49. No attempt was made to present a design wave height h_b. The four lowest values of $(b_o/b_b)^{1/2}$ given in the above tabulation dictate that the wave was exceedingly small (considering its small height in the open ocean), a condition that was not present at either of the two given locations for any of these tsunamis. The magnitude of these terms does infer, however, that no wave magnification takes place in the open ocean

due to gross wave refraction. Local severe discontinuities will undoubtedly cause local wave amplitude increases even in the open ocean; however, an unusually large amplitude associated with any tsunami is probably due to severe shore refraction, shoaling conditions, and the resonance of the particular nearshore area. Comparison of tsunami heights at various locations mentioned in Part IV shows wave heights for which all wave-height magnification factors (refraction, shoaling, and friction) have already been considered. It is seen that tsunamis of equal periods passing through equal water depths will exhibit equal wave-height increases due to shoaling. The time of travel of the tsunamis shown in figs. 17-25 is very close to that presented in the literature.[6,21,22]

PART IV: PROBABILITY OF OCCURRENCE OF TSUNAMIS OF VARIOUS HEIGHTS AT CRESCENT CITY

Frequency Distribution of Tsunamis of Various Heights at Crescent City

50. The relation of the tsunami height versus frequency of occurrence for Hilo has been determined by Professor Cox, both on the basis of visual observations and marigraphic tide recordings.[23] The first group covers a period of about 130 years and the latter a shorter period of about 24 years. The heights refer to runup values, which are derived from the given bay heights by multiplying the latter values by 1.5. A significant fact recognized by Cox is that the frequency relation needs to be expressed differently depending on the magnitude of the heights. For the smaller heights a power law is indicated, whereas for the larger heights the logarithmic form is more appropriate. Our present interest is in the latter. Keeping in mind the frequency relation for bay tsunami heights, the Cox determinations were divided by 1.5 and are presented in fig. 27. Wiegel gives some similar results for Crescent City based on 16 observations[3] of which those relating to larger heights are also plotted in fig. 27. The curve representing average

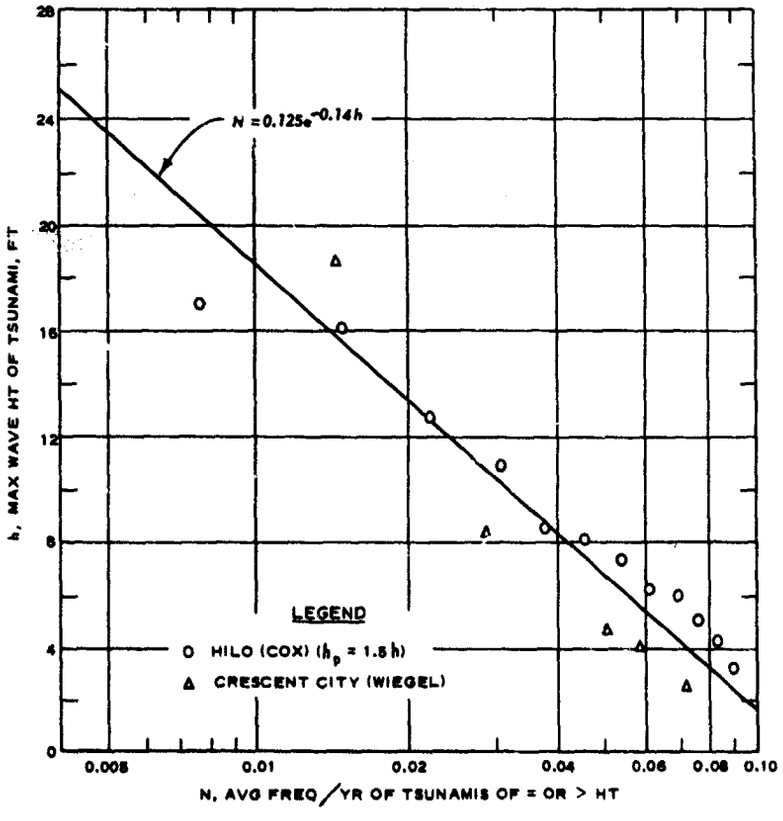

Fig. 27. Distribution function for maximum wave height

values from these two determinations has the equation

$$N = 0.125e^{-0.14\,h} \tag{25}$$

where N denotes the average frequency of occurrence of tsunamis of equal or greater height h (measured in feet).

Risk Evaluation

51. In arriving at a statistical interpretation of the distribution law shown above, the method adopted by Wiegel[3] has been followed. With N given by equation 25, the risk may be established using Poisson's rule

$$q = 1 - e^{-ND} \tag{26}$$

where D represents duration in years. Curves based on this relation are shown in fig. 28. The figure shows that there is about a 40 percent chance

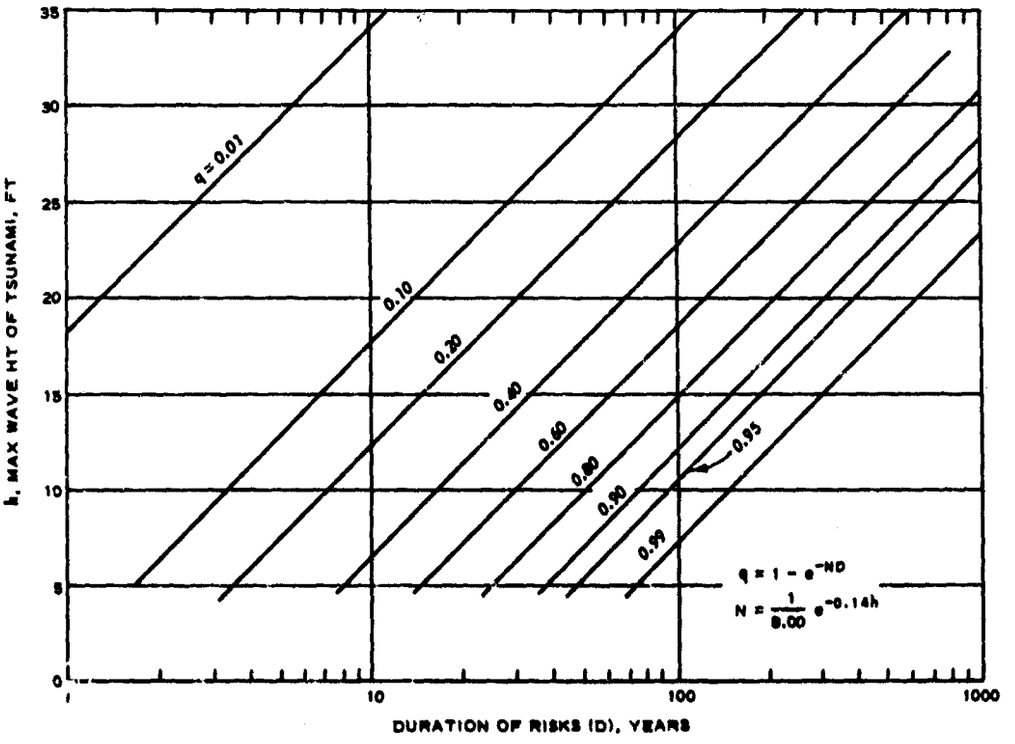

Fig. 28. Probability of maximum wave height exceeding a given value in a given duration

that a tsunami will strike Crescent City in a 100-year interval with a maximum wave height of at least 23 ft; furthermore, there is a 20 percent chance that such a wave will occur in a 45-year period, and a 95 percent chance that such a wave will strike the town within a period of 600 years. Agreeing with Wiegel, it will be remarked that an extension of tsunami heights to values much above those that have been observed may be erroneous.

Comparison of Tsunami Heights at Hilo and Crescent City

52. In the treatment shown above, a tacit assumption is made that a correlation exists between the tsunami heights at Hilo and Crescent City for a given instance of tsunami occurrence and that the correlation is one of equality. Table 2 shows the heights observed at Hilo and the heights observed at Crescent City or values reduced from the heights observed at San Francisco and the neighboring localities of Los Angeles and San Diego. On the basis of data obtained since 1948, it is found that, on the average, the Crescent City tsunami heights are 2.7 times greater than the values observed in San Francisco, Los Angeles, and San Diego (see fig. 29). The source of the data in table 2 relating to tsunamis 1 to 13, inclusive, is a catalog

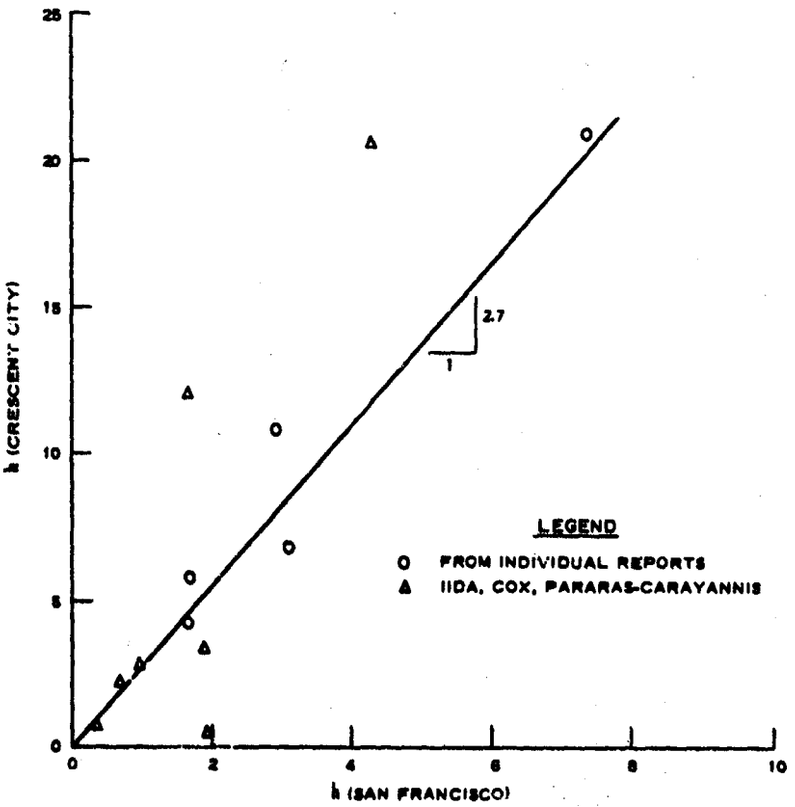

Fig. 29. Correlation of tsunami heights between San Francisco and Crescent City

prepared for the International Tsunami Information Center.[24] Additional sources of data for tsunamis 14 to 18, inclusive, are reports of the U. S. Coast and Geodetic Survey.[6,21,22] The heights refer to the maximum rise or fall noted during a tsunami. The values from table 2 are plotted in fig. 30. If the points relating to tsunamis 2, 3, 4, and 5 in table 2 are ignored, the remaining points suggest that, on the average, during a given tsunami the wave heights at Hilo and at Crescent City are similar.

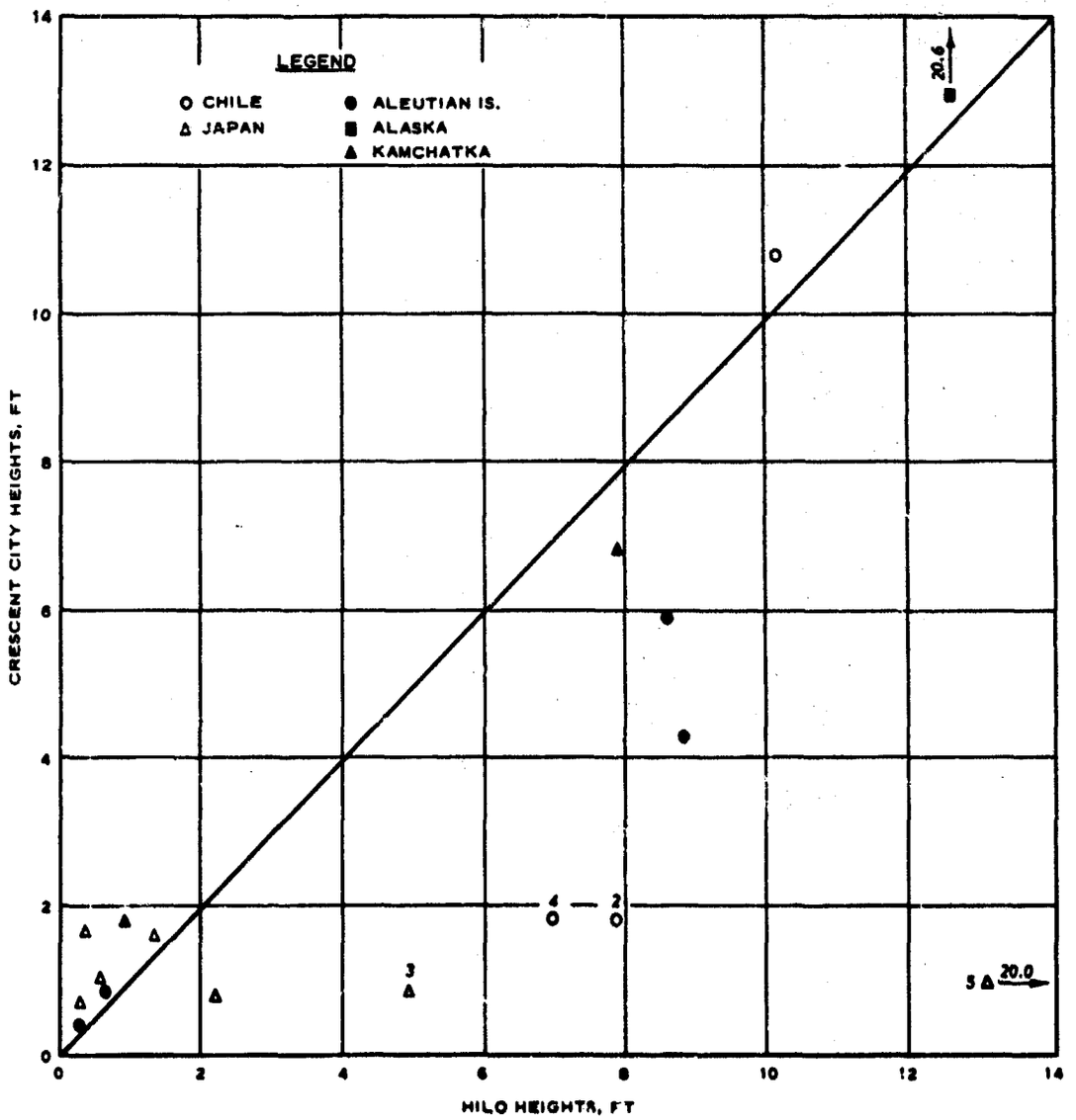

Fig. 30. Respective tsunami heights at Crescent City and Hilo for the same tsunami

Irregular Tsunami Heights at Hilo

53. It would not be amiss to reconsider tsunami cases 2, 3, 4, and 5, which show excessively large values. These are runup heights and even if an allowance is made for this fact, the reduced bay height values are still far higher than might be expected. From a tabulation given by Spaeth and Berkman,[6] it is inferred that the ratios of the tsunami heights at Hilo to those at Honolulu for the incidences of 1952, 1957, 1960, and 1964 are 1.79, 2.78, 1.75, and 4.62, respectively. The mean ratio, 2.73, may be used to infer the probable tsunami heights at Hilo. This reduction is done in table 3 for tsunamis 2, 3, 4, and 5 (as listed in table 2), and it is seen that the heights inferred for Hilo are of the same order of magnitude as the heights at Crescent City. Occasionally Hilo shows excessively high runup values for reasons difficult to assess.

Tsunami Height Attenuation with Distance Traveled

54. The data points of fig. 30 (a comparison of tsunami heights at Hilo and Crescent City) show scattering. This possibly could be explained on the basis of the distances of the observation localities from the tsunami generating area. Hilo is nearly a central point of the Pacific perimeter of earthquake activity. It is thus proper that the tsunami heights of any locality be compared with those at Hilo. For other points, the effect of distances of tsunami travel needs to be considered. This is particularly true for localities that exhibit resonant conditions. Distance affects the periods which, in turn, modify the magnification of waves in bays subject to resonance. Distance also modifies the tsunami heights. This matter is examined further in the next section.

55. In order to accurately correlate wave heights at Hilo and Crescent City, it is necessary to determine the dependence of wave height on travel distance. Unfortunately, this functional dependence has been determined for only very ideal cases and even there a certain amount of confusion exists.

56. The attenuation of wave height follows the general relation

$$h_b = h_o x^{-n} \tag{27}$$

where

h_b = wave height at a distance x from the source

h_o = wave height at the source

The relation is unmanageable in this form since the wave does not travel in a straight line from point to point. The above equation was derived from measurements and theory for constant average depth conditions and the approximate values for the exponent n are tabulated below.[25]

Case	n	Case	n
Three-dimensional:		Two-dimensional:	
Leading waves	5/6	Leading waves	1/3
Wave body	1	Wave body	1/2

Since the tsunami-generating earthquakes occur along a fault line, the wave form may actually be somewhere between these two extremes.

57. Tsunami wavelengths are of such magnitude that tsunamis may be considered shallow-water waves and the amplitude-to-depth ratio is small enough to be negligible. The wave speed is thus very nearly equal to the limiting value

$$C = \sqrt{g H_o} \tag{28}$$

where

C = wave celerity

g = the gravitational constant

H_o = the depth of the water

One would expect, therefore, to obtain a degree of correlation between wave height and time of travel shown by the general form

$$h_t = h_1 t^{-m} \tag{29}$$

where, in this case, h_1 is the wave height after one hour of travel, t is the travel time in hours, m is a curve fitting coefficient, and h_t is the wave height after t hours of travel. Available data for the 1960

tsunami which originated off the Chilean coast are plotted in figs. 31-34. The travel time on all the figures was determined by the time of arrival of the first wave as detected by tidal gaging stations. Attempts were made to correlate time with both the initial wave height and the maximum oscillation of the water surface. Figs. 31 and 33 exhibit a very high degree of scatter, so the values were averaged over convenient intervals and plotted on log-log paper. A straight line was fitted to the log-log plot by the least squares method in the general form of equation 29 and the resulting plots are shown as figs. 32 and 34.

58. The wave height is seen to diminish with an increase in time according to the general exponential relation; however, the data are too erratic to use as a basis for predicting wave-height distribution. It is generally believed that the nearshore conditions have a much greater effect on the wave height than travel distance. Wave measurements would have to be made in the open ocean to avoid the complicating factors due to nearshore and harbor topography.

Singularity of 1964 Alaskan Tsunami

59. In fig. 30 Crescent City wave heights are compared with those of Hilo Bay, and the Crescent City height from the 1964 Alaskan tsunami is close to the first rise of the water surface. Importantly, the largest wave height observed was that of the fifth wave; it rose about 23 ft, and indicates a very large disparity from the curve purportedly showing the trend in the correlation of heights between Hilo Bay and Crescent City. This large disparity cannot be explained on the basis of travel time from the generating area to these localities under consideration. If one considers h_c and h_h to be the tsunami heights at the shelf approaches to Crescent City and to Hilo Bay, respectively, and T_c and T_h to be the travel times of the tsunami wave from the generating area to these localities, then according to the relation shown in the previous section,

$$\frac{h_c}{h_h} = \left(\frac{T_c}{T_h}\right)^{5/6} \qquad (30)$$

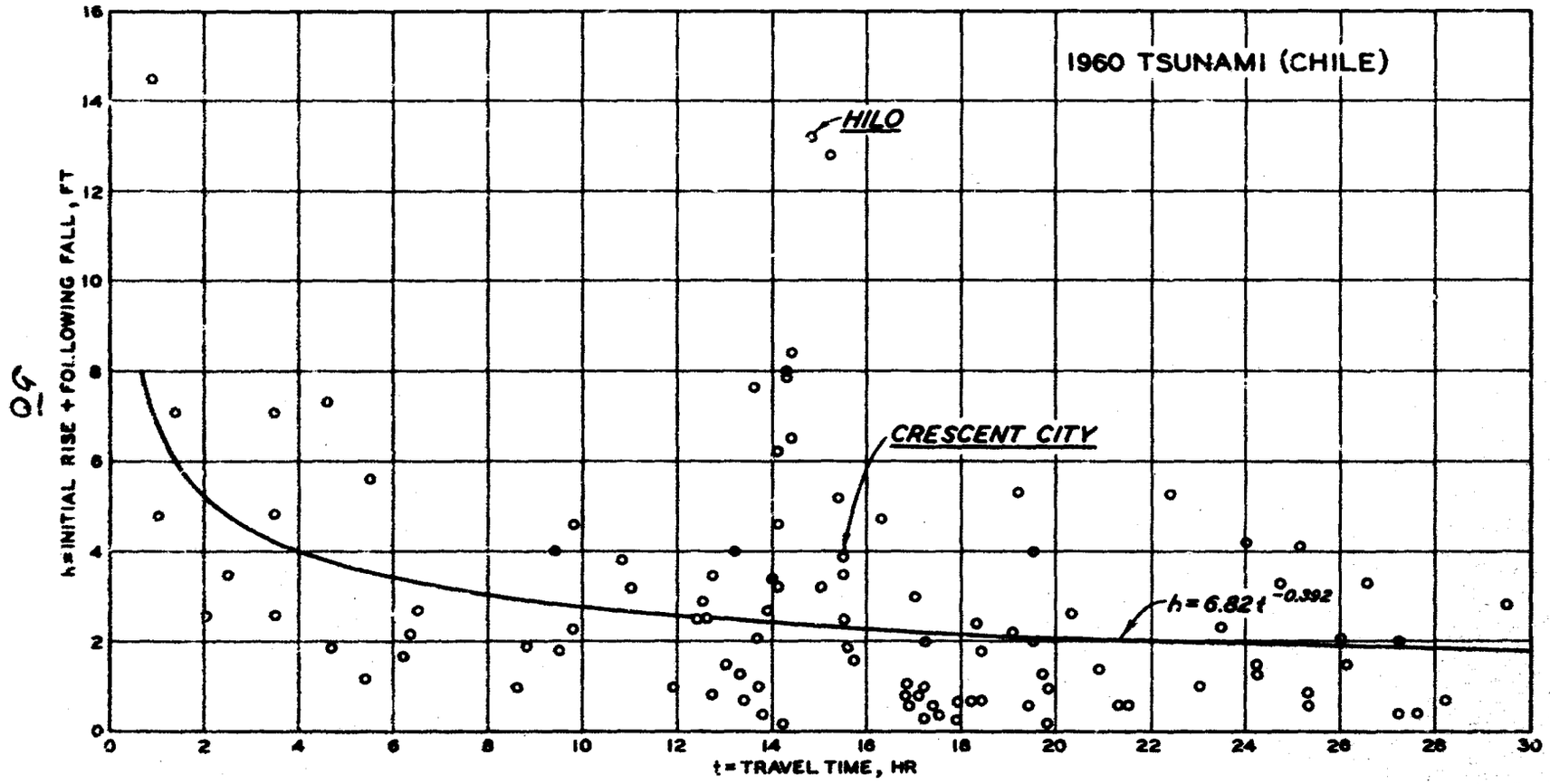

Fig. 31. Initial wave height versus travel time

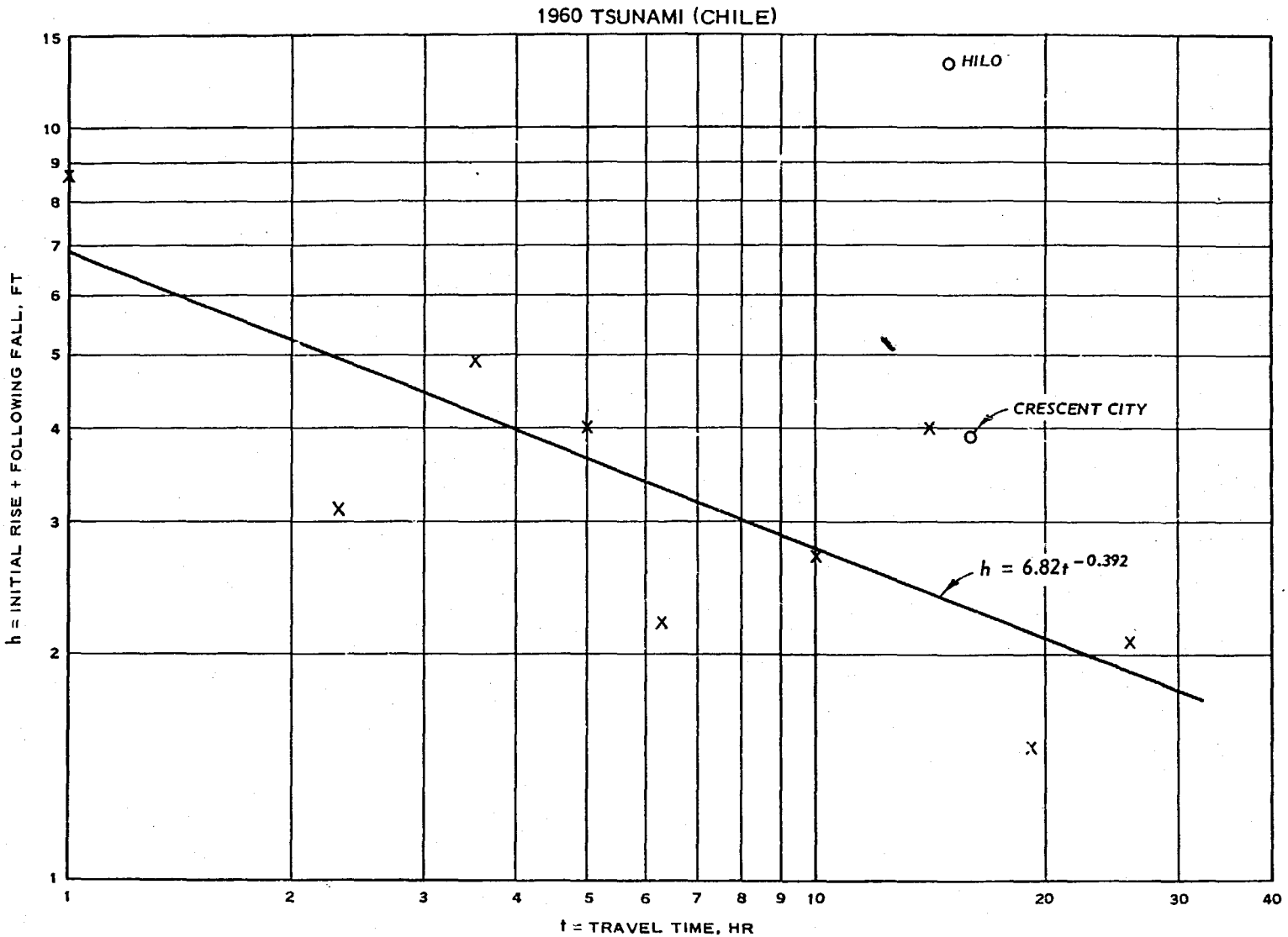

Fig. 32. Log-log plot of information in fig. 31

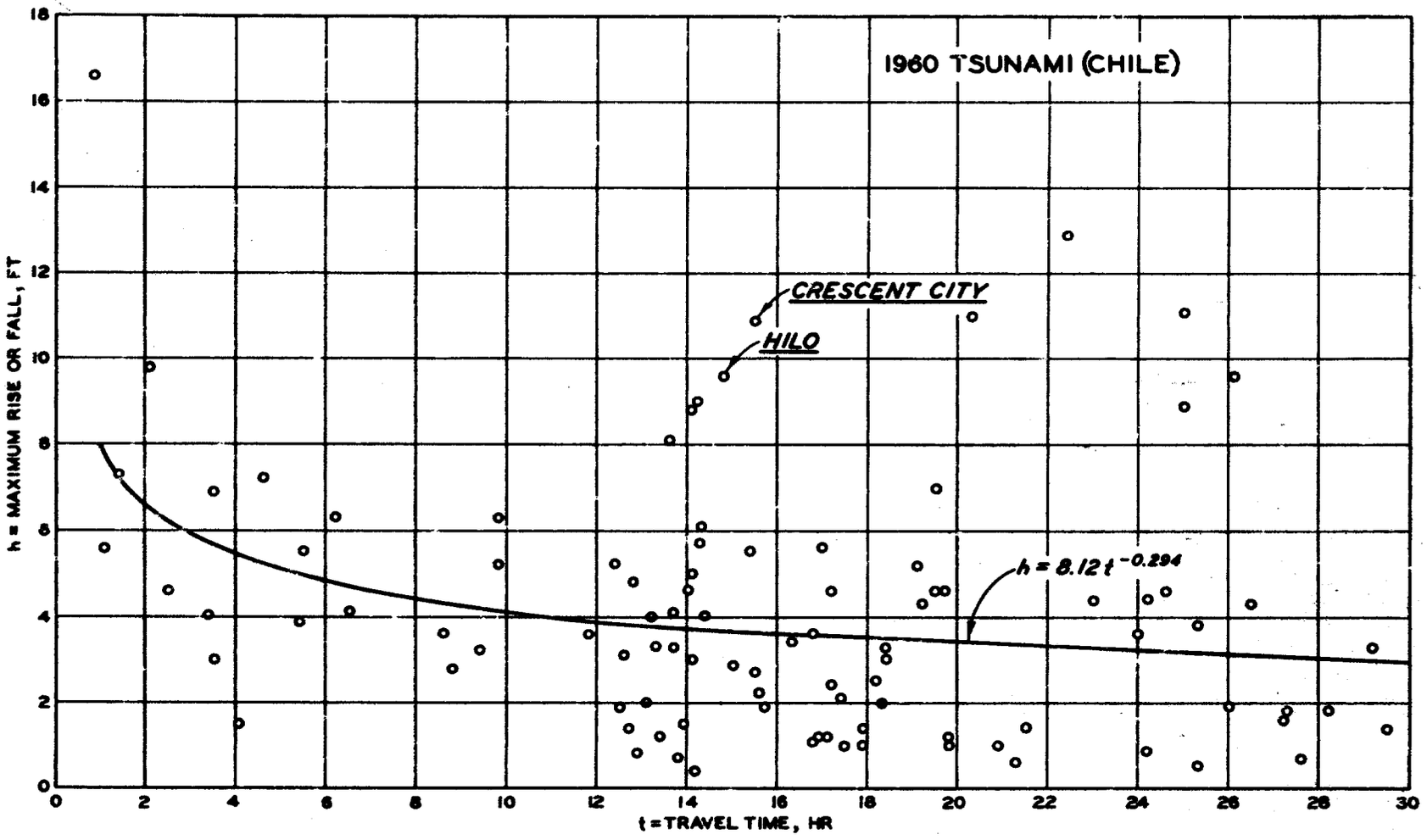

Fig. 33. Maximum rise or fall versus travel time

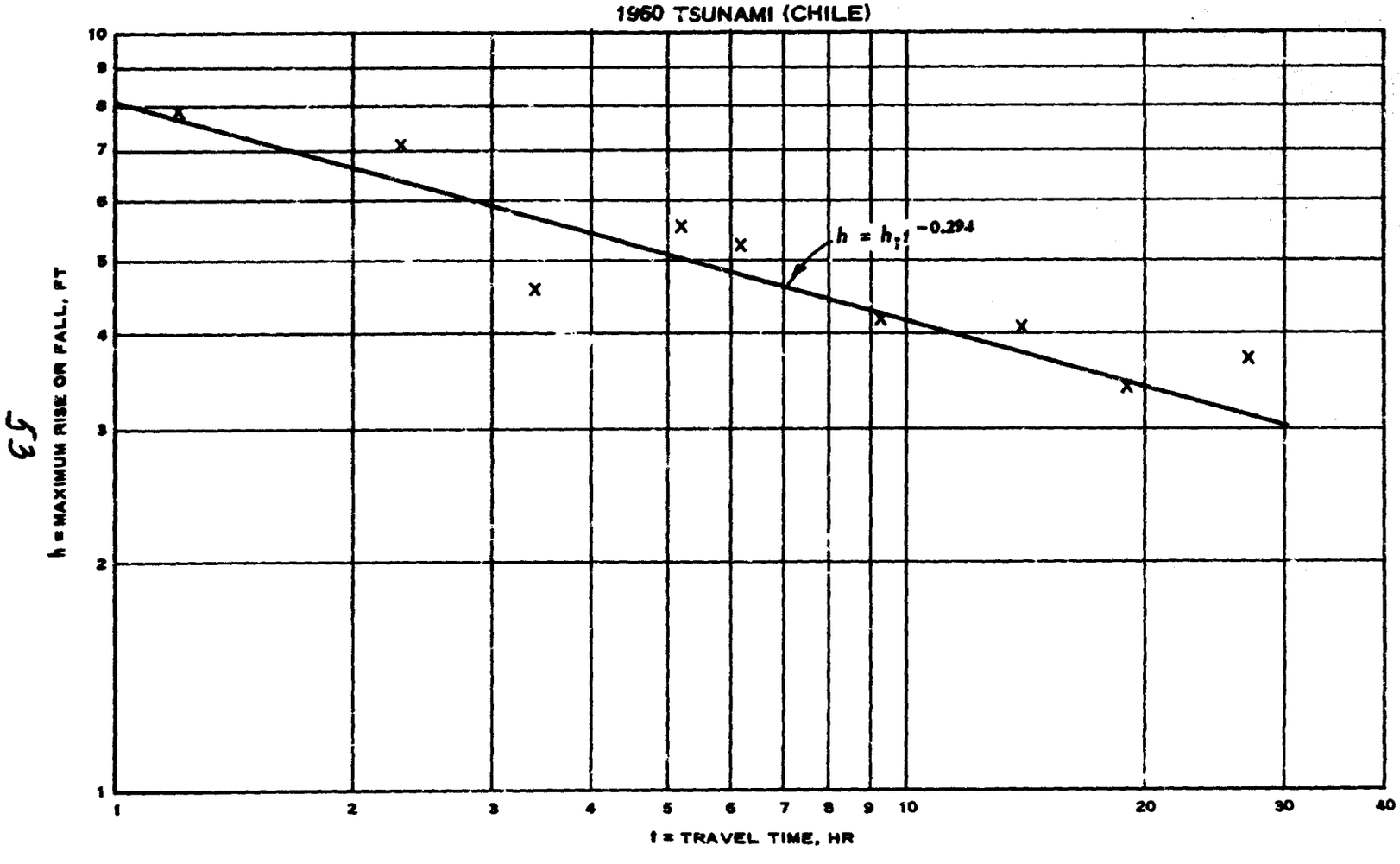

Fig. 34. Log-log plot of information in fig. 33

Spaeth and Berkman[6] give T_h = 325 min and T_c = 243 min, and hence h_c/h_h = 1.27 . Refraction analysis shows that the energy reductions at these two localities are also of approximately similar values. Thus, one needs to seek other factors for the anomaly. One possibility, of course, could be the presence of disparities in the resonant stages of the two localities during this particular tsunami. One would expect a higher wave magnification at Crescent City than that at Hilo Bay, if at Crescent City the quantity $\frac{T - T_{cr}}{T_{cr}}$ was almost nil, and at Hilo Bay, of a moderate amount. As precise determinations of the critical periods T_{cr} of the two localities are as yet not forthcoming, the matter cannot now be resolved. Another possibility could be an uneven concentration of energy along the crest of the wave front at the generating area. This is also a matter that is not amenable to an accurate determination.

60. Wilson has summarized much useful information relating the fault length, tsunami source dimension, tsunami height, and tsunami period and frequency with earthquake intensity.[1] Such information gives insight into the mechanism of tsunamis, but this is hardly adequate to predict what the tsunami heights at Crescent City would be if another earthquake occurred in the Alaskan area having an intensity of 8.5 on the Richter scale. The most relevant information desired is the frequency-height relation for Crescent City. From the latter point of view, the exaggerated disturbances of the 1964 Alaskan tsunami hardly fit the course of expected events of Crescent City, and one is forced to regard the manifestation as a singular event of rare probability.

PART V: FLUME TESTS AND RESULTS

61. Because of the long period and large height of the 1964 Crescent City tsunami, it was deemed necessary to make flume studies before final selection of the Crescent City model configuration.

Wave Generator and Flume

62. An existing 5-ft-wide, 100-ft-long concrete flume was used for preliminary testing. The object of the tests was to determine the characteristics of a long-period wave model.

63. A sketch of the pneumatic wave generator used in the majority of flume tests is shown in fig. 35. It consists of a rectangular steel vessel with a nozzle attached to the mouth of the tank. The top is provided with a valve leading to the aspirator and another set of valves leading to the open air. In a simple manner of operation, the flume water is raised from an initial level H_o, measured from the flume bottom, to a level H. During this process the air valves are closed. Next, the aspirator valve is closed and the air valves are opened. Assume that the initial wave of the efflux is rectangular in shape and is of constant height h. In the tentative design of the tank, use was made of the relation[26]

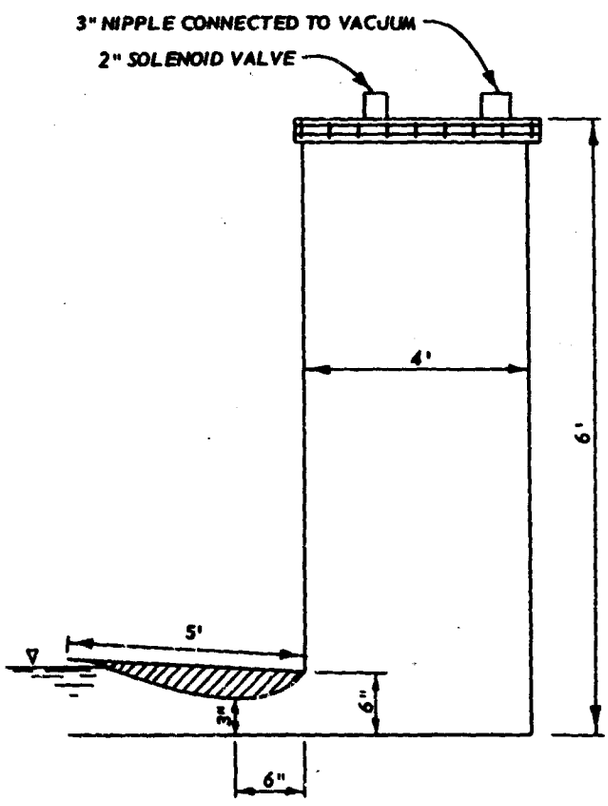

Fig. 35. Pneumatic wave generator used in the majority of flume tests

$$\frac{h}{H_o} = \left(\frac{H}{H_o} - 1\right)\left(1 - \frac{1}{4}\frac{h}{H_o}\right)\frac{k_1}{1 + \lambda} \tag{31}$$

which contains in addition to H_o, h, and H, the quantities k_1 and λ. The significance of k_1 is shown in the following statements. Prior to the opening of the air valves the suction pressure in the tank is Δp_o, say

$$\Delta p_o = \rho g\ (H - H_o) \tag{32}$$

Following the opening of the air valves, the suction pressure is decreased to Δp_i, allowing the flow of water from the generator and

$$k_1 = \frac{\Delta p_o - \Delta p_i}{\Delta p_o} \tag{33}$$

The value of k_1 may vary between 0.06 and 0.10 by a proper selection of the air gap in the tank and the aperture sizes of the valves. A good value to take is $k_1 = 0.085$. The quantity λ is related to the energy loss in the area of the nozzle and would have a reasonable value of 0.4.[26]

64. The generator was designed with the present 1:125 undistorted scale model of the Crescent City coast and the sea environment in mind. The prototype depth of water in the approaches to the harbor is approximately 62 ft. This gives a model depth H_o of 0.5 ft. A prototype design wave of 30 ft would have a value $h = 0.24$ ft. Entering equation 31 with the quantities $h = 0.24$ ft, $H_o = 0.5$ ft, $\lambda = 0.4$, and $k_1 = 0.085$ yields $H = 5.0$ ft. Allowing 1 ft for the air space, the height of the generator tank would be 6 ft. To determine the length of the tank, it is imagined that after the efflux from the tank is completed, the generated wave is triangular in shape and extends from the generator to the model coast. This distance is about 80 ft in the model. At the front, the height of wave is 0.5 ft. Thus, the wave area is 20 sq ft, requiring that the length of the tank be 4 ft.

Model Scale Relations

65. The derivation of scale relations becomes more meaningful if

based on physical relations. Tsunami model waves are essentially translation waves where the particle velocities in a vertical section are nearly constant. The appropriate dynamic and kinematic equations are, ignoring friction,

$$\frac{\partial u}{\partial t} + u \frac{\partial u}{\partial x} + g \frac{\partial h}{\partial x} = 0 \tag{34}$$

$$\frac{\partial h}{\partial t} + \frac{\partial}{\partial x} (UH) = 0 \tag{35}$$

These may be put in dimensionless form. For this, velocities are measured in terms of $\sqrt{gH_o}$, horizontal lengths in terms of L, a characteristic length, and vertical distances, depths, and wave elevations in terms of H_o, a characteristic depth, and time, in terms of a characteristic time, the wave period T. In other words, putting

$$u = \frac{U}{\sqrt{gH_o}}$$

$$\zeta = \frac{x}{L}$$

$$\eta = \frac{h}{H_o}$$

$$\delta = \frac{H}{H_o}$$

$$\tau = \frac{t}{T}$$

the dynamic and kinematic equations become

$$\frac{\partial u}{\partial \tau} + \frac{\partial u}{\partial \zeta} + \frac{\partial \eta}{\partial \zeta} = 0$$

$$\frac{\partial \eta}{\partial \tau} + \frac{\partial}{\partial \zeta} (u\delta) = 0$$

provided that

$$\frac{L}{T\sqrt{gH_o}} = \text{constant}$$

Thus, if the model be constructed affinely similar to the prototype, that is at corresponding points

$$\delta_m = \delta_p$$

then, at corresponding points

$$u_m = u_p$$

and

$$\eta_m = \eta_p$$

provided that

$$\left(\frac{L}{T\sqrt{gH_o}}\right)_m = \left(\frac{L}{T\sqrt{gH_o}}\right)_p$$

which is the scale for the periods. Let S be the scale for depths and r the model distortion, a quantity larger than unity. Then, with

$$S = \frac{H_p}{H_m}$$

$$rS = \frac{L_p}{L_m}$$

one has

$$T_m = \frac{1}{rS^{1/2}} T_p$$

66. Three series of tests were made for this part of the study. The first series was made using a horizontal and vertical scale of 1:125. This is the scale of the existing Crescent City model which was constructed at the WES for short-period wave studies. The horizontal scale was then enlarged to 1:375 (the vertical scale remaining 1:125) and the contours in

the flume floor remolded for the second series of tests. A set of hardware-cloth wave screens was then placed in front of the wave generator and the third series of tests was run using the same model scales as those used in the second series. The flume bottom configurations for the different series of tests are shown in fig. 36.

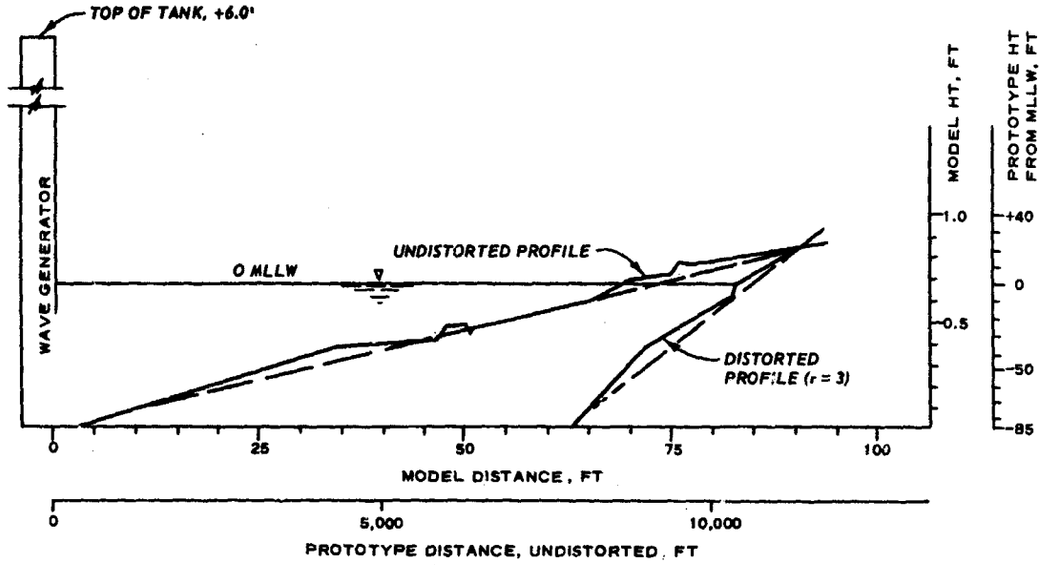

Fig. 36. Flume bottom configurations for the three series of tests

First Series of Tests, Undistorted Model

67. A typical wave record for the case of an undistorted model with a scale of 1:125 is shown in fig. 37. This series of tests was performed to investigate the possibility of utilizing the Crescent City model presently situated at the WES. It became evident from this series of tests that it was not possible to develop a sufficiently long-period model wave due to the interference of the resonant waves in the flume. The resonant characteristics of this size model cause undesirable interaction which makes it impossible to model even a half-period wave.

Second Series of Tests, Distorted Model Without Screens

68. A typical wave record for this case is shown in fig. 38. There

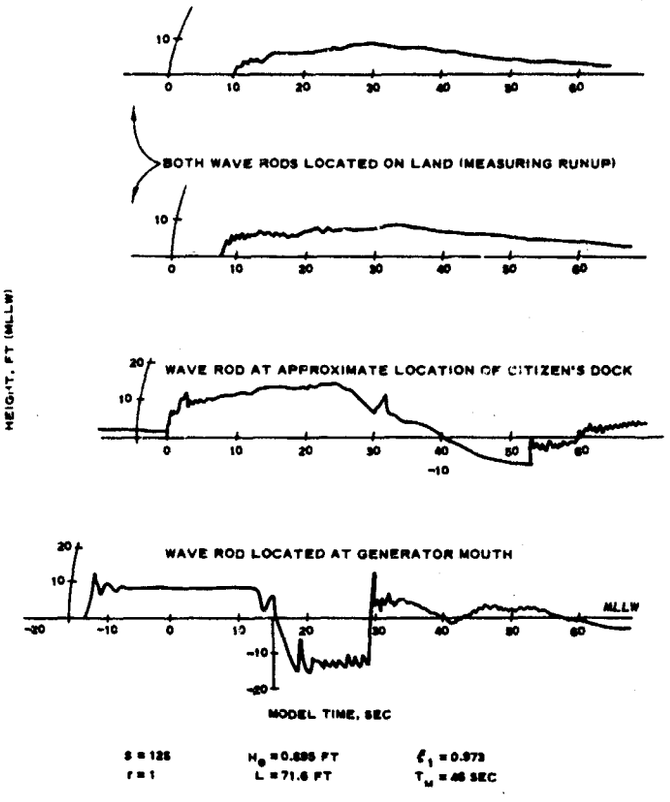

Fig. 37. Typical wave record in undistorted flume

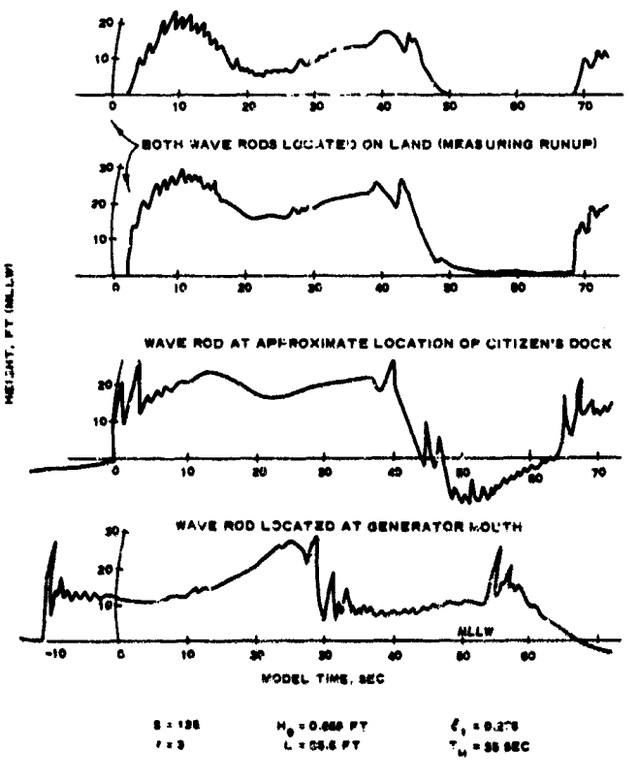

Fig. 38. Typical wave record in distorted flume; T_m = 35 sec

appear to be two objectionable characteristics in this case.

a. The wave record is very spiked with the initial stage of the wave being greatly affected by undesirable exit conditions of the wave generator.

b. The resonant characteristics of the model again make it impossible to input a wave of the desired period. The flume configuration consisted of a long uniform section up to the contoured area at the end of the flume. A "coupling effect" was evident with the two areas resonating independently at their own characteristic frequencies rather than as a whole.

Third Series of Tests, Distorted Model with Screens

69. Hardware-cloth wave screens were installed in the distorted model in an attempt to eliminate the objectionable peaks mentioned in the second series of tests. A typical wave record presented as fig. 39 shows that this objective was partially accomplished; however, the resonant interference at the barrier was still in great evidence and it was still impossible to generate a satisfactory model wave.

Similarity Rules for Wave Periods

70. In all three cases studied in the flume (undistorted profile, distorted profile without screens, and distorted profile with screens), the resonant characteristics of the basin interfered with the functioning of the model. Recognizing the fact that the resonance will always be strong unless an

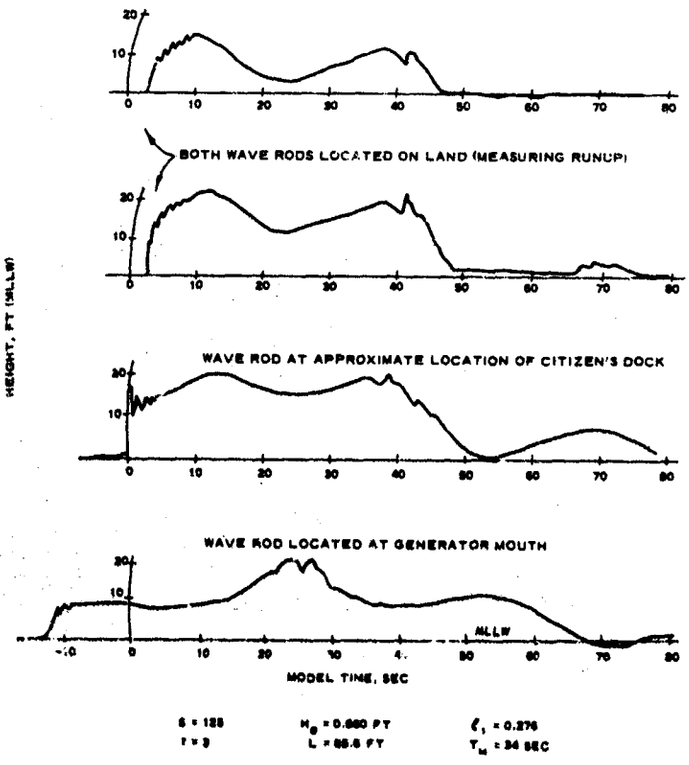

Fig. 39. Typical wave record in distorted flume with screens

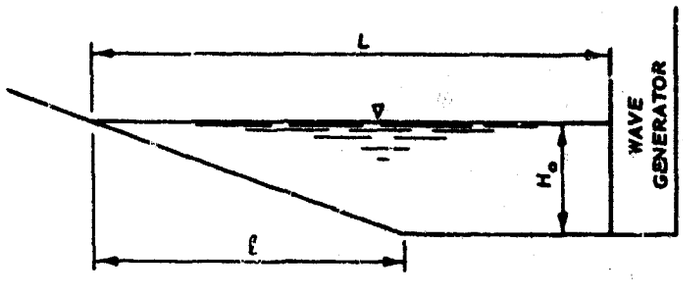

TERMINOLOGY: $\xi = \ell/L$

ℓ = FORESLOPE LENGTH

L = MODEL LENGTH

H = DEPTH AT WAVE GENERATOR

T = RESONANT WAVE PERIOD

	UNDISTORTED FLUME	DISTORTED FLUME	DISTORTED FLUME WITH SCREENS
ξ_1	0.97	0.30	0.28
L	70 FT	88 FT	86 FT
H_o	0.67 FT	0.70 FT	0.66 FT
TCALC	47 SEC	38 SEC	39 SEC
TOBS	46 SEC	35 SEC	35 SEC

Fig. 40. A comparison of theoretical and observed periods for different model configurations

extremely large model is built, it was realized that the model should be constructed to resonate at the desired period.

71. A theoretical analysis of a resonant model is included in Appendix E. The results of the theoretical development were verified by the preliminary model tests with the correlation between the observed and the calculated period shown in fig. 40. The theoretical analysis also indicated the similarity criteria to be used in designing a resonant model. The ratio of model period to prototype period was shown to be

$$\frac{T_m}{T_p} = \frac{1}{rS^{1/2}} \qquad (36)$$

where

r = distortion ratio = $\frac{S_H}{S_V}$

$S = S_V$ = vertical scale

T = period of oscillation

Furthermore, the resonant period for a triangular, two-dimensional basin with a closed end is found to be

$$T = 0.55 \frac{L}{H_o^{1/2}}$$

or

$$T_m = 0.55 \left(\frac{L_m}{\alpha_p r}\right)^{1/2} \qquad (37)$$

where

L = length of the basin

α = bottom slope

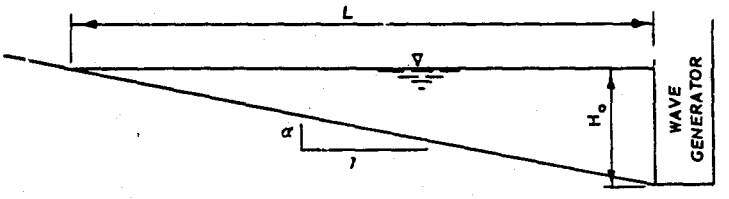

$$T_M = \frac{1}{rS^{1/2}} T_p$$

$$T_M = 0.55 \left(\frac{L_M}{\alpha_p r}\right)^{1/2}$$

WHERE:

T_p = 28 MIN = 1680 SEC

$S = H_p/H_M$ = VERTICAL SCALE

r = DISTORTION RATIO = $\frac{L_{op}}{L_{oM}} \cdot \frac{1}{S}$

α = OFFSHORE SLOPE
= 0.0060 FOR CRESCENT CITY

T = WAVE PERIOD (SEC)

L = HORIZONTAL LENGTH (FT)

H_o = DEPTH AT WAVE GENERATOR (FT)

	S = 125		S = 150		S = 175		S = 200	
r	T_M	L	T_M	L	T_M	L	T_M	L
1	150	445	137	374	127	320	119	282
2	75	223	68	183	63	158	60	143
3	50	149	45	120	42	105	39	91

Fig. 41. Model lengths for given scales and distortions

72. Employing these criteria, a resonant two-dimensional model can be designed for a particular observed prototype period. A table of possible model dimensions is presented in fig. 41. These values were calculated for a prototype period of 28 min and a bottom slope of 0.0060, both of which conditions were realized at Crescent City during the 1964 tsunami.

Problems for Future Study

73. One of the main findings of the aforementioned tests is that, in the model, the length of the sea area between the wave generators and the harbor should be great enough to create at least one cycle of the wave approximating that of the prototype. In the interest of economy of construction and to avoid an excessively long model, it is necessary that the model be distorted. A further requirement, as can be deduced from the analysis of scale, is that the model be constructed affinely with the prototype. This would mean that the bottom contours of the area from the harbor to the generator should be sloping. Based on these requirements, the model dimensions necessary for different depth scales and different distortions are summarized in fig. 41. A slightly modified wave generator (shown in fig. 42) will be used in any subsequent testing.

74. Among the problems to be considered is the manner of controlling the air valves that would lead to the formation of a well-shaped wave. The efficacy of screens to eliminate the secondary undulations related to the efflux of water from the generator needs to be examined anew. Another quite intriguing problem is the feasibility of utilizing the waves repeated in the flume following the initial operation of the generator tank.

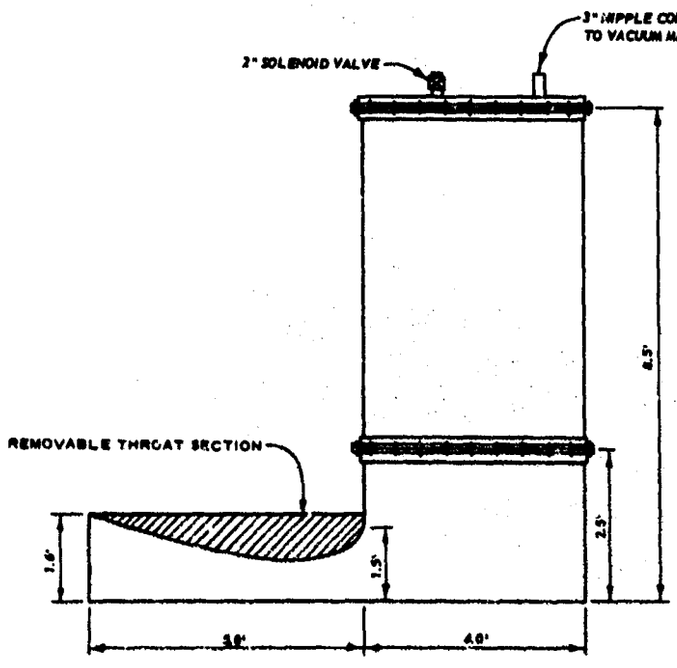

Fig. 42. Modified tsunami generator

75. One basic problem remaining is the effect of distortion on the runup. The necessity of the study was

particularly emphasized by Professor R. L. Wiegel in a conference held at the WES August 8-9, 1968. In the development of the analysis for the scales it was shown, tacitly, that similarity of the wave quantities, particle velocity and wave elevation, exists in the flume independently of distortion, provided that the period of the model is correctly selected. This is a consequence of the dynamic and kinematic equations applicable to the flume. The argument cannot be applied to the runup. Although resort may be made to another analysis to establish the runup extensions, it would be more satisfactory to resolve the question experimentally.

PART VI: CONCLUSIONS

76. Based on the results of the material presented in this report, it is concluded that:

a. The wave characteristics that should be used in the proposed model testing program to simulate the highest wave of the 1964 tsunami at Crescent City are a 23-ft, 28-min-period, rising tide with a maximum runup to about the +20 ft mllw contour.

b. Shelf resonance in the offshore Crescent City area is a key factor in the unusual height and duration of the 1964 tsunami, and probably, but to a lesser extent, of all other tsunamis causing a water-surface rise at Crescent City.

c. Linear spectral analyses performed on a portion of the 1960 tsunami record at Crescent City show that the contained periods of this tsunami coincide with those derived by Keulegan and Wilson to be the resonant oscillations of the offshore shelf area.

d. A digital computer program that allowed for the distortion present in maps drawn by Mercator projection was coded for tsunami refraction across the Pacific Ocean area and was tested successfully. Refraction diagrams computed and drawn by the above program for three recent tsunamis (Alaska, 1964; Chile, 1960; and Kamchatka, 1952) established nearshore wave-front patterns at Crescent City. These nearshore wave fronts will dictate the wave generator alignment in any subsequent model testing program. The refraction diagrams also showed that no overall tsunami height increase was caused by refraction in the open ocean.

e. The probability of occurrence studies indicated that tsunami heights at Hilo and Crescent City are similar and that the 1964 tsunami was a singular event with only a 20 percent probability of occurrence during any 45-year period.

f. The use of an undistorted tsunami model of the Crescent City area will not be feasible; and the sea environment of the model should be of such a magnitude that the fundamental period of the resonant oscillations of the model sea-to-land area corresponds to the largest period of the selected test wave.

g. Additional wave-flume tests are required to determine the optimum linear scales of the model and the required sea area that must be reproduced to ensure accurate reproduction of prototype tsunami action in the harbor and overbank areas at Crescent City.

LITERATURE CITED

1. Wilson, B. W. and Torum, A., "Final Report - Engineering Damage from the Tsunami of the Alaskan Earthquake of March 27, 1964," p 401, Sept 1967, prepared for Coastal Engineering Research Center by Science Engineering Associates, San Marino, Calif.

2. Van Dorn, W. G., "Source Mechanism of the Tsunami of March 28, 1964, in Alaska," Proceedings, Ninth Conference on Coastal Engineering, Lisbon, Portugal, June 1964, American Society of Civil Engineers, 1965, pp 166-190.

3. Wiegel, R. L., "Protection of Crescent City, California, from Tsunami Waves," Mar 5, 1965, Redevelopment Agency of the City of Crescent City, Berkeley, Calif.

4. Magoon, O. T., "Structural Damage by Tsunamis," Specialty Conference on Coastal Engineering, Santa Barbara, American Society of Civil Engineers, Oct 1965, pp 35-68.

5. Tudor, W. J., "Tsunami Damage at Kodiak, Alaska, and Crescent City, California, from the Alaskan Earthquake of 27 March 1964," Technical Note No. N-622, Nov 1964, Naval Civil Engineering Laboratory, Port Hueneme, Calif.

6. Spaeth, M. G. and Berkman, S. C., "The Tsunami of March 28, 1964, as Recorded at Tide Stations," ESSA Technical Report C&GS 33, July 1967, U. S. Coast and Geodetic Survey, Washington, D. C.

7. Piersol, A. G., "The Measurement and Interpretation of Ordinary Power Spectra for Vibration Problems," NASA CR-90, Sept 1964, National Aeronautics and Space Administration, Washington, D. C.

8. Moody, R. C., "Statistical Considerations in Power Spectral Density Analysis," Technical Products Co., Los Angeles, Calif.

9. _____, "Considerations in the Analysis of Random Wave Processes," Technical Products Co., Los Angeles, Calif.

10. Honda, K., Terada, T., and Isitani, D., "On the Secondary Undulations of Oceanic Tides," Philosophical Magazine, Series 6, 15, 1907, p 88.

11. Suda, K. and Seki, K., "On a Few Tsunami Waves Which Occurred Recently in the Pacific," Umito Sora (Sky and Water), 3, pp 95, 114 (in Japanese).

12. Goldsborough, G. R., "The Tidal Oscillations in an Elliptic Basin of Variable Depth," Proceedings, Royal Society of London, A, CXXX, 157, 1930.

13. Keulegan, G. H., "A Review of the Experimental Data Relative to the Pilot Model Study for the Design of the Hilo Harbor Tsunami Model," Miscellaneous Paper No. 2-883, Apr 1967, U. S. Army Engineer Waterways Experiment Station, CE, Vicksburg, Miss.

14. Housley, J. G., "Appendix A: Keulegan Memorandum of 15 May 1962, subject, 'Hilo Bay Tsunami Model,'" Pilot Model Study for the Design of the Hilo Harbor Tsunami Model, Research Report No. 2-3, Mar 1965, U. S. Army Engineer Waterways Experiment Station, CE, Vicksburg, Miss.

15. Ippen, A. T., ed., Estuary and Coastline Hydrodynamics, McGraw-Hill, New York, 1966, p 258.

16. Smail, L. L., Calculus, Appleton-Century-Crofts, New York, 1949, p 236.

17. Dobson, R. S., "Some Applications of a Digital Computer to Hydraulic Engineering Problems," Technical Report No. 80, pp 22-25, June 1967, Department of Civil Engineering, Stanford University, Stanford, Calif.

18. Wilson, W. S., "A Method for Calculating and Plotting Surface Wave Rays," Technical Memorandum No. 17, p 10, Feb 1966, U. S. Army Engineer Coastal Engineering Research Center.

19. Smith, S. M., Menard, H. W., and Sharman, G., "World-Wide Ocean Depths and Land Elevations Averaged for One Degree Squares of Latitude and Longitude," Scripps Institution of Oceanography, La Jolla, Calif.

20. Baer, L., "The Icosahedral-Gnomonic Projection and Grid of the World Ocean for Wave Studies," Report No. LR 20157, Lockheed-California Co., Oceanics Division.

21. Berkman, S. C. and Symons, J. M., "The Tsunami of May 22, 1960, as Recorded at Tide Stations," U. S. Coast and Geodetic Survey, Washington, D. C.

22. Zerbe, F. B., "The Tsunami of November 4, 1952, as Recorded at Tide Stations," Special Publication No. 300, 1953, U. S. Coast and Geodetic Survey, Washington, D. C.

23. Cox, D. C., "Tsunami Height-Frequency Relationship at Hilo," Nov 1964, Hawaii Institute of Geophysics, University of Hawaii.

24. Iida, K., Cox, D. C., and Pararas-Carayannis, G., "Preliminary Catalog of Tsunamis Occurring in the Pacific Ocean," Report No. HIG-67-10 (Data Report No. 5), Aug 1967, Hawaii Institute of Geophysics, University of Hawaii.

25. Wilson, B., Webb, L., and Hendrickson, J. A., "The Nature of Tsunamis, Their Generation and Dispersion in Water of Finite Depth," SN-57-2, Aug 1962, National Engineering Science Company, Pasadena, Calif.

26. Keulegan, G. H., "The Approximate Theories of Pneumatic Wave Generators," Research Report No. 2-7, Apr 1966, U. S. Army Engineer Waterways Experiment Station, CE, Vicksburg, Miss.

27. Lamb, H., Hydrodynamics, 6th ed., Dover Publications, New York, 1932.

Table 1

Confidence Levels of Amplitude Spectra

Time Interval	Effective Bandwidth cpm	e_s %	Degrees of Freedom n	70% Confident That Estimated Value Will Be		90% Confident That Estimated Value Will Be		99% Confident That Estimated Value Will Be	
				Greater Than	Less Than	Greater Than	Less Than	Greater Than	Less Than
0530-2400 hr	0.00194	68.1	4.3	--*	--	--	--	--	--
0530-2400 hr	0.00388	48.2	8.6	0.69 × TV**	1.25 × TV	0.44 × TV	1.75 × TV	0.20 × TV	2.50 × TV
0530-2400 hr	0.0097	30.5	21.6	0.82 × TV	1.15 × TV	0.65 × TV	1.50 × TV	0.43 × TV	1.90 × TV
0530-1300 hr	0.00194	107.0	1.75	--	--	--	--	--	--
0530-1300 hr	0.00388	75.8	3.49	--	--	--	--	--	--
0530-1300 hr	0.0097	47.7	8.74	0.70 × TV	1.18 × TV	0.46 × TV	1.70 × TV	0.225 × TV	2.47 × TV
1300-1700 hr	0.00194	147.0	0.930	--	--	--	--	--	--
1300-1700 hr	0.00388	107.5	1.93	--	--	--	--	--	--
1300-1700 hr	0.0097	65.3	4.66	--	--	--	--	--	--
1700-2400 hr	0.00194	111.0	1.63	--	--	--	--	--	--
1700-2400 hr	0.00388	78.1	3.26	--	--	--	--	--	--
1700-2400 hr	0.0097	49.5	8.14	0.70 × TV	1.21 × TV	0.45 × TV	1.75 × TV	0.21 × TV	2.60 × TV

* Less than 5 degrees of freedom (cannot read values from fig. 9).
** TV = true value.

Table 2

Tsunami Heights for Hilo and Crescent City

(From Reference 24)

No.	Date	Generating Area	Honolulu, ft	Hilo, ft	San Francisco, ft	Crescent City, ft
1	1883 Aug 26	Krakatoa Volcano	0.79	2.16*	0.33	0.9**
2	1896 June 15	Sanriku	0.33	7.9	0.67	1.8**
3	1906 Aug 17	Talcahuano	0.33	4.9	0.33	0.9**
4	1922 Nov 10	N. Chile	0.98	6.9	0.67	1.8**
5	1923 Feb 4	E. Kamchatka	2.9	20.0	0.33	0.9**
6	1923 Apr 13	E. Kamchatka	0.67	0.98	0.67	1.8†
7	1927 Nov 4	Point Argaello	0.06	0.33	0.1	0.3†
8	1928 June 16	Mexico	0.16	0.66	--	--
9	1933 Mar 3	Sanriku	0.33	0.33	0.66	1.8†
10	1944 Dec 7	Kii	0.33	0.90*	0.33†	0.9†
11	1946 Dec 21	Nankaido, Japan	0.33	0.90*	0.33	0.98
12	1952 Mar 4	Tokachi, Hokkaido	0.67	0.33	1.98	0.67
13	1963 Oct 12	S. Kuril Island	0.67	1.31	--	1.64
14	1946 Apr 1	E. Aleutian Island	1.94(4.1)††	26.6	0.98(1.7)	3.0(5.9)
15	1952 Nov 4	E. Kamchatka	2.3(4.4)	12.1(7.9)	1.96(3.5)	3.6(6.8)
16	1957 Mar 9	Adak Island	1.97	8.9	0.67	4.3
17	1960 May 22	S. Chile	3.3(5.5)	37.8(9.6)†	1.64(2.9)	12.1(10.9)
18	1964 Mar 28	Prince William Island	1.64(2.7)	6.9(12.5)†	4.25(7.4)	20.6(20.6)

* From correlation with Honolulu heights (Hon. heights × 2.73).
** From correlation with San Francisco heights (S.F. heights × 2.7)(see fig. 29).
† Nearby station.
†† Numbers in parentheses refer to C&GS reports or other.

Table 3

Comparison of Honolulu and Hilo Heights for Tsunamis with Large Runup at Hilo

No.	Date	Generating Area	Hilo, ft	Hono-lulu, ft	Hilo Reduced,* ft	Crescent City, ft
2	1896 June 15	Sanriku	7.9	0.33	0.90	1.81
3	1906 Aug 17	Talcahuano	4.9	0.33	0.90	0.89
4	1922 Nov 10	N. Chile	6.9	0.98	2.68	1.84
5	1923 Feb 4	E. Kamchatka	20.0	2.9	7.91	0.9

* Values shown for "Hilo Reduced" are Honolulu values multiplied by 2.73.

APPENDIX A: COMPUTER PROGRAM FOR TSUNAMI REFRACTION

Explanation of Variables and Program Listing

1. The program, for which a listing is given, is written in FORTRAN II and has been run successfully on the GE-225 computer at the U. S. Army Engineer Waterways Experiment Station, Vicksburg, Miss. The program gives output suitable for the off-line Calcomp 750 plotter system at the same installation.

2. The compilation takes approximately 150 sec, and the program executes at the approximate rate of three points per second on the GE-225. These execution times include reading the data for a 35 x 35 grid and printing output every 50 points.

Program: 22-Z5-074, Waterways Experiment Station

3. Input Variables

MM	The number of grid intersections along the x-axis.
NN	The number of grid intersections along the y-axis.
NOR	The number of rays to be refracted during one run.
NPRINT	Frequency for printed output.
GRID	The length in inches along one edge of a grid square.
H(I,J)	Depth data at the grid intersections (Note: $I \leq MM$, $J \leq NN$).
X,Y	Coordinates (in inches) of the starting point for each ray.
ANGLE	Initial direction of the wave ray, measured in degrees counterclockwise from the positive x-axis.
DELTAX	Computational x increment (Δx) measured in feet.
DIST	The number of feet corresponding to the length of a grid square (measured at the equator).
CONV	Conversion factor to change the depth readings to feet.
TIMEX	Dictates the number of seconds of actual wave travel between tic marks placed on the ray. (Note: The wave-front positions may be marked TIMEX seconds apart on the ray.)

TIME . . . . . The time in seconds at the beginning of a wave ray computation.

4. Output Variables

ANGLE, X,Y, TIME . . . . . As previously described except applied to the successive computational steps instead of the initial conditions.

DEPTH . . . . . The interpolated depth in feet at successive computational points.

5. Variables Not Previously Defined

HE(1),HE(2),...HE(10). . Depths at grid intersections used for surface fitting computations.

SMALLX,SMALLY . . . . . Distances, in feet, of the point of interest measured from H(I,J) .

PHWRTX,PHWRTY . . . . . $\frac{\partial H}{\partial x}, \frac{\partial H}{\partial y}$ found from the surface fitting procedure.

D2YDX2 . . . . . $\frac{d^2y}{dx^2}$

DYDX . . . . . $\frac{dy}{dx}$

DELTAY . . . . . The increment of $y,(\Delta y)$, computed from a given increment of $x,(\Delta x)$.

DELTAT . . . . . The time increment between successive points of calculations.

6. It must be noted that the format for the depth data is not variable but, of course, may be changed to suit the needed requirements.

7. The plotting steps are incorporated as an integral part of the program. A set of x-, y-axes are drawn with MM tic marks placed on the x-axis and NN tic marks placed on the y-axis. These tic marks are placed GRID inches apart and the axes form a reference by which the plotter output may be overlaid on the original map and the rays (which are drawn by the Calcomp plotter) traced from the plotter sheet to the original map.

8. Because of main memory limitations in the GE-225, the maximum size grid that can be used is 35 x 35.

9. A program listing and an example of input for the computer program are found on the following pages.

PROGRAM LISTING

```
C     THEORETICAL TSUNAMI STUDY FOR CRESCENT CITY,CALIFORNIA
C     JOHN HARRISON   22-25-074
C     PROGRAM COMPUTES AND PLOTS REFRACTION DIAGRAMS FOR A TSUNAMI
      DIMENSION H(35,35),HE(10)
      TANF(ANGRAD)=SINF(ANGRAD)/COSF(ANGRAD)
      G=32.174
      READ 1,MM,NN,NOR,NPRINT,GRID
    1 FORMAT(4I10,F10.5)
      LL=0
      READ 2,((H(I,J),I=1,MM),J=1,NN)
    2 FORMAT (7F10.3)
      CALL PLOT(0.0,-30.0,-3)
      CALL PLOT(0.0,5.0,-3)
      MMP= MM-1
      NNP= NN-1
      CALL TMK(0.0,0.0,GRID,MMP,0.1,0.0,1.0,1.0)
      CALL TMK(0.0,0.0,GRID,NNP,-0.1,90.0,1.0,1.0)
      CALL PLOT(0.0,0.0,-3)
 1002 READ 3,X,Y,ANGLE,DELTAX,DIST,CONV,TIMEX,TIME
      MPRINT = 1
      LL=LL+1
    3 FORMAT(8F10.3)
      NEB=1
      TIMES=TIMEX
      PRINT 14
   14 FORMAT(1H1,2X,10HANGLE(DEG),5X,16HX COORDINATE(IN),5X,16HY COORDIN
     1ATE(IN),8X,9HTIME(SEC),12X,10HDEPTH(FT.))
  999 ANGRAD=ANGLE*0.0174532925
  602 I=1.+X/GRID
      J=1.+Y/GRID
  625 HE(1)=H(I,J)*CONV
      HE(2)=H(I+1,J)*CONV
      HE(3)=H(I+2,J)*CONV
      HE(4)=H(I,J+1)*CONV
      HE(5)=H(I,J+2)*CONV
      HE(6)=H(I+1,J+1)*CONV
      HE(7)=H(I+1,J-1)*CONV
      HE(8)=H(I,J-1)*CONV
      HE(9)=H(I+2,J+1)*CONV
      HE(10)=H(I+1,J+2)*CONV
  502 XX=I-1
      YY=J-1
      XFEET= DIST*X/GRID
      YFEET= DIST*Y/GRID
      SMALLX = XFEET-XX*DIST
      SMALLY = YFEET-YY*DIST
```

PROGRAM LISTING (cont'd)

```
      E1=(HE(4)*HE(8)-2.*HE(1))/(2.*DIST*DIST)
      B1=(HE(4)-HE(1)-E1*DIST*DIST)/DIST
      C1=(HE(6)-HE(7)-2.*B1*DIST)/(2.*DIST*DIST)
      D1=(HE(1)+HE(3)-HE(6)-HE(7)+2.*E1*DIST*DIST)/(2.*DIST*DIST)
      A1=(HE(3)-HE(1)-4.*D1*DIST*DIST)/(2.*DIST)
      E2=(HE(5)-2.*HE(4)+HE(1))/(2.*DIST*DIST)
      B2=(HE(4)-HE(1)-E2*DIST*DIST)/DIST
      D2=(HE(9)-HE(10)-HE(2)+HE(1)+B2*DIST+3.*E2*DIST*DIST)/(2.*DIST*DIS
     1T)
      A2=(HE(2)-HE(1)-D2*DIST*DIST)/DIST
      C2=(HE(9)-HE(1)-2.*A2*DIST-B2*DIST-4.*D2*DIST*DIST-E2*DIST*DIST)/
     1(2.*DIST*DIST)
      A=(A1+A2)/2.
      B=(B1+B2)/2.
      C=(C1+C2)/2.
      D=(D1+D2)/2.
      E=(E1+E2)/2.
      DEPTH=HE(1)+A*SMALLX+B*SMALLY+C*SMALLX*SMALLY+D*SMALLX*SMALLX+E*SM
     1ALLY*SMALLY
      PHWRTX=A+C*SMALLY*2.+D*SMALLX
      PHWRTY=B+C*SMALLX*2.+E*SMALLY
      IF (DEPTH-0.001)858,858,857
  858 PRINT 859
  859 FORMAT(48HRAY HAS REACHED SHORE. A NEW RAY WILL BE STARTED)
      GO TO 1001
  857 D2YDX2=(TANF(ANGRAD)*PHWRTX-PHWRTY)*(1.0+TANF(ANGRAD)*TANF(ANGRAD)
     1)/(DEPTH*2.)
      DYDX=TANF(ANGRAD)+D2YDX2*DELTAX
      ANGNEW=ATANF(DYDX)*57.29577951
      DELTAY=DELTAX*TANF(ANGRAD)+(D2YDX2*DELTAX*DELTAX)/2.
      DELTAT=(SQRTF(DELTAX*DELTAX+DELTAY*DELTAY))/SQRTF(G*DEPTH)
      GO TO (4000,4001),NEB
 4001 MPRINT=MPRINT+1
      IF(MPRINT-NPRINT)4003,4004,4004
 4004 MPRINT=1
 4000 PRINT 800,ANGLE,X,Y,TIME,DEPTH
  800 FORMAT(3X,F10.4,9X,F7.3,13X,F7.3,8X,F14.4,10X,F14.3)
 4003 GO TO (814,815),NEB
  814 CALL PLOT(X,Y,3)
      NEB=2
      GO TO 816
  815 CALL PLOT(X,Y,2)
  816 IF(TIME-0.01)817,818,817
  818 CALL TMK(X,Y,0.0,1.0,.10,ANGLE,1.0,1.0)
  817 IF(TIMES-TIME)887,819,825
  819 CALL TMK(X,Y,0.0,1.0,.10,ANGLE,1.0,1.0)
      GO TO 888
  887 TIDIFF=TIME-TIMES
      PLOTX=(SQRTF(G*DEPTH)*TIDIFF*GRID)/(SQRTF(1.+DYDX*DYDX)*DIST)
      PLOTY=DYDX*PLOTX
      IF (ANGNEW) 901,900,901
  900 PLOTX=X-PLOTX
      PLOTY=Y
```

PROGRAM LISTING (cont'd)

```
      CALL TMK(PLOTX,PLOTY,0.0,1,0.1,ANGLE,1.0,1.0)
      CALL PLOT (X,Y,3)
      GO TO 888
  901 PLOTX=X-PLOTX
      PLOTY=Y-PLOTY
      CALL TMK(PLOTX,PLOTY,0.0,1,0.1,ANGLE,1.0,1.0)
      CALL PLOT (X,Y,3)
  888 TIMES=TIMES+TIMEX
  825 TIME=TIME+DELTAT
      DELTAX=DELTAX*GRID/DIST
      DELTAY=DELTAY*GRID/DIST
      X=X+DELTAX
      Y=Y+DELTAX
      ANGLE=ANGNEW
      IF(ANGLE+88.0)3002,3002,3001
 3001 IF(ANGLE-88.0)3000,3002,3002
 3002 PRINT 3003
 3003 FORMAT(52HANGLE IS BETWEEN 89 DEG AND 271 DEG. START A NEW RAY)
      GO TO 1001
 3000 DELTAX=DELTAX*DIST/GRID
      XXX=MM
      YYY=NN
      XXXX=(XXX+2.)*GRID
      YYYY=(YYY+2.)*GRID
      ZZZZ=GRID*2.
      IF(XXXX-X)1009,1009,1000
 1009 PRINT 5000
 5000 FORMAT(35HRAY IS GOING OFF RIGHT SIDE OF PLOT)
      GO TO 1001
 1000 IF(YYYY-Y)5001,5001,1010
 5001 PRINT 5002
 5002 FORMAT(28HRAY IS GOING OFF TOP OF PLOT)
      GO TO 1001
 1010 IF(ZZZZ-Y)999,5003,5003
 5003 PRINT 5004
 5004 FORMAT(31HRAY IS GOING OFF BOTTOM OF PLOT)
 1001 IF(LL-NOR)1025,1003,1003
 1025 PRINT 800 ,ANGLE,X,Y,TIME,DEPTH
      GO TO 1002
 1003 CALL PLOT(0.0,0.0,0.999)
      PRINT 800 ,ANGLE,X,Y,TIME,DEPTH
      REWIND 3
      READ 1, JOHN
      END
```

TYPICAL SET OF INPUT DATA

Dimensions of the Depth Grid: 35 35

Number of runs to be drawn: 2

Number of computations per printout: 50

Length of a grid square (in.): 8.53

35 values = first complete line of depth values

Depth grid (values in fathoms times cosine squared of the latitude)

3988.	3143.	2912.	2952.	3691.	4165.	4393.
4764.	4766.	4748.	4697.	4728.	4720.	4575.
4318.	4556.	4476.	3899.	3415.	3475.	3441.
3387.	3348.	3538.	3751.	3354.	2922.	3098.
3783.	3938.	3999.	3843.	3949.	3597.	4101.
4219.	3826.	3234.	2943.	3370.	3770.	4187.
4444.	4578.	4638.	4781.	4644.	4614.	4538.
4388.	4318.	4296.	4135.	3873.	3738.	2938.
2727.	2856.	3805.	3178.	2975.	2918.	3650.
3626.	3678.	3841.	3905.	4130.	4127.	4486.
4328.	4189.	3557.	3450.	3479.	3575.	4181.
4533.	4736.	4772.	4768.	4875.	4984.	4639.
4545.	4618.	4464.	3468.	3526.	3586.	3368.
3328.	3346.	3373.	3115.	2993.	2692.	2891.
3139.	3484.	3229.	3416.	4052.	4138.	4337.
4491.	3966.	3793.	3784.	3641.	3741.	3725.
4283.	4517.	4660.	4546.	4577.	4408.	4522.
4495.	4328.	4376.	3958.	3958.	3962.	3517.
4228.	3977.	3887.	3887.	3115.	3186.	3471.
3988.	3728.	3865.	4028.	4111.	4194.	4276.
4412.	3941.	3945.	3845.	4083.	4218.	4088.
4172.	4438.	4558.	4545.	4575.	4606.	4453.
4411.	4354.	4281.	3878.	3818.	3984.	4325.
4117.	3928.	3768.	3637.	3755.	3548.	3731.
3955.	4137.	4096.	4188.	4264.	4229.	4348.
4629.	4031.	3728.	3942.	3912.	4069.	4078.
4066.	4377.	4478.	4353.	4388.	4475.	4388.
4252.	4516.	4476.	4055.	4152.	4531.	4671.
4492.	3722.	3523.	3391.	3365.	3226.	3789.
4292.	4367.	4338.	4338.	4423.	4423.	4423.
4556.	4565.	4396.	4213.	4119.	3831.	3645.
3695.	3802.	4028.	4238.	4258.	4593.	4427.
4483.	4561.	4689.	4712.	4838.	5048.	4872.
4728.	4324.	3884.	3984.	4215.	4126.	4669.
4643.	4642.	4688.	4659.	4588.	4588.	4588.

INPUT DATA (cont'd)

DEPTH GRID (cont'd)

4690.	4652.	4783.	4893.	4353.	4174.	3965.
3944.	4126.	4410.	4014.	4499.	4595.	4578.
4701.	4839.	4874.	4753.	4898.	4998.	4984.
4576.	4805.	4882.	4123.	4525.	4553.	4923.
4747.	4753.	4762.	4762.	4762.	4762.	4762.
4926.	4648.	4591.	4693.	4587.	4522.	4233.
4218.	4299.	4468.	4712.	4753.	4808.	4758.
4729.	4996.	5178.	5020.	5054.	5168.	4911.
4587.	3743.	3972.	4342.	4530.	5008.	5045.
4933.	4933.	4933.	4933.	4933.	4933.	4933.
5132.	5698.	5513.	5513.	5445.	5386.	5368.
4967.	4968.	5017.	5344.	5462.	5518.	5556.
5684.	5651.	5590.	5807.	6014.	5946.	4876.
4456.	4582.	4843.	4925.	5126.	5763.	5857.
5027.	5118.	5118.	5118.	5118.	5118.	5118.
5221.	5233.	5192.	5144.	5041.	4878.	4787.
4722.	4636.	4684.	4778.	4750.	4837.	4858.
4550.	4533.	4502.	5271.	5370.	4751.	4523.
4562.	4774.	4676.	4616.	5134.	5828.	5866.
5241.	5236.	5293.	5297.	5297.	5379.	5362.
5235.	5439.	5378.	5350.	5298.	5135.	5218.
5094.	4957.	4869.	4944.	5020.	5178.	5182.
5118.	5271.	4934.	4987.	5158.	4765.	4496.
4583.	5153.	5171.	4971.	5308.	5216.	5281.
5189.	5097.	5414.	5441.	5388.	5408.	5368.
5615.	5570.	5578.	5546.	5488.	5347.	5348.
5298.	5022.	4928.	5002.	5162.	5313.	5228.
5268.	5248.	4923.	4942.	5112.	4996.	4987.
5817.	5518.	5598.	5685.	5692.	5574.	5567.
5459.	5389.	5605.	5591.	5463.	5591.	5605.
5685.	5581.	5642.	5508.	5477.	5349.	5591.
5265.	5063.	4936.	4845.	5124.	5186.	5248.
5378.	5311.	5234.	5258.	5377.	5361.	5242.
5381.	5655.	6004.	6251.	5890.	5765.	5787.
5935.	5900.	5745.	5725.	5648.	5646.	5646.
5629.	5629.	5622.	5617.	5546.	5549.	5651.
5112.	5073.	5198.	5112.	5252.	5260.	5128.
5229.	5128.	5255.	5555.	5521.	5599.	5603.
5783.	6182.	6224.	6192.	6165.	6095.	6049.
5973.	5795.	5598.	5579.	5747.	5717.	5651.
5722.	5644.	5610.	5642.	5598.	5540.	5695.
5514.	5492.	5373.	5052.	4787.	4897.	4862.
5253.	5231.	5382.	5593.	5630.	5328.	5766.
5903.	6171.	6250.	6129.	5960.	6239.	6103.
6001.	3939.	5892.	5878.	5904.	6154.	6464.
5544.	5544.	5649.	5649.	5649.	5649.	5544.
5696.	5620.	5630.	5606.	5681.	5381.	5293.
5435.	5415.	4952.	4970.	5504.	5561.	5644.
5925.	6278.	6252.	6178.	6242.	6257.	6112.
5968.	5839.	6011.	6208.	6256.	6347.	6332.

DEPTH GRID (cont'd)

5747.	[illegible]	[illegible]	355[illegible]	5657.	5657.	5657.
[illegible]7.	5657.	5657.	5657.	5657.	5967.	5929.
6087.	5445.	5682.	5799.	5731.	5851.	5877.
5986.	5838.	5788.	6185.	5921.	5983.	5917.
5159.	6114.	6074.	6070.	6076.	6052.	6081.
5248.	5539.	5645.	5639.	5608.	5953.	5953.
5718.	5891.	5688.	5792.	5881.	5991.	6157.
6325.	6134.	6304.	6688.	6484.	5980.	6046.
6227.	6259.	6255.	6269.	6096.	6020.	6018.
6009.	6155.	6258.	6388.	6095.	6352.	6272.
5446.	5483.	5541.	5681.	5676.	5708.	5843.
5898.	6028.	6018.	6122.	6232.	6344.	6456.
6478.	5808.	5943.	5953.	6598.	6661.	6575.
6565.	6582.	6511.	6486.	6456.	6456.	6456.
6344.	6344.	6344.	6456.	6465.	6465.	6539.
5480.	5544.	5455.	5568.	5682.	5792.	5796.
5918.	6072.	5682.	5970.	6251.	6478.	6705.
6819.	6692.	6721.	6721.	6814.	6797.	6781.
6781.	6781.	6621.	6466.	6451.	6484.	6418.
6312.	6398.	6484.	6581.	6518.	6522.	6526.
5486.	5742.	5804.	5874.	5742.	5861.	5946.
6314.	6376.	6383.	6396.	6614.	6731.	6963.
6849.	7065.	6963.	6933.	6963.	6789.	6731.
6718.	6674.	6674.	6615.	6615.	6674.	6674.
6674.	6674.	6674.	6674.	6615.	6615.	6615.
5348.	5940.	5975.	5818.	5818.	5929.	6183.
6285.	6434.	6589.	6642.	6745.	7068.	7168.
7115.	6996.	6996.	7174.	7115.	6879.	6879.
6768.	6768.	6768.	6768.	6768.	6879.	6879.
6879.	6879.	6879.	6879.	6768.	6768.	6768.
5793.	7145.	6544.	6384.	5989.	5938.	6052.
6175.	6658.	6961.	6899.	7021.	7088.	7384.
6836.	6977.	7322.	7262.	7208.	7021.	6961.
6899.	6837.	6944.	6944.	6999.	7021.	7021.
7088.	7080.	7050.	7021.	7021.	6961.	6961.
6434.	6733.	6997.	6859.	6185.	5939.	6088.
6061.	6434.	6805.	6928.	7052.	7177.	7548.
7039.	7257.	7323.	7363.	7299.	7177.	7052.
7052.	6928.	6928.	6928.	7138.	7353.	7326.
7299.	7299.	7238.	7177.	7177.	7177.	7177.
5836.	7143.	7266.	7377.	6508.	6318.	6285.
6129.	6320.	6697.	6886.	7283.	7268.	7013.
6622.	6529.	6949.	6916.	7064.	6886.	6759.
6886.	6949.	7013.	7076.	7268.	7393.	7582.
7845.	7899.	7868.	7664.	7582.	7520.	7455.
5126.	6333.	8295.	8270.	6847.	6718.	6590.
6202.	6202.	6590.	6847.	7365.	7365.	6460.
5498.	5685.	6460.	6460.	6541.	6613.	6460.
6720.	6977.	7105.	7235.	7495.	7623.	8010.
8400.	8532.	8532.	8270.	7458.	7367.	7358.

1999.	6849.	7744.	7395.	7199.	7262.	6846.	
6340.	6386.	6458.	6585.	6371.	6348.	5844.	
5814.	5499.	5982.	6874.	6498.	6562.	6581.	
6823.	7144.	7361.	7058.	8037.	8346.	8791.	
8392.	7889.	7827.	7661.	7787.	7841.	8854.	
618.	1976.	6478.	7486.	7152.	7128.	7152.	
6476.	6339.	6298.	6207.	5735.	5943.	5195.	
5128.	5363.	5438.	7668.	6873.	6372.	5561.	
6758.	6907.	7525.	7931.	8776.	9289.	9195.	
7032.	7885.	6427.	6653.	7332.	8011.	8761.	
247.	342.	2488.	5255.	6568.	7359.	7327.	
6899.	4589.	6268.	5855.	5566.	5192.	5152.	
5378.	5546.	6138.	6737.	6622.	6474.	7481.	
7388.	7221.	6723.	6225.	6872.	6861.	5364.	
5188.	4852.	4634.	4698.	4952.	5460.	6062.	
0.	0.	646.	3956.	6833.	7512.	7347.	
7879.	6438.	6342.	6173.	5694.	5213.	5398.	
5376.	5576.	6784.	7533.	7541.	7451.	7458.	
7438.	4598.	3545.	2934.	2934.	2158.	2262.	
2867.	1845.	1606.	1671.	1671.	2719.	3542.	
0.	0.	3731.	6821.	6935.	7448.	7471.	
6946.	6835.	6928.	6618.	6894.	5460.	5485.	
5669.	5981.	6464.	6483.	6798.	6526.	6272.	
5196.	4511.	4141.	4283.	4339.	4486.	4248.	
4264.	4337.	4306.	4532.	4814.	4474.	4383.	
0.	0.	0.	1765.	7988.	7991.	7988.	
7418.	7480.	7451.	7625.	6781.	5715.	5836.	
6248.	6654.	6559.	5931.	5567.	4994.	4957.	
5189.	5323.	6435.	7285.	7280.	7290.	7825.	
6956.	6681.	6766.	6809.	6715.	7163.	7897.	
0.	0.	0.	4874.	5438.	7489.	7585.	
7598.	7491.	6892.	6294.	6344.	6267.	6367.	
6495.	5964.	5468.	5282.	5837.	6713.	7217.	
7026.	7136.	6890.	6763.	6581.	6219.	5683.	
5514.	5438.	5482.	5589.	5541.	5938.	6310.	
0.	0.	0.	0.	2754.	2899.	2893.	
2889.	2991.	3938.	3961.	4019.	3940.	3759.	
3578.	3556.	3517.	4155.	4350.	4562.	4533.	
4456.	4489.	4077.	3758.	3536.	3267.	2546.	
2303.	2372.	2348.	2524.	2972.	2925.	2906.	

DEPTH GRID (in ft)

18.30	9.13	-39.1	10000.	304699.47	6.0	1000.	0.0
13.28	11.10	-17.1	10000.	304699.47	6.0	1000.	0.0

X, Y coordinates of ray origin

Initial ray angle (deg.)

Deltax (Δx) Computational Increment (ft)

Length of a grid square at 0° latitude (ft)

Conversion from fathoms to feet

Time interval between wave fronts (sec)

Time at the beginning of a ray

APPENDIX B: TRANSFORMATION OF WAVE MOTION ON THE EARTH'S SURFACE TO A MERCATOR REPRESENTATION OF THAT SURFACE

1. Latitudinal and meridional lines of a sphere may be represented on a map so that the latitudes are horizontal, parallel lines and the longitudes are vertical, parallel lines. Such a representation is termed a Mercator projection and is orthomorphic (i.e., the distortion is uniform in all directions at each point on the map).

2. Let Δx_o = elementary length on a parallel of latitude, ψ

Δy_o = elementary length on a meridian, ϕ

R = radius of the sphere

$\Delta x_o = R\Delta\phi \cos\psi$

$\Delta y_o = R\Delta\phi$

3. Let Δx and Δy be corresponding lengths on a Mercator map. Since the projection is orthomorphic,

$$\frac{\Delta x}{\Delta x_o} = \frac{\Delta y}{\Delta y_o} = n$$

Since two consecutive meridians separated by $\Delta\phi$ are represented on the Mercator map by parallel lines separated by $\Delta x = R\Delta\phi$, we have

$$\frac{\Delta x}{\Delta x_o} = \frac{R\Delta\phi}{R\Delta\phi \cos\psi} = \sec\psi = n$$

Therefore,

$$\frac{\Delta y}{\Delta y_o} = n = \sec\psi = \frac{\Delta y}{R\Delta\psi}$$

Then

$$\frac{\Delta y}{\Delta\psi} = R \sec\psi$$

$$y = R\int_o^{\psi} \sec\psi \, d\psi$$

and

$$y = R \log \tan\left(\frac{\pi}{4} + \frac{\psi}{2}\right)$$

Considering a unit sphere where $R = 1$,

$$e^{y} = \tan\left(\frac{\pi}{4} + \frac{\psi}{2}\right) \tag{B1}$$

Also, it can be shown that

$$e^{y} = \sec \psi + \tan \psi \tag{B2}$$

4. The above derivation shows that the distances on a sphere are magnified by the factor $\sec \psi$ on a Mercator representation of this sphere. The present problem is to determine a method of plotting wave motion which takes place on the earth's surface on a Mercator map. This is accomplished in the present methodology by multiplying the actual input depths by the secant squared of the latitudinal angle ψ . Since

$$V_o = \sqrt{gH_o}$$

$$V = \sqrt{gH_o \sec^2 \psi} = \sec \psi \sqrt{gH_o}$$

and

$$V = V_o \sec \psi$$

The time element dt is invariable since

$$dt = \frac{ds}{V} = \frac{dS_o \sec \psi}{V_o \sec \psi} = \frac{dS_o}{V_o}$$

5. This subjective reasoning can be proved in more definite form. Referring to fig. B1, the basic refraction equation is:

$$\frac{d\theta}{ds} = \frac{1}{C}\left(\sin \theta \frac{\partial C}{\partial x} - \cos \theta \frac{\partial C}{\partial y}\right)$$

where

$$\sin \theta = \frac{dy}{ds} = \frac{dy}{\sqrt{(dx)^2 + (dy)^2}} = \frac{1}{\sqrt{\left(\frac{dx}{dy}\right)^2 + 1}}$$

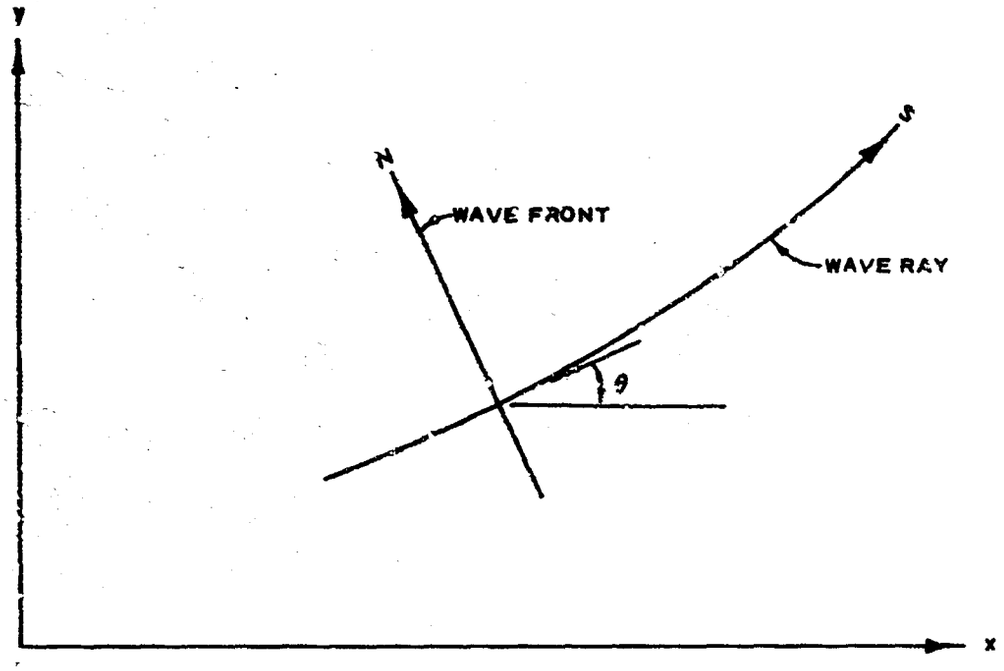

Fig. B1. Wave ray notation

$$\cos\theta = \frac{dx}{ds} = \frac{1}{\sqrt{1 + \left(\frac{dy}{dx}\right)^2}}$$

and

$$\begin{cases} \frac{\partial C}{\partial y} = \frac{1}{2} KH^{-1/2} \frac{\partial H}{\partial y} \\ \frac{\partial C}{\partial x} = \frac{1}{2} KH^{-1/2} \frac{\partial H}{\partial x} \end{cases}$$

where $C = KH^{1/2}$.

Therefore

$$\frac{d\theta}{ds} = \frac{1}{2H} \frac{\partial H}{\partial x} \frac{1}{\sqrt{\left(\frac{dx}{dy}\right)^2 + 1}} - \frac{1}{2H} \frac{\partial H}{\partial y} \frac{1}{\sqrt{1 + \left(\frac{dy}{dx}\right)^2}}$$

Also

$$\frac{d\theta}{ds} = \frac{\dfrac{d^2y}{dx^2}}{\left[1 + \left(\dfrac{dy}{dx}\right)^2\right]^{3/2}}$$

$$\frac{\dfrac{d^2y}{dx^2}}{\left[1 + \left(\dfrac{dy}{dx}\right)^2\right]^{3/2}} = \frac{1}{2H}\left[\frac{\dfrac{\partial H}{\partial x} \cdot \dfrac{dy}{dx}}{\sqrt{1 + \left(\dfrac{dy}{dx}\right)^2}} - \frac{\dfrac{\partial H}{\partial y}}{\sqrt{1 + \left(\dfrac{dy}{dx}\right)^2}}\right]$$

$$\frac{d^2y}{dx^2} = \frac{1 + \left(\dfrac{dy}{dx}\right)^2}{2H}\left(\frac{\partial H}{\partial x}\frac{dy}{dx} - \frac{\partial H}{\partial y}\right) \qquad (B3)$$

Now

$$e^y = \sec \phi + \tan \phi$$

$$\tan \phi = e^y - \sec \phi$$

$$\tan^2 \phi = e^{2y} - 2e^y \sec \phi + \sec^2 \phi$$

and

$$\sec^2 \phi - 1 = \tan^2 \phi$$

so

$$2e^y \sec \phi = 1 + e^{2y}$$

$$\sec \phi = \frac{1}{2}(e^y - e^{-y}) = \cosh y$$

The depths are transformed so that

$$H = H_o \sec^2 \phi \qquad (B4)$$

In a sea of uniform depth

$$H = H_o \sec^2 \phi = H_o \cosh^2 y$$

$$\frac{\partial H}{\partial y} = 2H_o \cosh y \sinh y$$

$$\frac{1}{H}\frac{\partial H}{\partial y} = \frac{2H_o \cosh y \sinh y}{H_o \cosh^2 y} = 2 \tanh y \qquad (B5)$$

Substituting equation B5 into equation B3 and noting that $\frac{\partial x}{\partial x} = 0$ (in this case)

$$\frac{d^2y}{dx^2} = -\frac{1}{2} \cdot 2 \tanh y \left[1 + \left(\frac{dy}{dx}\right)^2\right] \qquad (B6)$$

Then, taking x as a function of y,

$$\frac{dy}{dx} = \frac{1}{\frac{dx}{dy}}$$

$$\frac{d^2y}{dx^2} = \frac{d}{dx}\left(\frac{dx}{dy}\right)^{-1} = \frac{d}{dy}\left(\frac{dx}{dy}\right)^{-1}\frac{dy}{dx}$$

$$\frac{d^2y}{dx^2} = -\frac{\frac{d^2x}{dy^2}}{\left(\frac{dx}{dy}\right)^3}$$

$$\frac{d^2x}{dy^2} = -\frac{d^2y}{dx^2}\left(\frac{dx}{dy}\right)^3 = \tanh y \left(\frac{dx}{dy}\right)^3 \left[1 + \left(\frac{dy}{dx}\right)^2\right] \qquad (B7)$$

$$\frac{d^2x}{dy^2} = \tanh y \left[\left(\frac{dx}{dy}\right)^3 + \frac{dx}{dy}\right]$$

$$\frac{d}{dy}\left(\frac{dx}{dy}\right)^2 = 2 \tanh y \left[\left(\frac{dx}{dy}\right)^4 + \left(\frac{dx}{dy}\right)^2\right]$$

Setting

$$\left(\frac{dx}{dy}\right)^2 = \eta \qquad (B8)$$

we have

$$\frac{d\eta}{dy} = 2 \tanh y(\eta^2 + \eta)$$

$$\frac{d\eta}{\eta + \eta^2} = 2 \tanh y \, dy$$

$$\frac{d\eta}{\eta} - \frac{d\eta}{1 + \eta} = 2 \tanh y \, dy$$

Integrating

$$\ell n \, \eta - \ell n \, (1 + \eta) = 2 \, \ell n \cosh y + \ell n \, C_1$$

or

$$\frac{\eta}{1 + \eta} = C_1^2 \cosh^2 y \tag{B9}$$

since

$$\eta_o = \left(\frac{dx}{dy}\right)_o^2 = \cot^2 \phi$$

where ϕ is the angle between the ray and the x-axis. At $y = 0$, C_1 is evaluated as

$$C_1^2 = \frac{\eta_o}{1 + \eta_o}$$

6. For example, if the ray follows the equator, $\theta = 0$, $\cot^2 \theta = \infty$, and C_1 becomes unity. If the ray follows a meridian. $\theta = 90^\circ$, $\cot^2 \theta = 0$, and $C_1^2 = 0$. Now

$$\eta = C_1^2 \cosh^2 y + \eta C_1^2 \cosh^2 y$$

or

$$\eta = \frac{C_1^2 \cosh^2 y}{1 - C_1^2 \cosh^2 y}$$

$$\eta = \left(\frac{dx}{dy}\right)^2 = \frac{\cosh^2 y}{C_1^{-2} - \cosh^2 y}$$

$$\frac{dx}{dy} = \frac{\cosh y}{\sqrt{C_1^{-2} - 1 - \sinh^2 y}}$$

Setting

$$C_1^{-2} - 1 = K^2$$

$$\frac{dx}{dy} = \frac{\cosh y}{\sqrt{K^2 - \sinh^2 y}}$$

Then integrating

$$x - x_o = \int_o^y \frac{\cosh y \, dy}{\sqrt{K^2 - \sinh^2 y}} \qquad \text{(B10)}$$

by setting

$$\sinh y = z$$

$$d(\sinh y) = \cosh y \, dy = dz$$

$$x - x_o = \int_o^{\sinh^{-1} z} \frac{dz}{\sqrt{K^2 - z^2}} = \sin^{-1}\left(\frac{z}{K}\right) \Bigg|_o^{\sinh^{-1} z}$$

one obtains

$$\sin (x - x_o) = \frac{\sinh y}{K} \qquad \text{(B11)}$$

Differentiating equation B11 yields

$$\cos (x - x_o) \, dx = \frac{\cosh y}{K} \, dy$$

$$\frac{dx}{dy} = \frac{\cosh y}{K \cos (x - x_o)} \qquad \text{(B12)}$$

Also

$$\sin^2 (x - x_o) = \frac{\sinh^2 y}{K^2} \qquad \text{(B13)}$$

Then

$$\cos^2 (x - x_o) = 1 - \frac{\sinh^2 y}{K^2} \qquad \text{(B14)}$$

Combining equations B13 and B14 into equation B12 one obtains

$$\frac{dx}{dy} = \frac{\cosh y}{\sqrt{K^2 - \sin^2 y}} \tag{B15}$$

The tsunami travel time can be represented by the equation

$$t = \int_{S_1} \frac{ds}{V} \tag{B16}$$

where

S_1 is the path of the ray

V is the velocity over the path on a Mercator map

The velocities have been assumed to be

$$V_o = \sqrt{gH_o} \ , \ V = V_o \sec \phi$$

Therefore

$$t = \frac{1}{V_o} \int_{S_1} \frac{ds}{\sec \phi} \tag{B17}$$

7. In order to test the depth transformation, consider a wave initiated at $x = 0$, $y = 0$, and traveling to the meridian $x = \frac{\pi}{2}$. Equation B17 becomes

$$t = \frac{1}{V_o} \int_0^{\pi/2} \frac{\sqrt{1 + \left(\frac{dy}{dx}\right)^2}\, dx}{\cosh y} \tag{B18}$$

Equation B15 becomes

$$\left(\frac{dy}{dx}\right)^2 = \frac{K^2 - \sinh^2 y}{\cosh^2 y}$$

$$1 + \left(\frac{dy}{dx}\right)^2 = \frac{K^2 - \sinh^2 y + \cosh^2 y}{\cosh^2 y} = \frac{1 + K^2}{\cosh^2 y}$$

Therefore

$$t = \frac{\sqrt{1 + K^2}}{V_o} \int_o^{\pi/2} \frac{dx}{\cosh^2 y} \qquad (B19)$$

From equation B11, equation B19 becomes

$$t = \frac{\sqrt{1 + K^2}}{V_o} \int_o^{\pi/2} \frac{dx}{1 + K^2 \sin^2 (x - x_o)}$$

and, when $x_o = 0$,

$$t = \frac{\sqrt{1 + K^2}}{V_o} \int_o^{\pi/2} \frac{dx}{1 + K^2 \sin^2 x} \qquad (B20)$$

Equation B20 can be integrated by the formula

$$\int \frac{dx}{a^2 + b^2 \sin^2 x} = \frac{1}{a\sqrt{a^2 + b^2}} \tan^{-1} \left(\frac{\sqrt{a^2 + b^2} \tan x}{a} \right)$$

so that

$$t = \frac{\sqrt{1 + K^2}}{V_o} \left[\frac{1}{\sqrt{1 + K^2}} \tan^{-1} \left(\sqrt{1 + K^2} \tan x \right) \right]_o^{\pi/2}$$

$$t = \frac{1}{V_o} \left(\frac{\pi}{2} - 0 \right) = \frac{\pi}{2V_o}$$

8. It can be concluded from the development given above that all waves starting from $(x,y) = 0,0$ reach the meridian $x = \frac{\pi}{2}$ at the same time. Since this fact can be immediately understood to occur on a sphere covered with a uniform depth of ocean, and has been shown to occur under the proposed transformation of depths onto a Mercator map, the proposed transformation is justified.

9. A refraction diagram drawn by digital computer techniques utilizing the above presentation (and previously discussed at length) is shown in fig. B2. This refraction takes place across an idealized ocean which everywhere covers the earth's surface to an equal depth.

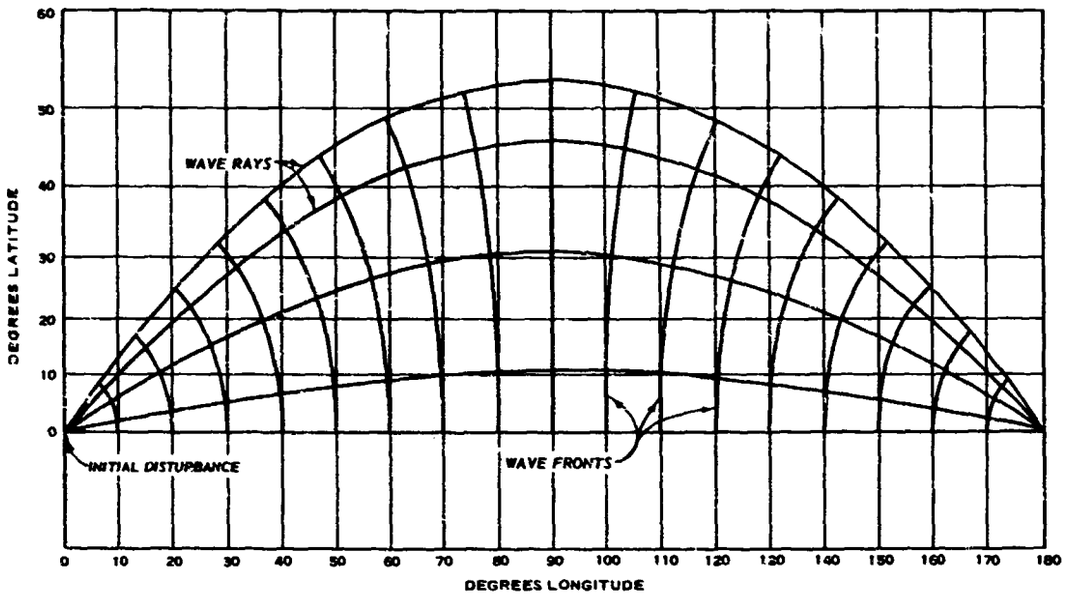

Fig. B2. Representation of wave refraction on Mercator map

APPENDIX C: TSUNAMI REFRACTION IN THE AREA OF A THEORETICAL ISLAND

1. In order to test the numerical technique for drawing refraction diagrams, it was deemed necessary to check the solution against a closed solution for a special case. A circular island of the idealized dimensions shown in fig. C1 was chosen as a model.

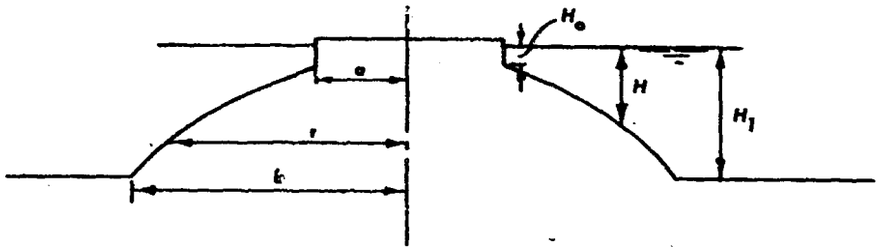

Fig. C1. Profile of island used to test refraction program

2. While considering a circular island, it is convenient to transform the refraction equation

$$\frac{d^2y}{dx^2} = \frac{1}{2H}\left(\frac{dy}{dx}\frac{\partial H}{\partial x} - \frac{\partial H}{\partial y}\right)\left[1 + \left(\frac{dy}{dx}\right)^2\right] \tag{C1}$$

into polar coordinates r and θ so that

$$\left.\begin{aligned} x &= r\cos\theta \\ y &= r\sin\theta \end{aligned}\right\} \tag{C2}$$

First, we write equation C1 as

$$K = \frac{\frac{1}{2H}\left(\frac{dy}{dx}\frac{\partial H}{\partial x} - \frac{\partial H}{\partial y}\right)}{\sqrt{1 + \left(\frac{dy}{dx}\right)^2}} \tag{C3}$$

where the radius of curvature of a curve K in rectangular coordinates is defined as

$$K = \frac{\frac{d^2y}{dx^2}}{\left[1 + \left(\frac{dy}{dx}\right)^2\right]^{3/2}} \qquad (C4)$$

In polar coordinates

$$K = \frac{r^2 + 2r'^2 - rr''}{\left(r^2 + r'^2\right)^{3/2}} \qquad (C5)$$

where

$$r' = \frac{\partial r}{\partial \theta}$$

and

$$r'' = \frac{\partial^2 r}{\partial \theta^2}$$

Now

$$\frac{dy}{dx} = \frac{r' \sin\theta + r\cos\theta}{r'\cos\theta - r\sin\theta}$$

and

$$1 + \left(\frac{dy}{dx}\right)^2 = \frac{(r'\cos\theta - r\sin\theta)^2 + (r'\sin\theta + r\cos\theta)^2}{(r'\cos\theta - r\sin\theta)^2}$$

$$= \frac{r'^2(\cos^2\theta + \sin^2\theta) + r'r(\theta) + r^2(\sin^2\theta + \cos^2\theta)}{(r'\cos\theta - r\sin\theta)^2}$$

$$1 + \left(\frac{dy}{dx}\right)^2 = \frac{r'^2 + r^2}{(r'\cos\theta - r\sin\theta)^2} \qquad (C6)$$

From equation C3

$$K\sqrt{1 + \left(\frac{dy}{dx}\right)^2} = \frac{1}{2H}\left(\frac{dy}{dx}\frac{\partial H}{\partial x} - \frac{\partial H}{\partial y}\right) \qquad (C7)$$

and from equations C5 and C6

$$K\sqrt{1+\left(\frac{dy}{dx}\right)^2} = \frac{r + 2r'^2 - rr''}{(r^2 + r'^2)(r' \cos\theta - r \sin\theta)} \qquad (C8)$$

The terms of equation C7 are expanded as follows:

$$\frac{\partial H}{\partial x} = \frac{\partial H}{\partial r}\frac{\partial r}{\partial x} + \frac{\partial H}{\partial \theta}\frac{\partial \theta}{\partial x}$$

$$\frac{\partial H}{\partial y} = \frac{\partial H}{\partial r}\frac{\partial r}{\partial y} + \frac{\partial H}{\partial \theta}\frac{\partial \theta}{\partial y}$$

and

$$\frac{\partial r}{\partial x} = \cos\theta \ , \ \frac{\partial r}{\partial y} = \sin\theta$$

$$\frac{\partial \theta}{\partial x} = -\frac{\sin\theta}{r} \ , \ \frac{\partial \theta}{\partial y} = \frac{\cos\theta}{r}$$

Now since

$$\frac{dy}{dx} = \frac{r' \sin\theta + r\cos\theta}{r' \cos\theta - r \sin\theta}$$

$$\frac{1}{2H}\left(\frac{dy}{dx}\frac{\partial H}{\partial x} - \frac{\partial H}{\partial y}\right)$$

$$= \frac{\frac{1}{2H}\left[(r' \sin\theta + r\cos\theta)\frac{\partial H}{\partial x} - (r' \cos\theta - r\sin\theta)\frac{\partial H}{\partial y}\right]}{r' \cos\theta - r \sin\theta} \qquad (C9)$$

Considering these terms separately

$$\left(r' \sin\theta + r\cos\theta\right)\frac{\partial H}{\partial x} = \left(r' \sin\theta + r\cos\theta\right)\left(\cos\theta\frac{\partial H}{\partial r} - \frac{\sin\theta}{r}\frac{\partial H}{\partial \theta}\right)$$

$$= r' \sin\theta\cos\theta\frac{\partial H}{\partial r} + r\cos^2\theta\frac{\partial H}{\partial r} - \frac{r'}{r}\sin^2\theta\frac{\partial H}{\partial \theta} - \sin\theta\cos\theta\frac{\partial H}{\partial \theta}$$

$$\left(r' \cos\theta - r \sin\theta\right) \frac{\partial H}{\partial y} = \left(r' \cos\theta - r \sin\theta\right) \left(\sin\theta \frac{\partial H}{\partial r} + \cos\theta \frac{\partial H}{\partial \theta}\right)$$

$$= r' \cos\theta \sin\theta \frac{\partial H}{\partial r} - r \sin^2\theta \frac{\partial H}{\partial r} + \frac{r'}{r} \cos^2\theta \frac{\partial H}{\partial \theta} - \cos\theta \sin\theta \frac{\partial H}{\partial \theta}$$

Therefore

$$(r' \sin\theta + r \cos\theta) \frac{\partial H}{\partial x} - (r' \cos\theta - r \sin\theta) \frac{\partial H}{\partial y} = r \frac{\partial H}{\partial r} - \frac{r'}{r} \frac{\partial H}{\partial \theta}$$

and

$$\frac{1}{2H} \left(\frac{dy}{dx} \frac{\partial H}{\partial x} - \frac{\partial H}{\partial y}\right) = \frac{\frac{1}{2H} \left(r \frac{\partial H}{\partial r} - \frac{r'}{r} \frac{\partial H}{\partial \theta}\right)}{r' \cos\theta - r \sin\theta}$$

Now, combining equations C7, C8, and C9 yields

$$r^2 + 2r'^2 - rr'' = \frac{1}{2H} \left(r \frac{\partial H}{\partial r} - \frac{r'}{r} \frac{\partial H}{\partial \theta}\right) \left(r^2 + r'^2\right) \qquad \text{(C10)}$$

Equation C10 is the refraction equation in polar coordinates.

3. Let us assume that the island is symmetrical so that

$$\frac{\partial H}{\partial \theta} = 0$$

Therefore

$$r^2 + 2r'^2 - rr'' = \frac{1}{2H} \left(r \frac{dH}{dr}\right) \left(r^2 + r'^2\right) \qquad \text{(C11)}$$

The hypothetical island is illustrated in fig. C1 and is defined by the equations

$$H = H_o \left(\frac{r}{a}\right)^2 \qquad a < r < b$$

$$H = H_1 = H_o \left(\frac{b}{a}\right)^2 \qquad b < r$$

$$\frac{\partial H}{\partial r} = 2H_o \left(\frac{r}{a^2}\right)$$

$$\frac{r}{H}\frac{\partial H}{\partial r} = 2$$

Simplifying equation C11 according to these boundary conditions yields

$$r^2 + 2r'^2 - rr'' = r^2 + r'^2 \qquad \text{(C12)}$$

or

$$-rr'' + r'^2 = 0$$

$$-r\frac{d^2r}{d\theta^2} + \left(\frac{dr}{d\theta}\right)^2 = 0 \qquad \text{(C13)}$$

Now one may solve equation C13 for θ as a function of r ;

$$\frac{dr}{d\theta} = \frac{1}{\frac{d\theta}{dr}}$$

$$\frac{d^2r}{d\theta^2} = -\frac{\frac{d^2\theta}{dr^2}}{\left(\frac{d\theta}{dr}\right)^3}$$

and equation C13 becomes

$$r\frac{d^2\theta}{dr^2} + \frac{d\theta}{dr} = 0 \qquad \text{(C14)}$$

The solution of equation C14 is

$$\theta = C_1 \log r + C_2 \tag{C15}$$

In order to solve for the two constants in equation C15, consider a plan view of the given island shape (fig. C2). The x-axis is situated parallel

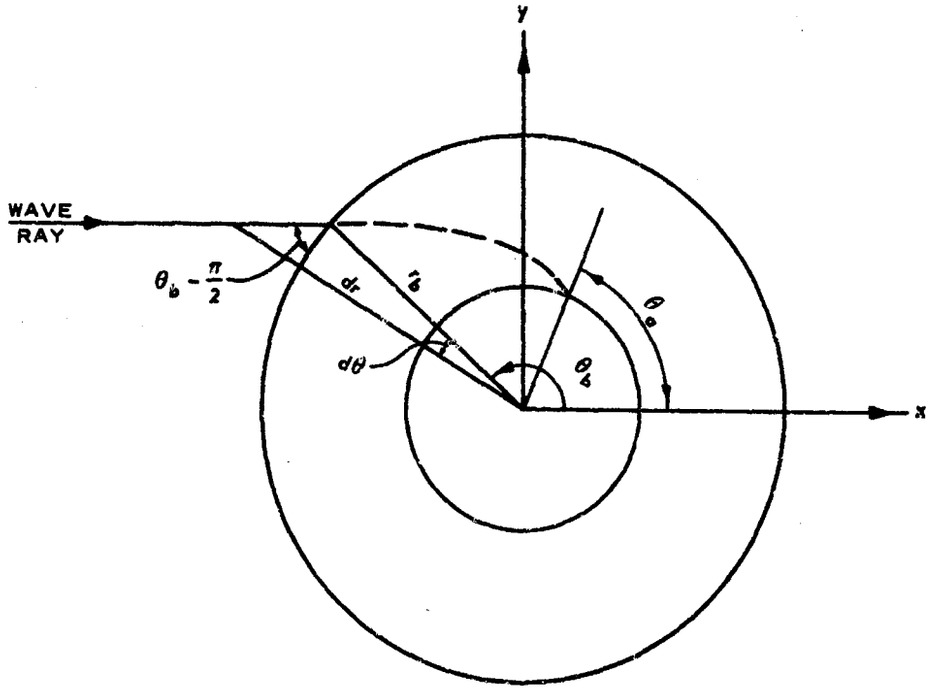

Fig. C2. Plan view of theoretical island showing refraction of one wave ray

to the incident ray direction and all angles are measured in the usual counterclockwise direction from the positive x-axis.

4. At the point of entrance of the ray to the island's influence

$$\frac{dr}{rd\theta} = \tan\left(\theta_b - \frac{\pi}{2}\right) = -\cot\theta_b \tag{C16}$$

Therefore

$$\frac{d\theta}{dr} = \frac{-\tan\theta_b}{r_b}$$

From equation C15

$$\frac{d\theta}{dr} = \frac{C_1}{r_b}$$

and therefore

$$C_1 = -\tan \theta_b \qquad (C17)$$

C_2 is eliminated by considering (r_b,θ_b) and another arbitrary point (r,θ) on the shelf so that

$$\theta_b = C_1 \log r_b + C_2$$

and

$$\theta = C_1 \log r + C_2$$

yielding

$$\theta - \theta_b = -\tan \theta_b \log \frac{r}{r_b} \qquad (C18)$$

Thus, the equation of a ray entering the surroundings of the island at the point $r = r_b$, $\theta = \theta_b$ is

$$\theta = \theta_b - \tan \theta_b \log \frac{r}{r_b} \qquad (C19)$$

The ray will reach the island coast zero contour (at $r = a$) at an azimuth of

$$\theta_a = \theta_b - \tan \theta_b \log \frac{a}{b} \qquad (C20)$$

5. An example of the foregoing discussion is shown below. If

$$\theta_b = 135^\circ = \frac{3\pi}{4}$$

$$\tan \theta_b = -1$$

so that

$$\theta_a = \frac{3\pi}{4} + \log \frac{a}{b}$$

Typical values of θ_a (with $\theta_b = \frac{3\pi}{4}$) for various values of the ratio $\frac{a}{b}$ are tabulated below:

$\frac{a}{b}$	$\log \frac{a}{b}$	θ_a
0.5	-0.693	1.666
0.4	-0.916	1.443
0.3	-1.204	1.155
0.2	-1.609	0.750
0.1	-2.303	0.057

6. Fig. C3 shows a typical refraction pattern around the given island shape to which the specific dimensions shown in the figure have been assigned. The results given by the accepted computer program agree very closely with those produced by the theoretical treatment.

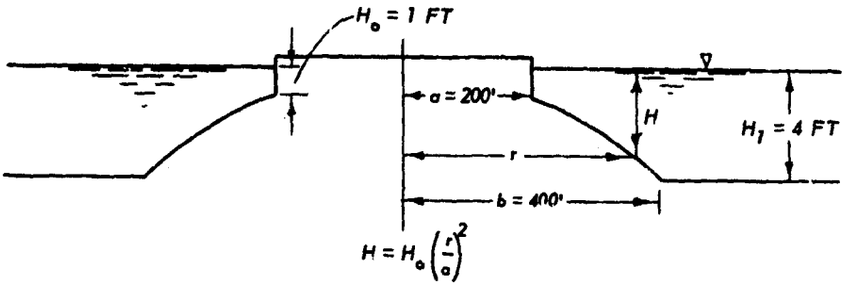

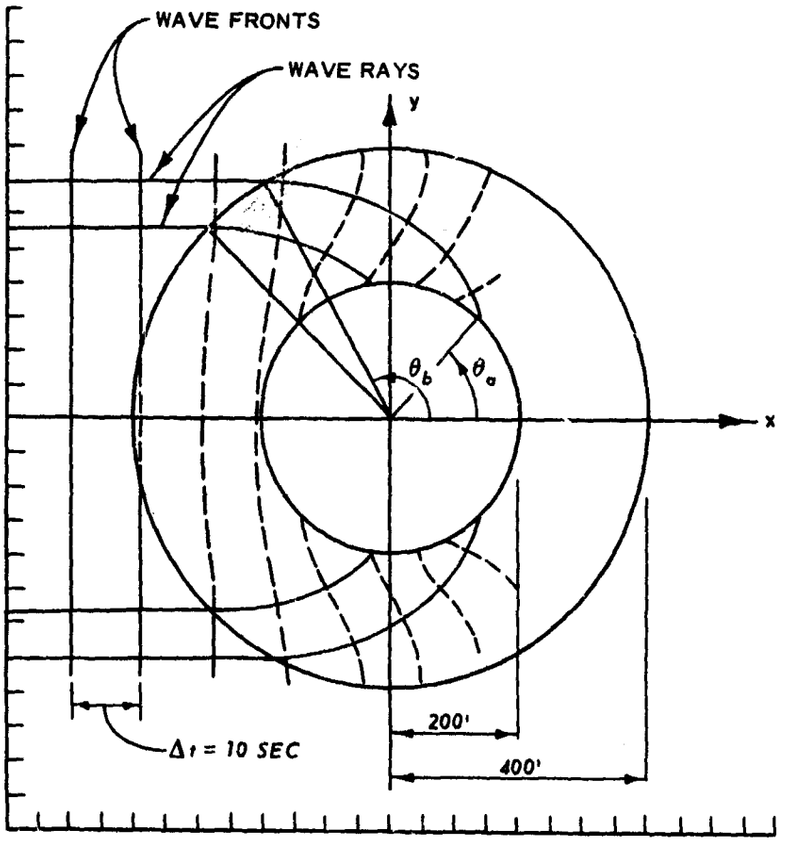

Fig. C3. Typical refraction pattern around the theoretical island

APPENDIX D: SHELF OSCILLATIONS IN THE CRESCENT CITY AREA

1. One may consider the oscillations of an ocean shelf by analyzing the simplified two-dimensional model shown in fig. D1. The model configuration consists of

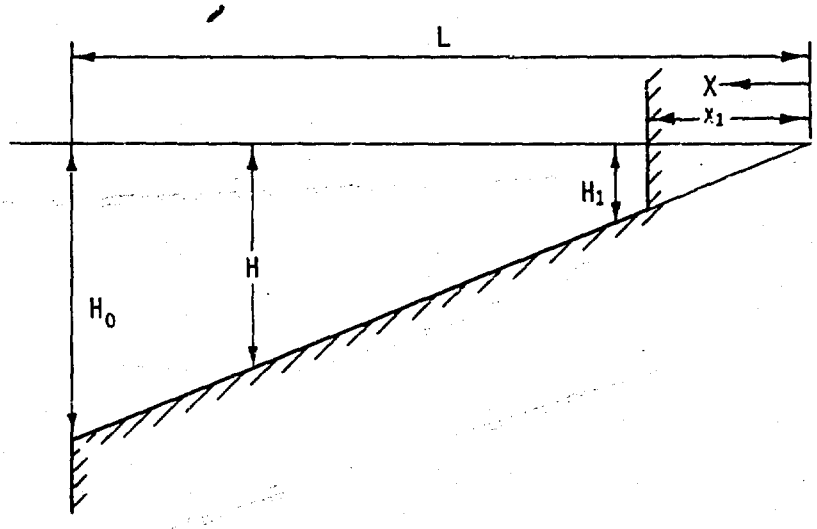

Fig. D1. Two-dimensional model shelf

a uniformly sloping shelf which drops off to infinity at the ocean end and is terminated by a vertical wall near the land.

2. Let the distance x be measured from the point of intersection of the still-water surface and the shelf slope. The shelf then extends from the point $x = x_1$ to $x = L$. The depth of water varies uniformly as

$$H = H_o \frac{x}{L} \tag{D1}$$

3. Denoting the surface disturbance as h, the velocity of water in a section x by u, and the time by t, the equation of motion becomes

$$\frac{\partial u}{\partial t} = -g \frac{\partial h}{\partial x} \tag{D2}$$

where g is the gravitational acceleration. The conservation of mass equation is

$$\frac{\partial h}{\partial t} + \frac{\partial}{\partial x}(Hu) = 0 \qquad (D3)$$

These relations assume that the amplitude h is small in comparison with the depth H, that the vertical acceleration is negligible, and that the velocity u is uniform across the section. The waves induced are assumed to be shallow-water waves.

4. The elimination of u from equations D2 and D3 yields

$$\frac{\partial^2 h}{\partial t^2} - g\frac{\partial}{\partial x}\left(H\frac{\partial h}{\partial t}\right) = 0 \qquad (D4)$$

As we are interested in standing wave oscillations over the shelf, let

$$h = \eta \cos \sigma t \qquad (D5)$$

$$u = V \sin \sigma t \qquad (D6)$$

where $\sigma = \frac{2\pi}{T}$ and T is the period of the oscillation. Substituting from equation D5 into equation D4 yields

$$g\frac{d}{dx}\left(H\frac{d\eta}{dt}\right) + \sigma^2\eta = 0 \qquad (D7)$$

Now, let us suppose that x is measured in terms of L, and write

$$\xi = \frac{x}{L} \qquad (D8)$$

also

$$\xi = \frac{H}{H_o}$$

Equation D7 transforms to

$$\frac{d}{d\xi}\left(\xi\frac{d\eta}{d\xi}\right) + K\eta = 0 \qquad (D9)$$

where

$$K = \frac{\sigma^2 L^2}{g H_o} \tag{D10}$$

Equation D9 may be written as

$$\xi \frac{d^2 \eta}{d\xi^2} + \frac{d\eta}{d\xi} + K\eta = 0 \tag{D11}$$

We may set

$$\theta = 2\xi^{1/2} K^{1/2} \tag{D12}$$

and write equation D11 as

$$\frac{d^2 \eta}{d\theta^2} + \frac{1}{\theta} \frac{d\eta}{d\theta} + \eta = 0 \tag{D13}$$

which is a Bessel equation of zero order and hence

$$\eta = AJ_o(\theta) + BK_o(\theta) \tag{D14}$$

where J_o and K_o are zero order Bessel functions of the first and second kind, respectively. The height of the disturbance is

$$h = \left[AJ_o(\theta) + BK_o(\theta)\right] \cos \sigma t \tag{D15}$$

If the oscillations of the open sea are given at $x = L$ to be

$$h = \eta_o \cos \sigma t \tag{D16}$$

then

$$\eta_o = AJ_o(\theta_L) + BK_o(\theta_L) \tag{D17}$$

where

$$\theta_L = 2 K^{1/2}$$

5. A second relation similar to equation D17 involving, likewise, the constants A and B should be obtained. At the point $\xi = \xi_1$ the particle velocity is defined.

6. Reconsider equation D2 and substitute from equations D5 and D6.

$$\rho u = -\varepsilon \frac{d\eta}{dx} \tag{D18}$$

or

$$\rho u = \frac{\varepsilon K}{L} \frac{d\eta}{d\xi} \tag{D19}$$

This can also be written as

$$K^{1/2} \frac{\rho}{\rho_c} \frac{V}{\sqrt{gL_0}} = -\frac{d\eta}{d\xi} \tag{D20}$$

Differentiating equation D15 with respect to θ,

$$\frac{d\eta}{d\theta} = AJ_0'(\theta) + BK_0'(\theta)$$

and since

$$J_0'(\theta) = -J_1(\theta)$$

and

$$K_0'(\theta) = -K_1(\theta)$$

we have

$$\frac{d\eta}{d\theta} = -AJ_1(\theta) - BK_1(\theta) \tag{D21}$$

Now

$$\frac{d\eta}{d\xi} = \frac{d\eta}{d\theta}\frac{d\theta}{d\xi} \quad \text{and} \quad \frac{d\theta}{d\xi} = \frac{2K}{\theta}$$

so that

$$\frac{d\eta}{d\xi} = \frac{2K}{\theta} \frac{d\eta}{d\theta} \tag{D22}$$

Substituting equation D22 into equation D21 yields

$$\frac{d\eta}{d\xi} = \frac{-2K}{\theta} \left[AJ_1(\theta) + BK_1(\theta) \right]$$

and from equation D20 the velocity relation is

$$H_o \frac{V}{\sqrt{gh_o}} = \frac{2K}{\theta} \left[AJ_1(\theta) + BK_1(\theta) \right] \tag{D23}$$

where

$$\theta = 2\xi^{1/2} K^{1/2}$$

At the coast, $\xi = \xi_1$, the particle velocity $u = 0$, and hence V vanishes and

$$AJ_1(\theta_1) + BK_1(\theta_1) = 0 \tag{D24}$$

where

$$\theta_1 = 2\xi_1^{1/2} K^{1/2} \tag{D25}$$

Solving for A and B from equations D18 and D24

$$A = \frac{K_1(\theta_1)\eta_o}{\Delta} \tag{D26}$$

$$B = \frac{-J_1(\theta_1)\eta_o}{\Delta} \tag{D27}$$

where

$$\Delta = J_o(\theta_L)K_1(\theta_1) - J_1(\theta_1)K_o(\theta_L) \tag{D28}$$

Substitute into equation D15 so that

$$\frac{\eta}{\eta_o} = \frac{J_o(\theta)K_1(\theta_1) - K_o(\theta)J_1(\theta_1)}{\Delta} \qquad \text{(D29)}$$

7. The solution of the above equations is presented in the following statements. When the waves which excite the shelf system occur at a fundamental frequency of the shelf, the wave heights at the shore $\xi = \xi_1$ will become infinite (under the original assumptions). For various values of ξ_1, we can determine the roots of

$$\Delta = J_o(\theta_L)K_1(\theta_1) - J_1(\theta_1)K_o(\theta_L) \qquad \text{(D28 bis)}$$

The values are shown in table D1 in terms of N where

$$N = \frac{T\sqrt{gH_o}}{L} = \frac{4\pi}{2\alpha^{1/2}} \qquad \text{(D30)}$$

Table D1

N Values for Various Values of ξ_1

ξ_1	N_1	N_2	N_3	N_4	N_5
0	5.226	2.276	1.432	1.006	0.782
0.01	5.129	2.202	1.381	1.003	--
0.022	5.013	2.112	1.319	0.954	--
0.04	4.880	2.016	1.250	0.904	--
0.09	4.511	1.797	1.104	0.7936	--
0.16	4.045	1.558	0.950	--	--

Note: $N = \dfrac{T\sqrt{gH_c}}{L} = \dfrac{4\pi}{2K^{1/2}}$

$\xi_1 = \dfrac{x_1}{L}$

APPENDIX E: STANDING WAVES IN TSUNAMI MODEL CHANNELS

1. For simplicity in argument it will be assumed that the harbor and bay environments in the tsunami model can be approximated by the special channel configuration shown in fig. E1.

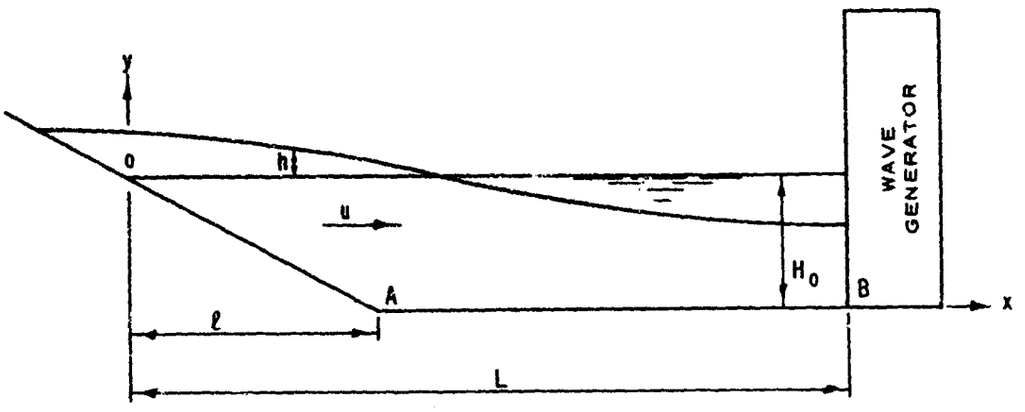

Fig. E1. Idealized channel configuration

Along the distance OA, the harbor and bay area is correctly contoured. Along the distance AB, the water depth is constant. The wave generator placed at B constitutes a barrier, and at this point the particle velocity u vanishes when flow from or into the generator has ceased. For the successful operation of the model it is desired that the period of the standing waves in this particular channel be greater than or equal to the tsunami model period. Although in principle it is always desirable that harbor and bay contours be reproduced up to the foot of the generator, this may not be possible because of cost considerations. In any case one must have an expression for the period of the slowest oscillation.

Law of depth:

$$\left.\begin{aligned} H &= H_o \frac{x}{\ell} \qquad 0 < x < \ell \\ H &= H_o \qquad \ell < x < L \end{aligned}\right\} \tag{E1}$$

Dynamic equation:

$$\frac{\partial u}{\partial t} = -g \frac{\partial h}{\partial x} \tag{E2}$$

Continuity condition:

$$\frac{\partial h}{\partial t} + \frac{\partial}{\partial x}(Hu) = 0 \qquad \text{(E3)}$$

Details of these relations can be found in reference 27. From equations E2 and E3

$$\frac{\partial^2 h}{\partial t^2} - g\frac{\partial}{\partial x}\left(H\frac{\partial h}{\partial x}\right) = 0 \qquad \text{(E4)}$$

Introducing

$$h = \eta \cos \sigma t \ , \ \sigma = \frac{2\pi}{T} \qquad \text{(E5)}$$

equation E4 gives

$$\sigma^2\eta + g\frac{\partial}{\partial x}\left(H\frac{\partial \eta}{\partial x}\right) = 0$$

Introducing

$$\xi = \frac{x}{L} \ , \ \xi_1 = \frac{\ell}{L} \qquad \text{(E6)}$$

the last equation becomes

$$\sigma^2\eta + \frac{gH_o}{L^2}\frac{d}{d\xi}\left(\frac{H}{H_o}\frac{d\eta}{d\xi}\right) = 0 \qquad \text{(E7)}$$

Also

$$K = \frac{\sigma^2 L^2}{gH_o} \qquad \text{(E8)}$$

whereupon

$$\frac{d}{d\xi}\left(\frac{H}{H_o}\frac{d\eta}{d\xi}\right) + K\eta = 0 \qquad \text{(E9)}$$

One must consider two solutions of the equation, first for the range

$0 < \xi \leq \xi_1$ and second for the range $\xi_1 < \xi \leq 1$. For the first range

$$\frac{H}{H_o} = \frac{\xi}{\xi_1} \tag{E10}$$

and equation E9 becomes

$$\xi \frac{d^2\eta_1}{d\xi^2} + \frac{d\eta_1}{d\xi} + K\xi_1\eta_1 = 0 \tag{E11}$$

Subject to the condition that η_1 is finite at $\xi = 0$, the proper solution is (Lamb[27])

$$\eta_1 = A_1 J_o \left(2\xi^{1/2} \xi_1^{1/2} K^{1/2}\right) \tag{E12}$$

For the range $\xi_1 < \xi \leq 1$, since $\frac{H}{H_o} = 1$, equation E9 becomes

$$\frac{d^2\eta_2}{d\xi^2} + K\eta_2 = 0 \tag{E13}$$

and the solution is

$$\eta_2 = A_2 \cos K^{1/2} \xi + B_2 \sin K^{1/2} \xi \tag{E14}$$

Now at $\xi = 1$, $u = 0$ and thus $\frac{d\eta_2}{d\xi} = 0$. By differentiation

$$\frac{d\eta_2}{d\xi} = K^{1/2} \left(-A_2 \sin K^{1/2} \xi + B_2 \cos K^{1/2} \xi\right) \tag{E15}$$

and

$$A_2 \sin K^{1/2} = B_2 \cos K^{1/2}$$

or

$$B_2 = A_2 \tan K^{1/2} \tag{E16}$$

At the section through A, $\xi = \xi_1$, and both η and $\frac{d\eta}{d\xi}$ are continuous. Hence,

$$\left.\begin{aligned} &\eta_1 = \eta_2 \ , \ \xi = \xi_1 \\ \text{and} \\ &\frac{d\eta_1}{d\xi} = \frac{d\eta_2}{d\xi} \ , \ \xi = \xi_1 \end{aligned}\right\} \tag{E17}$$

Then from equations E12 and E14

$$A_1 J_o \left(2\xi_1 K^{1/2}\right) = A_2 \cos K^{1/2} \xi_1 + B_2 \sin K^{1/2} \xi_1 \tag{E18}$$

and

$$A_1 K^{1/2} J_o' \left(2\xi_1 K^{1/2}\right) = K^{1/2} \left(-A_2 \sin K^{1/2} \xi_1 + B_2 \cos K^{1/2} \xi_1\right)$$

or

$$A_1 J_o' \left(2\xi_1 K^{1/2}\right) = -A_2 \sin K^{1/2} \xi_1 + B_2 \cos K^{1/2} \xi_1 \tag{E19}$$

Making use of equation E16

$$A_1 J_o \left(2\xi_1 K^{1/2}\right) = A_2 \left(\cos K^{1/2} \xi_1 + \tan K^{1/2} \sin K^{1/2} \xi_1\right) \tag{E20}$$

and

$$A_1 J_o' \left(2\xi_1 K^{1/2}\right) = A_2 \left(-\sin K^{1/2} \xi_1 + \tan K^{1/2} \cos K^{1/2} \xi_1\right) \tag{E21}$$

Dividing equation E21 by equation E20 and utilizing the rule

$$J_o'(\quad) = -J_1(\quad) \tag{E22}$$

one has

$$\frac{-J_1\left(2\xi_1 K^{1/2}\right)}{J_o\left(2\xi_1 K^{1/2}\right)} = \frac{\tan K^{1/2} - \tan K^{1/2}\,\xi_1}{1 + \tan K^{1/2} \tan K^{1/2}\,\xi_1}$$

or more simply

$$\frac{J_1\left(2\xi_1 K^{1/2}\right)}{J_o\left(2\xi_1 K^{1/2}\right)} = -\tan\left[K^{1/2}\,(1 - \xi_1)\right] \tag{E23}$$

The roots of this equation of least value for specified values of ξ_1, through equation E8, determine the periods T of the slowest oscillation.

2. Determination of the periods is simpler for the two extreme cases represented by $\xi_1 = 0$ and $\xi_1 = 1$. Consider the first case, $\xi_1 = 0$. Since $J_1(0) = 0$, from equation E23

$$\tan K^{1/2} = 0 \tag{E24}$$

and hence

$$K^{1/2} = \pi\,, \quad K = \pi^2$$

Substitute this into equation E8 to obtain

$$T = \frac{2L}{\sqrt{gH_o}} \tag{E25}$$

a well known result.

3. Taking the second case $\xi_1 = 1$, as $J_o(2K^{1/2})$ is finite, equation E23 yields

$$J_1(2K^{1/2}) = 0 \tag{E26}$$

the root of the smallest value being

$$2K^{1/2} = 3.8317$$

which gives

$$K = 4.0530$$

Substituting this in equation E8, one has

$$T = 3.121 \frac{L}{\sqrt{gH_o}} \tag{E27}$$

4. The determination of the roots of equation E23 for other values of ξ_1 must be carried out by trials. Some other determinations of $K^{1/2}$ are given in table E1, along with the corresponding values of N in the expression

$$T = N \frac{L}{\sqrt{gH_o}}, \quad N = \frac{2\pi}{K^{1/2}} \tag{E28}$$

Table E1

Values of $K^{1/2}$ and N for Various Values of ξ_1

ξ_1	$K^{1/2}$	N
0.0	3.142	2.000
0.10	3.137	2.002
0.20	3.100	2.026
0.30	3.007	2.090
0.33	2.952	2.128
0.40	2.837	2.214
0.50	2.642	2.378
0.60	2.454	2.560
0.70	2.285	2.750
0.80	2.141	2.934
0.90	2.020	3.110
0.75	2.210	2.843
1.00	2.013	3.121